

A Dislocation Based Technique for the
Simulation of the Fatigue Growth of Initiated
Microcracks

M. Edstorp

May 28, 2003

Abstract

A dislocation based mathematical model for the fatigue growth of microcracks is presented. The model considers the crystallographic structure of the component in which the crack is initiated, and plastic work is modelled in a detailed way by the emission and movements of dislocations.

To implement the model, we develop in detail a mathematical technique for approximating the different quantities that are treated in the model. Lastly, the usefulness of the technique is evaluated by performing simulations of crack problems using a computer code, and the tool is then applied to crack problems that concern the interaction between a microcrack and the grain boundaries of a composite material.

'A crack in an elastic solid – is a distribution of dislocations on the crack plane' [10].

Contents

1	Introduction	4
1.1	Preface and acknowledgements	4
1.2	Problem formulation	4
1.3	Preliminaries	5
1.3.1	Dislocations	5
1.3.2	A summary of available techniques for crack problems and something about the governing boundary value problem	13
1.3.3	Examples of numerical methods for singular integral equations	29
1.4	Simplifications of the problem and assumptions on its data . .	37
2	A dislocation based model of the fatigue growth of initiated microcracks	39
2.1	Load stepping	39
2.2	The modelling of the grain boundaries, glide planes and crack	39
2.3	The governing boundary value problem and how to obtain its data	41
2.4	Modelling plasticity	42
2.4.1	Dislocation glide and climb	42
2.4.2	The Equilibrium Arrangement of Dislocations and the EAD-iteration	43
2.4.3	Dislocation annihilation	44
2.5	Dislocation emission and crack tip shielding	44
2.6	Crack growth	46
2.7	A flow scheme for the simulation	47
3	A technique for simulating the fatigue growth of initiated microcracks based upon the model	48
3.1	The boundary equation formulation of the governing boundary value problem	48
3.2	Discretizing the equations	50
3.2.1	The ansatz	50
3.2.2	The Gauss-Jacobi method, the Lobatto-Chebyshev method and crack kink singularity correction	52
3.3	Solving the resulting linear system	56

3.4	The problem of plasticity induced crack closure	56
3.5	Computing stress intensity factors	57
4	An implementation of the technique	58
4.1	Evaluating the code by comparing stress intensity approxima- tions with handbook tables	58
4.2	Evaluating the code by examining stress field approximations .	60
4.3	Examining the effects of dislocations on the stress intensity . .	62
4.4	Evaluating the crack growth model	62
5	Applications of the implementation	67
5.1	A first application; No grain boundaries	67
5.2	A second application; Simple grain boundaries	78
5.3	A third application; Sophistscated grain boundaries, a com- plicated geometry and several glide planes	89
5.4	Conclusions and future work	96

1 Introduction

1.1 Preface and acknowledgements

This project was carried out in cooperation with *The Swedish National Testing and research institute* (SP), for the author's master of science diploma in engineering mathematics at Chalmers University of Technology. The author would like to thank Tekn.Dr. Erland Johnson, the project supervisor at SP, and Prof. Kenneth Eriksson the project examiner and supervisor at Chalmers, for their support.

1.2 Problem formulation

We wish to develop a mathematical model that can be used to predict the behaviour of short cracks in different composite granular materials subject to external high cyclic loading, and develop a tool for the computer simulation of the possible growth of such cracks.

In developing the model, we wish to consider the mesostructure of the material constituting the component. We focus on crystalline composites, and hence take into account the crystallographic defects that are present, as well as those defects that appear due to stress concentration. Furthermore, for reasons that will become clear later, we will consider the material to be purely elastic, which means that we will not seek to treat the effects of the plastic zone around the crack tip through an adjustment of the linear elasticity equations. Instead we wish to model the plastic work by the emission and movements of defects of a special kind, namely dislocations, see section 1.3.1.

The crack is assumed to be situated in a single grain, and initiated at a free boundary. Hence, at a particular time, it is the geometry of the grain in which the crack is located, the magnitude of the loading on the grain, the crystallographic glide planes of the grain, the defects present in the grain, and also the shape of the crack itself, that determine the crack growth. It is exactly the above mentioned circumstances that influence the size of the three *stress intensity factors* (see for example [4]), quantities that in a purely elastic material completely characterize the stresses and strains in the close vicinity of the crack tip (see [9]). In linear elastic fracture mechanics theory, a basic assumption is that it is the crack tip stresses alone that govern whether the crack will grow or not. It is therefore crucial that we find these stress intensity factors, and much of our attention will be directed towards this matter.

A microcrack that does not extend over more than one single grain is not likely to influence the usefulness of the component. It is rather the transgranular fracture that makes it possible for the crack to develop into a macrocrack and cause severe harm. It is because of this that the prediction of the behaviour of the crack tip as it approaches the grain boundary is of special interest; In other words, we wish to investigate how well grain boundaries act as a barriers for dislocation motion and crack advance.

1.3 Preliminaries

1.3.1 Dislocations

Physically, a dislocation is a flaw in the crystallographic structure of a material that 'dislocates' the atoms (or molecules) from their equilibrium positions, i.e. their locations in the ideal crystal, causing the interatomic forces to create what is mathematically known as a stress field. Hence, the mathematical object modelling a dislocation is a source of stress originating from a disturbance in the space lattice. We will consider the type of dislocation known as the *straight edge dislocation*, which is formed by the insertion into the crystal lattice of an extra atomic half plane, at the edge of which the dislocation is considered to be located. When the lattice is projected onto a plane orthogonal to the dislocation edge, as when a plain strain state is considered, the straight edge dislocation may be treated as a point.

Since the dislocation is a source of stress, it is natural to assign to it a strength. Considering further that different dislocations can have different orientation, it is adequate to associate with each one of them a vector. This vector is known as the burgers vector b of the dislocation. The formal definition of b can be found in [2] and [3]. From this definition it can be seen that a burgers vector can be associated with any finite number of dislocations. We will disregard the actual number of dislocations represented by a burgers vector, and recognize only its size and direction.

Another interesting property of dislocations is that the stresses and displacements induced by a dislocation only depend upon its burgers vector. Different lattice defects can have the same burgers vector, but it follows that one need not consider the actual nature of the flaw.

In the following we constrain our study to straight edge dislocations. The atoms on the edge of the inserted half plane can be considered to lack an atomic bond over a crystal plane. More realistically, a number of neigh-

bouring atoms are dislocated near the edge, merely altering the bonds in a small vicinity. This is pedagogically described by Andrade's model for dislocation motion described in [2]. For simplicity, we consider the edge atoms to completely lack a bond over the crystal plane, while the other atoms in the vicinity retain their perfect crystal bonds (though dislocated). From this point of view it can be understood that the dislocation can move along the crystal plane due to a force applied in such a way that the bonds of the nearest edge-neighbour are connected to the edge, leaving their former neighbours lacking bonds over the crystal plane. A repetition of this procedure causes what is known as *glide*. The crystal plane in question is called the *glide plane* of the dislocation, and the dislocation moving by glide is called a *glide dislocation*. Thus, what we have is a set of mobile (point) sources of stress.

Figure 1 schematically describes how a straight edge dislocation is created and how it glides. It specifically illustrates that when a dislocation is created, another defect is created with such a burgers vector that the sum of the burgers vectors of both flaws is zero.

The critical force needed to cause the glide induces a stress τ_{crit} in the body. This stress is termed the *critical resolved shear stress* and is discussed in connection with the modelling of dislocation motion in section 2.4.1. It was originally the difference between the theoretically obtained values of the critical resolved shear stress and the experimentally obtained values that stimulated the study of crystal defects, see [2].

As has already been stated, a crystalline state is modelled by a three dimensional lattice. Every lattice is characterized by its *unit cell*, and this unit cell defines a finite set of possible glide planes. Hence the number of possible directions in which a dislocation can move is limited, causing an anisotropy in the material, see further [1]. Note that edge dislocations can also move by what is known as *climb*. Climb occurs when a *climb dislocation* moves in a direction perpendicular to the glide plane. The set of 'climb planes' are also limited by the microstructure. For example, in a crystal consisting of face-centered cubic unit cells, glide usually takes place along one of the $\{111\}$ lattice planes in one of the three directions $\langle 110 \rangle$ ([2]).

In dislocation modelling, it is common to treat dislocation constellations other than single dislocations. For example, in our case, we might very well employ the plane dislocation dipole of length l , which is made up from two dislocations with similar strength but opposite direction burgers vectors b and $-b$, placed on the same plane. In a two dimensional analysis, the dipole may thus be treated as an area of inserted material; One of the constituting

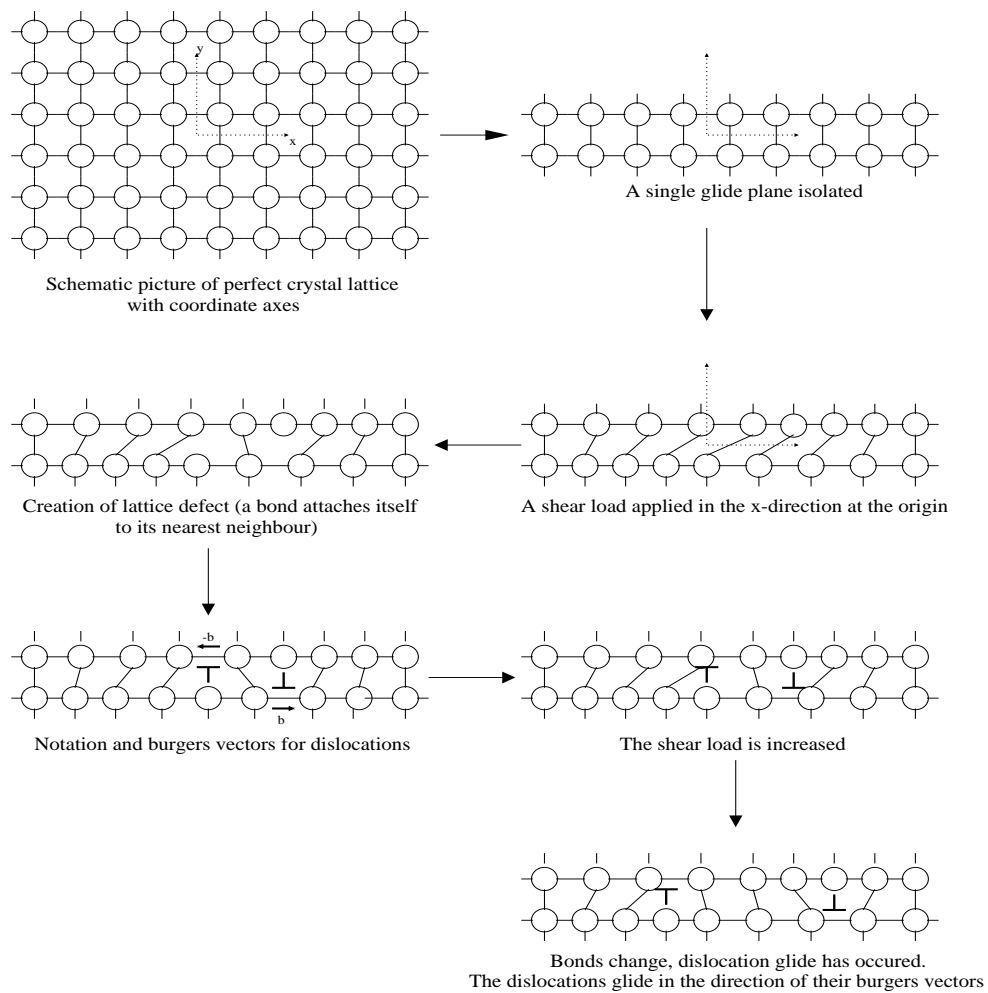


Figure 1: The birth of a straight edge dislocation

dislocations is made up from an inserted half plane of material 'of thickness $\|b\|$ ', and cutting this plane off at the length l creates another dislocation of equal strength but of opposite direction burgers vector! The area of the inserted material is then $\|b\| \times l$.

Figures 2 through 5 show contour plots of the shear and direct stress fields in the vertical direction arising from the precense of different dislocations in a half plane. Note specifically that the shear stress (as well as the direct stress in the *horizontal* direction) vanish on the free edge of the half plane (the left edge of the plot).

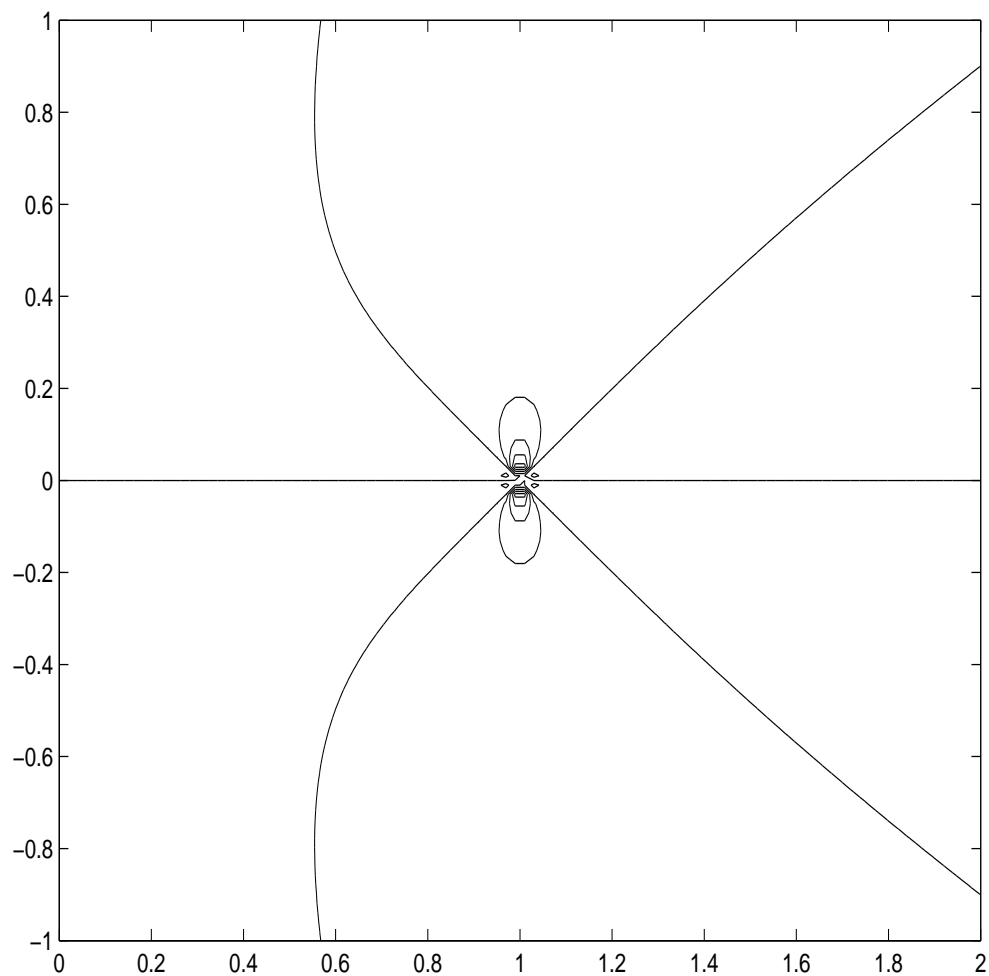


Figure 2: The direct stress around a dislocation with a burgers vector in the horizontal direction. Note specifically that the direct stress is zero on the horizontal axis.

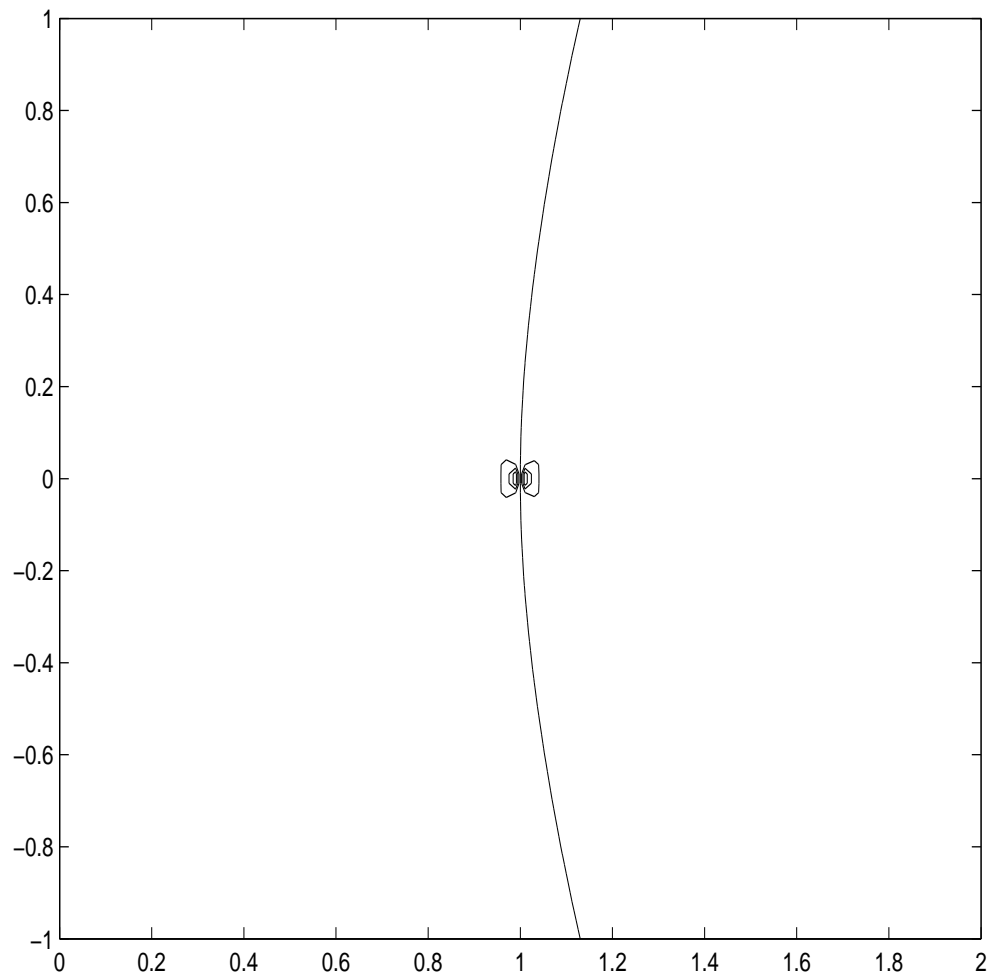


Figure 3: The direct stress around a dislocation with a burgers vector in the vertical direction.

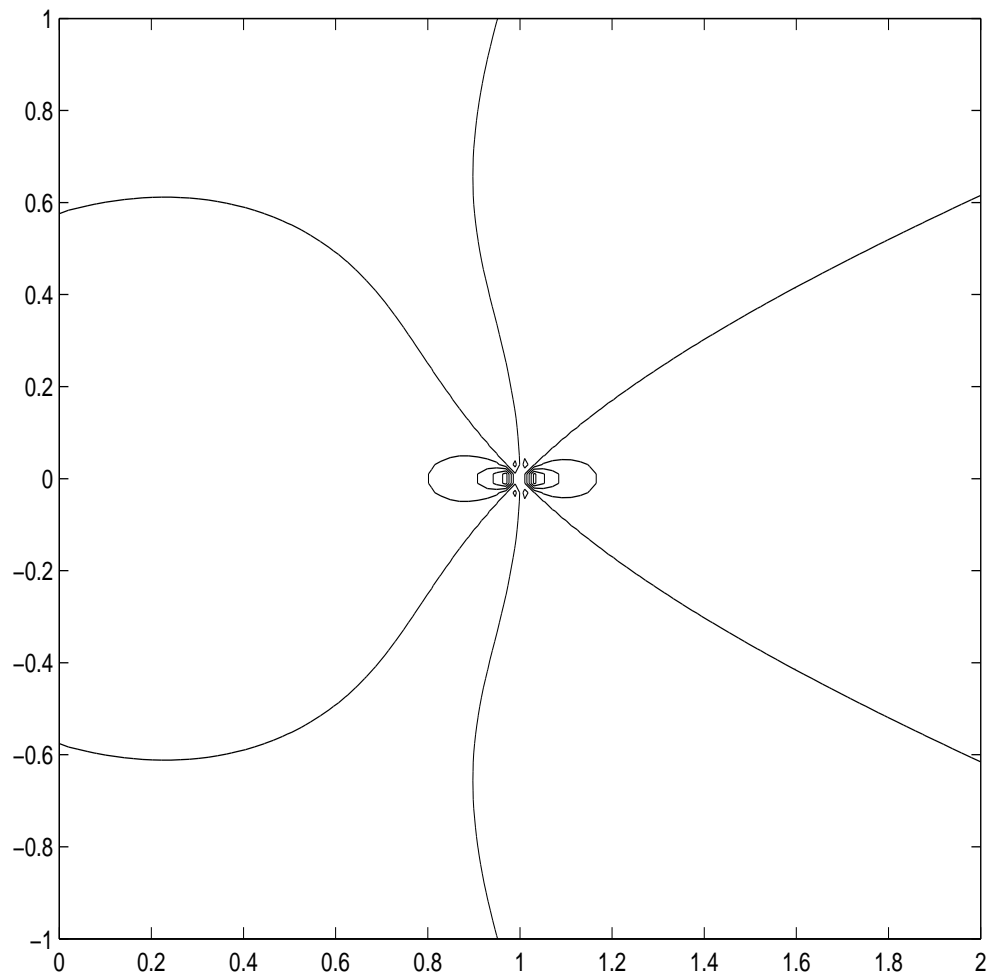


Figure 4: The shear stress around a dislocation with a burgers vector in the horizontal direction.

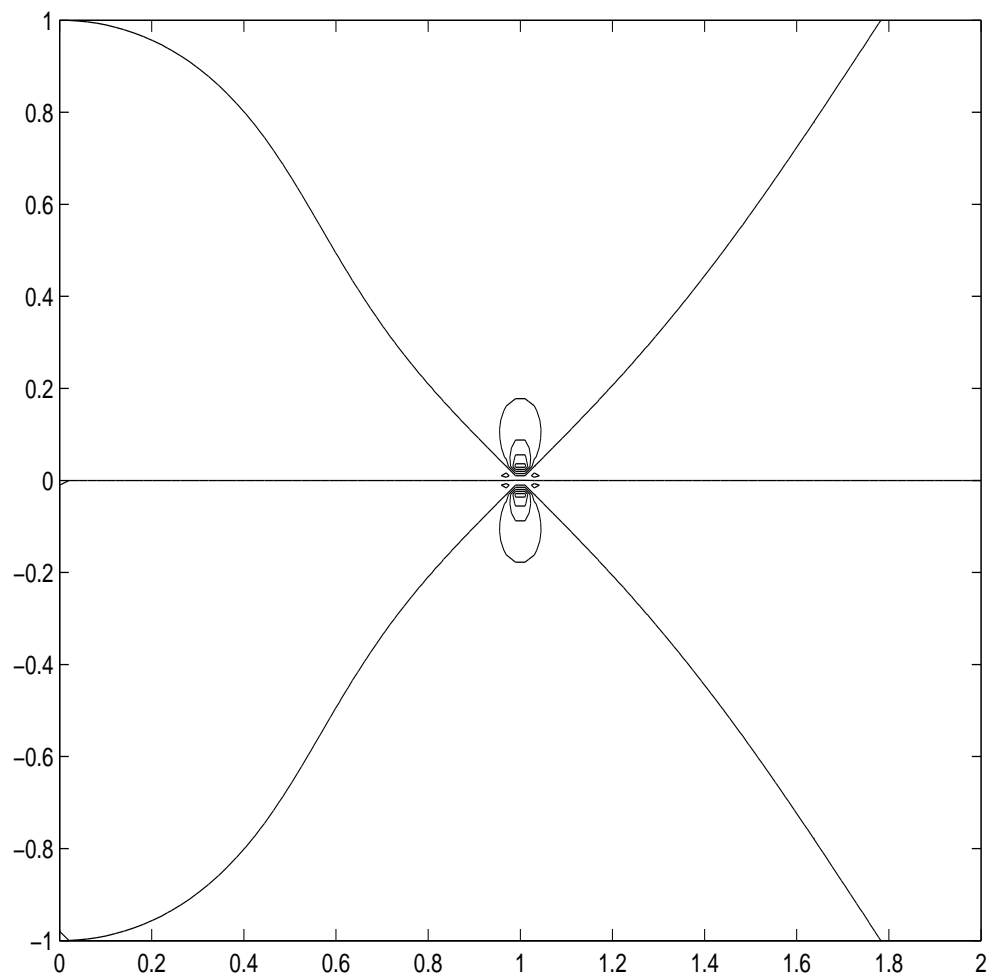


Figure 5: The shear stress around a dislocation with a burgers vector in the vertical direction. Note specifically that the shear stress is zero on the horizontal axis.

1.3.2 A summary of available techniques for crack problems and something about the governing boundary value problem

Below is a summary of available techniques for solving crack problems. The aim of the summary is to clarify which technique we prefer to use for solving our specific problem. The different techniques will be explained with reference to a time independent two dimensional (plain strain) problem. Since the length scales involved in this problem are small, we may, without restricting the physical relevance, model the component by the (right) half plane Ω_h and the grain by a simply connected and bounded subset Ω_g of Ω_h , with piecewise smooth boundary. The boundaries of these sets will be denoted by Γ_h and Γ_g respectively. (For the crack to initiate at a free boundary as specified in the problem formulation, we must have that $\Gamma_g \cap \Gamma_h \neq \emptyset$.) To write down a boundary value problem for this crack problem, we need to define the concept of a crack. In the applications considered in this study, the separation between the crack faces is always vanishingly small in comparison with the size of the domain, so that the domain with the crack is of *the same shape* as the domain without the crack. The crack locus can thus be represented by a contour Γ_c that is a subset of Ω_g . Even though we have assumed that the separation between the crack faces is vanishingly small, we must allow the values of the displacements, stresses and strains at every point along Γ_c to differ between the crack planes. Thus the displacements, stresses and strains are not single-valued along Γ_c . In general, the two values of the displacements will differ along some points along Γ_c , since if they are equal along the whole length of the crack then the crack is fully closed, which is generally not the case in applications such as ours. For this reason we understand that if the crack is open, then the displacement field must vary rapidly at the crack tip to satisfy the condition of continuity that is enforced in the non-cracked material. Indeed, infinite displacement gradients appear, and one of the major tasks when deriving techniques for crack problems is to accomodate the methods to this behaviour. Furthermore, the assumption we have made about the separation between the crack faces being vanishingly small can now be interpreted as one of the basic assumptions made in all linear elastic fracture mechanics applications, since the separation between the crack faces is determined by the displacements along the faces, and these must be small for the linear elastic fracture mechanics theories to be valid.

For the time being we assume that there is only one simply connected crack contour Γ_c , and that Γ_c is a subset of the horizontal axis. (According to

the problem formulation, Γ_c is in the interior of Ω_g , and one endpoint of Γ_c coincides with a point on $\Gamma_g \cap \Gamma_h$.) Even though the crack is considered to be a single contour, the analysis carried out in the derivations of many of the techniques explained below is much simplified if one considers the boundary value problem in which the upper and lower crack faces Γ_+ and Γ_- are separated by a strictly positive distance δ and joined at the crack tip by a parabola. Taking this approach, the boundary value problem with our definition of the crack can be obtained by setting $\delta = 0$. To define the domain in this auxiliary boundary value problem some adjustment of the geometry is required. These adjustments will not affect our discussion of the different techniques. See for example [8], [22] or [21] for a somewhat more thorough analysis.

We now introduce some notation. From now on, all vectors are treated as column vectors.

$f : \Omega_h \rightarrow \mathbb{R}^2$	a body force per unit thickness
$\sigma : \Omega_h \rightarrow \mathbb{R}^{2 \times 2}$	a symmetric stress tensor
$\varepsilon : \Omega_h \rightarrow \mathbb{R}^{2 \times 2}$	a symmetric strain tensor
$t : \Gamma_g \setminus \Gamma_h \rightarrow \mathbb{R}^2$	a boundary traction vector
$p^+ : \Gamma_+ \rightarrow \mathbb{R}^2$	a pressure on the upper crack face
$p^- : \Gamma_- \rightarrow \mathbb{R}^2$	a pressure on the lower crack face
K_I, K_{II}	global stress intensity factors
$n : \Gamma_g \cup \Gamma_h \cup \Gamma_+ \cup \Gamma_- \rightarrow \mathbb{R}^2$	outward unit normal to the domains

Figure 6 shows a schematic picture of the above quantities and the grain.

There are (at least) two possible ways of defining the boundary value problem that governs the stress state in Ω_g as the boundaries Γ_+ and Γ_- are incorporated. Since we are interested in the stresses appearing in Ω_g , the naive approach is to prescribe some conditions on the stress along the boundaries, and enforce the stress field to satisfy the equations of equilibrium in Ω_g , resulting in the boundary value problem:

Given f , t , p^+ and p^- , find σ such that

$$\left\{ \begin{array}{ll} -\nabla \cdot \sigma - f = 0 & \text{in } \Omega_g \\ \sigma \cdot n = t & \text{on } \Gamma_g \setminus \Gamma_h \\ \sigma \cdot n = 0 & \text{on } \Gamma_g \cap \Gamma_h \\ \sigma \cdot n = -p^+ & \text{on } \Gamma_+ \\ \sigma \cdot n = -p^- & \text{on } \Gamma_- \end{array} \right. \quad (1)$$

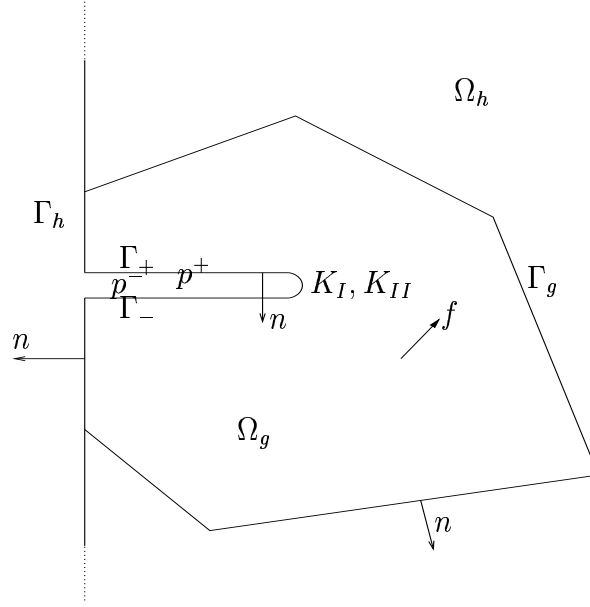


Figure 6:

The second condition in (1) simply means that the free boundary is traction free. In this version of the boundary value problem we control the tractions along the grain boundary, which is not always relevant. It is more convenient to apply a load at the 'ends' of the component. We choose to do so by symmetrically applying to the northern and southern remote boundaries a tensile load σ^∞ . A new version of the boundary value problem is

Given f , p^+ and p^- , find σ such that

$$\left\{ \begin{array}{ll} -\nabla \cdot \sigma - f = 0 & \text{in } \Omega_h \\ \sigma \cdot n = 0 & \text{on } \Gamma_h \\ \sigma \cdot n = -p^+ & \text{on } \Gamma_+ \\ \sigma \cdot n = -p^- & \text{on } \Gamma_- \\ \lim_{|x| \rightarrow \infty} \sigma(x) = \begin{bmatrix} 0 & 0 \\ 0 & \sigma^\infty \end{bmatrix} & \end{array} \right. \quad (2)$$

where the last boundary condition means that the components of σ should tend to the corresponding components of $\begin{bmatrix} 0 & 0 \\ 0 & \sigma^\infty \end{bmatrix}$ as x tends to infinity in any direction in Ω_h .

The usual way to obtain variational formulations of (1) and (2) is to pose the problems for the displacements and introduce a displacement condition along some part of the body to ensure well-posedness. Let us characterize the displacements in Ω_g and Ω_h by the vector-valued functions $u_g : \Omega_g \rightarrow \mathbb{R}^2$ and $u_h : \Omega_h \rightarrow \mathbb{R}^2$, and indicate that the stress and strain in Ω_g is induced by the displacements u by explicitly writing the u -dependence after the respective tensors, such as this: $\varepsilon(u), \sigma(u)$. We introduce also the virtual displacements (or 'test displacements') $u_g^* : \Omega_g \rightarrow \mathbb{R}^2$ and $u_h^* : \Omega_h \rightarrow \mathbb{R}^2$. By performing a scalar multiplication of (1) and (2) with u_g^* and u_h^* respectively, and using the divergence theorem we obtain the desired variational formulations:

Given f, t, p^+ and p^- , find $u_g \in V_g$ such that for all $u_g^* \in S_g$

$$\int_{\Omega_g} \sigma(u_g) : \varepsilon(u_g^*) = \int_{\Gamma_g \setminus \Gamma_h} t \cdot u_g^* - \int_{\Gamma_+} p^+ \cdot u_g^* - \int_{\Gamma_-} p^- \cdot u_g^* + \int_{\Omega_g} f \cdot u_g^* \quad (3)$$

and

Given f, p^+ and p^- , find $u_h \in V_h$ such that for all $u_h^* \in S_h$

$$\int_{\Omega_h} \sigma(u_h) : \varepsilon(u_h^*) = - \int_{\Gamma_+} p^+ \cdot u_h^* - \int_{\Gamma_-} p^- \cdot u_h^* + \int_{\Omega_h} f \cdot u_h^*, \quad (4)$$

where V_g, V_h, S_g and S_h are the appropriate trial and test spaces. These trial spaces should incorporate the essential conditions on the displacements. Furthermore, by a slight misuse of the word 'space', one can think of all methods we describe in this section as being derived from the variational formulations by using different test spaces. A very special test space for the problem (4) worth extra attention is the set S_h^* containing only the solutions $u_h^* : \Omega_h \rightarrow \mathbb{R}^2$ of the problems

$$\begin{cases} -\nabla \cdot \sigma(u_h^*) - f_h^* = 0 & \text{in } \Omega_h \\ \sigma(u_h^*) \cdot n = t_h^* & \text{on } \Gamma_h \cup \Gamma_+ \cup \Gamma_- \end{cases} \quad (5)$$

for different choices of virtual forces $f_h^* : \Omega_h \rightarrow \mathbb{R}^2$ and tractions $t_h^* : \Gamma_h \cup \Gamma_c \rightarrow \mathbb{R}^2$. For the problem (3) we can create the corresponding test space S_g^* as the solutions of the problem

$$\begin{cases} -\nabla \cdot \sigma(u_g^*) - f_g^* = 0 & \text{in } \Omega_g \\ \sigma(u_g^*) \cdot n = t_g^* & \text{on } \Gamma_g \cup \Gamma_+ \cup \Gamma_- \end{cases} \quad (6)$$

By using a symmetry in the stress-strain relationship (see [23] or [21]), we obtain Betti's reciprocal work theorem:

For any f, t, p^+, p^-, f_g^* and t_g^* and corresponding u_g and u_g^* satisfying (3) and (6) respectively, we have that

$$\int_{\Gamma_g \cup \Gamma_+ \cup \Gamma_-} t_g^* \cdot u_g + \int_{\Omega_g} f_g^* \cdot u_g = \int_{\Gamma_g} t \cdot u_g^* - \int_{\Gamma_+} p^+ \cdot u_g^* - \int_{\Gamma_-} p^- \cdot u_g^* + \int_{\Omega_g} f \cdot u_g^* \quad (7)$$

and for the entire half plane this theorem can be stated as

For any f, p^+, p^-, f_h^* and t_h^* and corresponding u_h and u_h^* satisfying (4) and (5) respectively, we have that

$$\int_{\Gamma_h \cup \Gamma_+ \cup \Gamma_-} t_h^* \cdot u_h + \int_{\Omega_h} f_h^* \cdot u_h = - \int_{\Gamma_+} p^+ \cdot u_h^* - \int_{\Gamma_-} p^- \cdot u_h^* + \int_{\Omega_h} f \cdot u_h^* \quad (8)$$

If we know the solution σ to eq. (1) (or (2)) explicitly, then of course we also know K_I and K_{II} since these can be deduced from the behaviour of σ near the crack tip. Aspects of the numerical computation of these stress intensity factors are left for section 1.3.3 and Chapter 3. Now let us summarize a few important techniques for solving crack problems.

Superposition

Most of the available techniques for determining stress fields utilize superposition in some form. Worth mentioning is the kind of superposition made possible by *Bueckners principle*, which is nicely explained in [6]. It is also concisely stated in [7]:

'The stress intensity factor for a crack in a body subjected to external forces is identical to that for a similar crack, subjected to internal pressure in a similar body which has no external forces acting on it. The internal pressure ... acting in the crack is equal to the stress that would exist normal to the crack-line along the crack-site in the uncracked body subjected to the external forces.'

It is important to note that Bueckners principle is valid not only when the body is subjected to external forces solely (i.e. forces applied at the edges of the component), but also includes cases when a mixture of external *and* internal forces (i.e forces that act at interior points of Ω_g) are present, as is explained in [9].

FEM

A finite element formulation of our crack problem can be obtained by setting $\delta = 0$ (the distance between the crack faces) in (3) or (4), and choosing trial- and test-spaces as the appropriate FE-spaces. These spaces should accommodate to the displacement discontinuity that inevitably appears along Γ_c , and special crack tip elements must be employed to capture the behaviour of the unknown at the crack tip.

Remember now that our overall problem also involves placing dislocations at interior points of Ω_g . As was stated in section 1.3.1, a dislocation is a point source of stress, i.e. a force. As we place a dislocation in Ω_g , it is also necessary to have knowledge of how this effects the stress field in Ω_g . Expressions for the influence on the stress field in isotropic material due to an arbitrarily placed dislocation with arbitrary burgers vector have been derived for a few simple geometrical configurations (for a summary, see [9]). These configurations include geometries such as interfacing half planes of elastically dissimilar material, quarter-planes, and other infinite media containing simply shaped inclusions. These expressions all have in common that they have been derived under the assumption that the domain does not contain a crack. Thus no such expression for the influence of a dislocation in our cracked component is available. One can obtain such an expression by solving (1) or (2) with a force term representing the dislocation. This does not avoid the necessity of obtaining a new such dislocation solution every time we consider a new crack, which is cumbersome. As long as we cannot overcome this problem, the FEM is of no use to us.

Collocation and Galerkin Boundary Element Method with Kelvin fundamental solution

To derive a boundary element formulation for our crack problem we consider the 'test spaces' S_g^* and S_h^* that were introduced earlier, and choose the virtual forces f_g^* and f_h^* as each of the functions $\delta_{\bar{x}}e_i$, $i = 1, 2$, where $\delta_{\bar{x}}$ is the dirac delta function with source point at \bar{x} and e_i is the i :th standard base vector in \mathbb{R}^2 . The formulations (6) and (5) compels us to also specify tractions along the boundaries. A popular approach is to define these tractions as the tractions appearing along Γ_g and Γ_h when the forces $\delta_{\bar{x}}e_i$, $i = 1, 2$ are applied in the entire plane. Let us write these tractions and the corresponding fundamental solutions in matrix form by denoting by $T_{ij}(\bar{x})$ and $U_{ij}(\bar{x})$ the traction and displacement in the j :th direction as a point load is applied

in the $i : th$ direction at \bar{x} . It can be understood from the context which domain the fundamental solution refers to, which is why the subscripts g and h are dropped. By using the fundamental solutions in Bettis reciprocal theorem (78), we obtain Somigliana's identity for the displacements at the interior point \bar{x} :

$$u_g(\bar{x}) = -\int_{\Gamma_g \cup \Gamma_+ \cup \Gamma_-} T_{ij}(\bar{x})u_g + \int_{\Gamma_g} U_{ij}(\bar{x})t - \int_{\Gamma_+} U_{ij}(\bar{x})p^+ - \int_{\Gamma_-} U_{ij}(\bar{x})p^- + \int_{\Omega_g} U_{ij}(\bar{x})f \quad (9)$$

$$u_h(\bar{x}) = -\int_{\Gamma_h \cup \Gamma_+ \cup \Gamma_-} T_{ij}(\bar{x})u_h - \int_{\Gamma_+} U_{ij}(\bar{x})p^+ - \int_{\Gamma_-} U_{ij}(\bar{x})p^- + \int_{\Omega_h} U_{ij}(\bar{x})f \quad (10)$$

Since we have not specified any essential boundary conditions neither in (5) nor in (6), it follows that the 'test spaces' S_g^* and S_h^* will contain infinitely many solutions that differ from each other by a constant. It follows from the divergence theorem that every such solution gives rise to the same equation, which is why it is sufficient to consider only two solutions (one for each force term). This one solution can for example be the one that tends to zero at infinity, which is the solution commonly referred to as the Kelvin fundamental solution.

We can obtain a boundary integral equation for the displacements by placing the source point \bar{x} on the boundary of the domain. The derivation of this equation invokes a limiting process which can be found in [21]. For the problem formulated with the grain as domain and with equal pressures acting on both crack faces, the equation is

$$\frac{1}{2}u_g(\bar{x}) = -CPV \int_{\Gamma_g \cup \Gamma_+ \cup \Gamma_-} T_{ij}(\bar{x})u_g + \int_{\Gamma_g} U_{ij}(\bar{x})t + \int_{\Omega_g} U_{ij}(\bar{x})f, \quad (11)$$

where the first integral on the right hand side must be treated as a Cauchy principal value integral. A boundary element formulation of our crack problem can now be derived by making an ansatz for the unknown and inserting it into (11). An advantage of BEM is that since (11) involves the values of the unknown along the boundary only, to obtain an approximate solution in the entire domain, we need only discretize the boundary and estimate the unknown dependent variable only on the resulting one-dimensional curve. This reduces the complexity of the problem in comparison with for example the FEM, that requires a two-dimensional mesh. One should keep in mind though, that the evaluation of the unknown at an interior point requires the

evaluation of the integrals in Somigliana's identity. Carrying on, we set $\delta = 0$, choose a set of collocation points along $\Gamma_g \cup \Gamma_+ \cup \Gamma_-$, and assemble a linear system of equations. This is where we run into problems since a collocation point at one crack face now coincides with another point on the other crack face. Every equation that a collocation gives rise to therefore involves two unknowns; the displacements on each side of the crack. Because each distinct collocation point along the crack produces an equation involving two new unknown values, the resulting linear system has no unique solution. Collocating at the same point on both crack faces introduces only one pair of unknown values, but it also gives rise to only one linear independent equation. Hence, this BEM-formulation is of no use to us.

One way to evade the mentioned difficulties is to decompose the domain in such a way that no subdomain contains the crack as an inner boundary (but rather as a pressurized outer boundary), and then enforce continuity of displacements (but not necessarily tractions) along the part of the boundary where the subdomains are connected to each other. If this multizone approach is taken, and special crack tip elements are used, it is possible to solve crack problems. If one wishes to model crack *propagation*, meaning that one needs to solve several crack problems with slightly different crack geometries, the multizone BEM implies that remeshing is needed every time the crack increments. This remeshing might be restricted to a few elements near the tip if the crack grows straight forward, but if we include the possibility of kinked cracks, we might have to make a new decomposition of the domain at every iteration. Hence, the multizone approach is not very well suited for our needs.

It should also be mentioned that one might very well make a Galerkin formulation of the boundary equations. This would require another integration which is cumbersome and time-consuming. What is more, in the Galerkin approach, one requires the residual of the integral equation to be orthogonal to a suitable test space. This orthogonality is defined via the L^2 scalar product, i.e. a weighted integral of the unknown where the weight is a test function. These integrals are often evaluated using a numerical quadrature which approximates the value of the integral by a weighted sum of the values of the integrand at a finite set of points. In this case, it turns out that Galerkin can be thought of as a weighted point collocation. On the other hand, point collocation is nothing but Galerkin when using delta functions as weights in the mentioned integrals. Thus, both approaches are related, which motivates that we in the following restrict ourselves to point collocation.

Collocation Displacement Discontinuity Method with Kelvin fundamental solution

Let us return to equations (9) and (10). By differentiating and using Hookes law we obtain Somiglianas identity for the stresses at the interior point \bar{x} . Since we are allowed to differentiate under the integral sign, these identities can be expressed in a similar fashion as (9) and (10) but with modified kernels. For the grain we have

$$\begin{aligned} \sigma(u_g(\bar{x})) = & - \int_{\Gamma_g \cup \Gamma_+ \cup \Gamma_-} S(\bar{x}) u_g + \int_{\Gamma_g} D(\bar{x}) t \\ & - \int_{\Gamma_+} D(\bar{x}) p^+ - \int_{\Gamma_-} D(\bar{x}) p^- + \int_{\Omega_g} D(\bar{x}) f \end{aligned} \quad (12)$$

and by incorporating the traction boundary condition along the free edge of the half plane, we get

$$\begin{aligned} \sigma(u_h(\bar{x})) = & - \int_{\Gamma_h \cup \Gamma_+ \cup \Gamma_-} S(\bar{x}) u_h \\ & - \int_{\Gamma_+} D(\bar{x}) p^+ - \int_{\Gamma_-} D(\bar{x}) p^- + \int_{\Omega_h} D(\bar{x}) f, \end{aligned} \quad (13)$$

where the scalar products with the kernels $S = \{S_{kij}\}$ and $D = \{D_{kij}\}$ are now taken with respect to the first index. We can obtain a boundary integral equation for the stresses by placing the source point \bar{x} on the boundary of the domain (see [21]). This equation is

$$\begin{aligned} \frac{1}{2} \sigma(u_g(\bar{x})) = & -HPV \int_{\Gamma_g \cup \Gamma_+ \cup \Gamma_-} S(\bar{x}) u_g \\ & + CPV \int_{\Gamma_g} D(\bar{x}) t - CPV \int_{\Gamma_+} D(\bar{x}) p^+ - CPV \int_{\Gamma_-} D(\bar{x}) p^- \\ & + \int_{\Omega_g} D(\bar{x}) f \end{aligned} \quad (14)$$

for the grain, and for the half plane it is

$$\begin{aligned} \frac{1}{2} \sigma(u_h(\bar{x})) = & -HPV \int_{\Gamma_h \cup \Gamma_+ \cup \Gamma_-} S(\bar{x}) u_h \\ & - CPV \int_{\Gamma_+} D(\bar{x}) p^+ - CPV \int_{\Gamma_-} D(\bar{x}) p^- \\ & + \int_{\Omega_h} D(\bar{x}) f, \end{aligned} \quad (15)$$

where the first integrals on the right hand sides are now interpreted in the Hadamard principal value sense (see [21]). Let us multiply (15) by the outward normal to obtain

$$\begin{aligned}
\frac{1}{2}\sigma(u_h(\bar{x})) \cdot n(\bar{x}) &= -HPV \int_{\Gamma_h \cup \Gamma_+ \cup \Gamma_-} n(\bar{x}) \cdot S(\bar{x}) u_h \\
&\quad -CPV \int_{\Gamma_+} n(\bar{x}) \cdot D(\bar{x}) p^+ - CPV \int_{\Gamma_-} n(\bar{x}) \cdot D(\bar{x}) p^- \\
&\quad + \int_{\Omega_h} n(\bar{x}) \cdot D(\bar{x}) f,
\end{aligned} \tag{16}$$

where the scalar products between the normal and the kernels are taken with respect to the third index. As we set $\delta = 0$, every point x^+ on the upper crack face coincides with a point x^- on the lower crack face. Thus, in the case $f \equiv 0$ we have (see [21] again) for such points that

$$\begin{aligned}
\frac{1}{2}\sigma(u_h^+(x^+)) \cdot n(x^+) + \frac{1}{2}\sigma(u_h^-(x^-)) \cdot n(x^-) &= \\
-HPV \int_{\Gamma_h} n(x^+) S(x^+) u_h - HPV \int_{\Gamma_c} n(x^+) S(x^+) u_h^+ + HPV \int_{\Gamma_c} n(x^-) S(x^-) u_h^- \\
-CPV \int_{\Gamma_c} n(x^+) \cdot D(x^+) p^+ - CPV \int_{\Gamma_c} n(x^-) \cdot D(x^-) p^-
\end{aligned} \tag{17}$$

where u_h^+ and u_h^- now refer to the displacements on the upper and lower crack faces respectively. The two *HPV*-integrals along the crack line have different signs because the integration paths have different orientations (according to the divergence theorem). Note that since $n(x^+) = -n(x^-)$ and (consequently) $S(x^+) = -S(x^-)$, it does not matter whether we use $n(x^+)S(x^+)$ or $n(x^-)S(x^-)$ in the above integrals. In the *CPV*-integrals the super index on the source point does matter though, since now $D(x^+) = D(x^-)$ because the fundamental solution is single-valued. Using these relationships we get

$$\begin{aligned}
\frac{1}{2}\sigma(u_h^+(x^+)) \cdot n(x^+) + \frac{1}{2}\sigma(u_h^-(x^-)) \cdot n(x^-) &= \\
-HPV \int_{\Gamma_h} n(x^+) S(x^+) u_h - HPV \int_{\Gamma_c} n(x^+) S(x^+) u_h^+ + HPV \int_{\Gamma_c} n(x^+) S(x^+) u_h^- \\
-CPV \int_{\Gamma_c} n(x^+) \cdot D(x^+) (p^+ - p)
\end{aligned} \tag{18}$$

We may incorporate the traction boundary conditions of (2) and substitute Δu_h for $u_h^+ - u_h^-$ on the crack line to obtain

$$\begin{aligned}
\frac{1}{2}(p^+(x^+) + p^-(x^+)) &= \\
-HPV \int_{\Gamma_h} n(x^+) S(x^+) u_h - HPV \int_{\Gamma_c} n(x^+) S(x^+) \Delta u_h \\
-CPV \int_{\Gamma_c} n(x^+) \cdot D(x^+) (p^+ - p), x \in \Gamma_c \\
0 &= \\
-HPV \int_{\Gamma_h} n(x^+) S(x^+) u_h - HPV \int_{\Gamma_c} n(x^+) S(x^+) \Delta u_h \\
-CPV \int_{\Gamma_c} n(x^+) \cdot D(x^+) (p^+ - p), x \in \Gamma_h
\end{aligned} \tag{19}$$

We can obtain an approximate solution of the above equation for the *displacement discontinuity* Δu_h along the crack line and the displacements along the other parts of the boundary by first making an ansatz for Δu_h along Γ_c and an ansatz for u_h along Γ_h , inserting it into (15) and choosing a set of collocation points on the boundary $\Gamma_h \cup \Gamma_+ \cup \Gamma_-$. The only unknown along the crack line is hence the crack opening displacement (COD). Furthermore, if the crack faces are equally pressurized ($p^+ = p^-$), the displacement discontinuity equation is simplified to

$$\begin{aligned} p^+(x) &= -HPV \int_{\Gamma_h} n(x)S(x)u_h - HPV \int_{\Gamma_c} n(x)S(x)\Delta u_h, x \in \Gamma_c \\ 0 &= -HPV \int_{\Gamma_h} n(x)S(x)u_h - HPV \int_{\Gamma_c} n(x)S(x)\Delta u_h, x \in \Gamma_h \end{aligned} \quad (20)$$

A similar equation can be derived for the problem for the grain. Still, even if we use a non-trivial body force, we cannot incorporate free dislocations into this formulation, since this BEM-formulation does not avoid the necessity of obtaining a new dislocation solution every time the crack increments.

Collocation Displacement Discontinuity Method with infinitesimal Dislocation Dipole fundamental solution (The distributed dipoles technique)

We are not confined to using the Kelvin fundamental solution in the derivation of BEM-formulations. Let us put some more effort into finding a good fundamental solution that takes into account the characteristics of our specific problem. The Kelvin solution was obtained as the limit as $\delta \rightarrow 0$ of the solution of the problem (5) with a special choice of virtual forces and tractions. Let us instead at the outset set $\delta = 0$ in (5), so that the fundamental problem is a crack problem. Let us also substitute the traction condition along the crack line by an essential boundary condition in the form of a specified displacement discontinuity along Γ_c . If we choose $f_h^* \equiv 0$, and the essential condition to be an infinite point displacement discontinuity at the point \bar{x} , we obtain the following fundamental problem:

$$\begin{cases} -\nabla \cdot \sigma(u_h^*) = 0 & \text{in } \Omega_h \\ \sigma(u_h^*) \cdot n = 0 & \text{on } \Gamma_h \\ \Delta u_h^* = \delta_{\bar{x}} e_i \end{cases} \quad (21)$$

Using the solution of this fundamental problem, Betti's theorem (8) turns into

$$\int_{\Gamma_+ \cup \Gamma_-} t_h^* \cdot u_h = - \int_{\Gamma_+} p^+ \cdot u_h^* - \int_{\Gamma_-} p^- \cdot u_h^* + \int_{\Omega_h} f \cdot u_h^* \quad (22)$$

which in the case $f_h \equiv 0$ is the same as

$$\int_{\Gamma_+} t_h^* \cdot u_h + \int_{\Gamma_-} t_h^* \cdot u_h = - \int_{\Gamma_+} p^+ \cdot u_h^* - \int_{\Gamma_-} p^- \cdot u_h^* \quad (23)$$

which in the case $p^+ = p^- = p$ because of the different orientations of the now coinciding crack faces is the same as

$$\int_{\Gamma_c} t_h^* \cdot u_h - \int_{\Gamma_c} t_h^* \cdot u_h = - \int_{\Gamma_c} p \cdot u_h^* + \int_{\Gamma_c} p \cdot u_h^* \quad (24)$$

which is easily seen to be equivalent to

$$\int_{\Gamma_c} t_h^* \cdot \Delta u_h = - \int_{\Gamma_c} p \cdot \Delta u_h^* \quad (25)$$

which according to the fundamental problem is the same as

$$\int_{\Gamma_c} t_h^* \cdot \Delta u_h = -p(\bar{x}) \quad (26)$$

Since the COD is zero along the crack except at \bar{x} , t_h^* are the tractions appearing along the crack line in the uncracked body. It turns out that the kernel t_h^* of equation (26) is strongly singular at \bar{x} , and the integral must be treated in the *HPV* sense.

If we solve (21), we can obtain a BEM-formulation of equation (26) by making an ansatz for the unknown Δu_h along Γ_c and collocating at a nice set of points along Γ_c . This way we have reduced the domain of the integral equation from the whole of the boundary to the crack alone. If we were to derive the same kind of equation for the problem posed in the grain, the domain of the integral equation would also include the grain boundaries, unless the traction free grain boundaries condition is incorporated in the fundamental problem. Let us for now focus on the equation (26). For this equation to be relevant we must find the fundamental solution, or more specifically, the tractions normal to the crack line given rise to by the fundamental solution. This can be done by considering an infinitely short but infinitely strong dislocation dipole situated at \bar{x} and oriented parallel or perpendicular to the crack line depending on whether $i = 2$ or $i = 1$ in (21). By the discussion in section 1.3.1 we understand that since a dipole is a piece of material of size $\|b\| \times l$, where l and b are the length and the strength of the dipole, the infinitely short and infinitely strong dipole is exactly the displacement discontinuity $\delta_{\bar{x}} e_i$! Since there is an explicit formula for the influence of such a dipole in a half plane (derived from the expression for a dislocation in a half plane), the main work has already been done. We now see that posing the

boundary value problem in the entire half plane instead of in the grain has the advantage that the fundamental solution (or *Green's function*) is already available, whilst if we include boundary conditions along Γ_g , we must derive a new fundamental solution every time we consider a new grain, which might not even be possible. Though, as previously mentioned, we could use the Green's function for the half plane when solving for the grain, but since the virtual tractions along Γ_g are not zero, the integral equation (22) would then include the unknown displacements along Γ_g , and thus we would not have managed to reduce the domain of the unknown to the crack alone.

Even though the equation (26) is very pretty, we have not yet found a way to incorporate the free dislocations into the BEM-formulation since the crack is still in the domain, ruining every chance of finding an exact expression for their influence on the stress field. However, by the use of Bueckners superposition principle, we can divide (2) (or (1)) into two simpler problems, in one of which the dislocations may be incorporated. Indeed, it should be clear that the left-hand side of (26) expresses the traction normal to Γ_c at \bar{x} induced by the distribution of infinitesimal dislocation dipoles with density $\Delta u_h : \Gamma_c \rightarrow \mathbb{R}^2$ ($\Delta u_h(x)$ is the strength of an infinitely short dipole at x , and the kernel $t_h^*(x)$ of (26) is the influence at \bar{x} of an infinitely short but infinitely strong dipole situated at x). Thus, finding the solution of (26) corresponds to inserting infinitely short dipoles, that is, pieces of material, into the crack. This insertion of additional material creates the internal pressure that is discussed in Bueckners principle. In mathematical terms, the use of Bueckners principle means that we can divide (2) (with traction free crack faces) into two subproblems;

Subproblem A. Find the stress induced in Ω_h by the far field loading and internal sources of stress (such as dislocations) in the *absence of the crack*. That is,

Find σ^A such that

$$\begin{cases} -\nabla \cdot \sigma^A - f = 0 & \text{in } \Omega_h \\ \sigma^A n = 0 & \text{on } \Gamma_h \\ \lim_{|x| \rightarrow \infty} \sigma^A(x) = T_\infty \end{cases} \quad (27)$$

where $T_\infty = \begin{bmatrix} 0 & 0 \\ 0 & \sigma^\infty \end{bmatrix}$

Subproblem B. Find the stress $\sigma^{\hat{B}}$ induced in Ω_h by the dipole density \hat{B} along Γ_c where \hat{B} is such that it leaves the crack traction free when superposed onto the stress field obtained in subproblem A. That is,

Find $\sigma^{\hat{B}}$ such that

$$\int_{\Gamma_c} t_h^* \cdot \hat{B} = -\sigma^A(\bar{x}) \cdot n, \bar{x} \in \Gamma_c \quad (28)$$

The stress field σ that solves (2) can now be obtained as $\sigma^A + \sigma^{\hat{B}}$. Since there is no stress concentration in subproblem A, the stress intensity factors for the overall problem are by ordinary superposition the same as for subproblem B.

Subproblem A above is easy to solve since the solution σ^A is obtained by superposing onto T_∞ the stress fields of the free dislocations, for which we have an expression. Once we have found σ^A , the dislocation density \hat{B} in subproblem B can be obtained as the solution of a singular integral equation of the first kind. The BEM-formulation of the equation (28) must employ special crack tip elements to take into account the square root behaviour of \hat{B} close to the crack tip. As we have obtained a BE-approximation of \hat{B} , we must also find $\sigma^{\hat{B}}$. This is done by inserting \hat{B} into an expression similar to the one on the left-hand side of (28), with the difference that we are now not only interested in two of the stress components but all three, and the source point \bar{x} can be located anywhere in Ω_h . This does not actually require much more work than we have already done, because the appropriate kernel can easily be derived from known expressions in much the same way as for t_h^* .

Bueckners superposition principle may seem a bit mystical at first sight, since the overall solution can be solved by the superposition of two solutions which are posed in different domains (one containing a crack, and the other uncracked), but by considering dislocation dipoles, we understand that both domains are actually the same uncracked body. Indeed, if the crack is considered as an inner contour along which the normal tractions are required to vanish, we can without altering the shape of the body let dislocation dipoles be distributed along the crack contour in such a fashion that the tractions induced along the crack by this distribution cancels those given rise to by the far field loading, thus leaving the crack traction free. The shape of the body is not considered to be altered by the insertion of the dipoles, because the displacements due to a dipole are infinitesimal in comparison with the

domain, and hence we can utilize ordinary superposition to add together the solutions obtained by considering the uncracked externally loaded body and the externally unloaded but internally loaded body separately.

When it comes to choosing a technique for this problem, the use of the Bueckner superposition in the distributed dipoles technique proves to be of crucial importance, since it is possible to include internal point sources of stress, i.e. dislocations, into the f -term in subproblem A. The domain in subproblem A does *not* contain a crack, and hence the expression for a dislocation in a half plane is valid.

It is common in dislocation modelling to consider the problem as to consist in placing a finite number of *finite* length and varying strength dipoles along the crack line in such a fashion that the crack faces are traction free at a set of selected points (often the midpoints of each dipole element). The primary unknowns are hence the different strengths of these dipoles, i.e. the sizes of the burgers vectors of the dislocations constituting the dipoles. With this approach, the discretization is so to speak performed in the modelling, and not once the governing equations are already posed. The same formulation of the problem can though be obtained by using piecewise constant elements in the BEM-formulation of the distributed infinitesimal dipoles technique.

The distributed dipoles technique is commonly used in dislocation modelling, see for example [16],[13] and [17].

A partial integration of the equations of the Collocation Displacement Discontinuity Method with infinitesimal Dislocation Dipole fundamental solution (The distributed dislocations technique)

Let us perform a partial integration w.r.t. the first coordinate in the left-hand side of the equation in (28). This requires the differentiation of $\hat{B}(x, 0)$ (the second argument is zero because the crack is a subset of the horizontal axis). It is not difficult to realize that if the crack opening displacement $\hat{B}(\cdot, 0)$ has a jump discontinuity of size b at x , then there is a dislocation with a burgers vector of size b situated at x . Furthermore, if the derivative $D_1\hat{B}(x, 0)$ is $-B(a-x)$ at x , then the *dislocation density* at the distance $a-x$ from the crack tip is $-B(a-x)$. Let us therefore write $-B(a-\cdot) = D_1\hat{B}(\cdot, 0)$ so that $B(r)$ is the dislocation density at the distance r from the crack tip. This implies the relation $\int_0^{a-x} B(r)dr - \int_0^a B(r)dr = COD(x) - COD(0)$, and setting $x = a$ gives $-\int_0^a B(r)dr = -COD(0)$ so we have that the crack opening displacement can be expressed via the dislocation density according

to the formula

$$COD(x) = \int_0^{a-x} B(r)dr \quad (29)$$

Let us also write T_h^* for the integral of t_h^* . We have already mentioned that the dipole density is zero at the crack tip (because the crack opening displacement is zero at the crack tip), and it turns out that the integrated kernel T_h^* is zero at the crack mouth. Hence the boundary terms in the following partial integration vanish:

$$\begin{aligned} \int_{\Gamma_c} t_h^* \cdot \hat{B} &= [T_h^* \hat{B}]_0^a - \int_{\Gamma_c} T_h^* \cdot D_1 \hat{B} = \\ \int_{\Gamma_c} T_h^*(x) \cdot B(a-x)dx &= - \int_a^0 T_h^*(a-r) \cdot B(r)dr = \\ \int_0^a T_h^*(a-r) \cdot B(r)dr & \end{aligned} \quad (30)$$

Thus we have established that the expression $\int_0^a T_h^*(a-r) \cdot B(r)dr$ gives the tractions due to the dislocation density B along Γ_c . To examine the influence on the tractions made by a dislocation with burgers vector b situated at the distance R from the crack tip we simply insert $B = \delta_R b$ into the expression (30) to obtain

$$\int_0^a T_h^*(a-r) \cdot \delta_R(r)bdr = T_h^*(a-R) \cdot b \quad (31)$$

which is exactly the kind of expression for the influence of a dislocation of size b at the distance R from the crack tip derived by many other investigators using other methods. From this we may conclude that the kernel $T_h^*(a-R)$ is exactly the already available expression that gives the influence of a dislocation when multiplied by the burgers vector. We have thus obtained a boundary equation formulation of our boundary value problem that involves only known expressions except for the dislocation density along the crack. This formulation is a version of the distributed dipoles technique, so we may still utilize Bueckners superposition principle and incorporate dislocations in the interior of Ω_h .

Differentiating the dipole density makes it square root singular at the crack tip, so when making a BEM-formulation for the unknown dislocation density B in the distributed dislocations technique, one must make use of singular crack tip elements. On the other hand, the kernel is not as singular as in the distributed dipoles technique, and it is sufficient to treat the integrals in the *CPV*-sense. It should also be noted that the same equations that one gets when using piecewise constant elements in the distributed dislocations technique can be obtained from the distributed dislocations tech-

nique when using as the only shape function (for each density component) on each geometrical element the sum of two equal strength but opposite signs delta-functions, with the points of influence of these delta-functions being the extreme points of the geometrical element.

The distributed dislocations technique shows some generality concerning crack geometries. Both curved and kinked cracks can be modelled by distributing edge dislocations of infinitesimal burgers vectors along Γ_c in such a way that the dislocation density $B : \Gamma_c \rightarrow \mathbb{R}^2$ gives rise to a stress field that satisfies the traction conditions in (2) when superposed onto the field induced in Ω_h by the external and internal forces in the absence of the crack. What is more, a grain boundary is by definition nothing but a distribution of dislocations. If for some reason one has made up ones mind on solving the problem (1), one can indeed 'cut out' Ω_g from a larger set by distributing dislocations along both Γ_g and Γ_c , and then apply boundary conditions on Γ_g to obtain an integral equation with domain $\Gamma_g \cup \Gamma_c$ (see [17]).

1.3.3 Examples of numerical methods for singular integral equations

We have seen that the method we can use for our problem is the distributed dislocations technique together with some BEM-formulation of the resulting singular integral equations. In this section we explore the efficiency of two different formulations together with point collocation.

We examine the problem that was introduced in section 1.3.2, where the crack is of length a , and for now we ignore the grain boundaries. We set $\sigma^\infty \equiv 1$, and let μ and ν denote the modulus of rigidity and Poisson's ratio of the material of which the component (the half plane) is composed. To derive the equation for this problem, we shall, according to the discussion in section 1.3.2, commence by solving subproblem A. It is obvious that $\sigma^A \equiv T_\infty$. Next, we want to solve subproblem B, that is, we want to determine the dislocation density $B : \Gamma_c \rightarrow \mathbb{R}^2$ in such a way that the crack faces are traction free, a condition that can be written

$$\begin{aligned} (\sigma_{12}^A + \sigma_{12}^B)(\Gamma_c) &= \{0\} \\ (\sigma_{22}^A + \sigma_{22}^B)(\Gamma_c) &= \{0\}. \end{aligned} \tag{32}$$

We know ([9]) that a dislocation with burgers vector b located at a point (ξ, χ) will at a point $x = (x_1, x_2)$ induce the stress σ^b such that

$$\begin{aligned}
\sigma_{11}^b(x) &= \frac{C^{-1}}{\pi} b \cdot G^{11}(x; \xi, \chi) \\
\sigma_{12}^b(x) &= \frac{C^{-1}}{\pi} b \cdot G^{12}(x; \xi, \chi) \\
\sigma_{22}^b(x) &= \frac{C^{-1}}{\pi} b \cdot G^{22}(x; \xi, \chi),
\end{aligned} \tag{33}$$

where $C = \frac{\kappa+1}{2\mu}$ and $\kappa = 3 - 4\nu$ is Kolosov's constant for plane deformation. The 'influence functions' $\{G^{ij} = (G_1^{ij}, G_2^{ij})^T\}_{i,j=1}^2$ in (33) are given by the expressions

$$\begin{aligned}
G_1^{11}(x; \xi, \chi) &= (x_2 - \chi) \left[-\frac{1}{r_1^2} + \frac{1}{r_2^2} - \frac{2(x_1 - \xi)^2}{r_1^4} + \frac{2(x_1 + \xi)^2}{r_2^4} \right. \\
&\quad \left. - \frac{4\xi(x_1 + \xi)}{r_2^4} + \frac{4\xi^2}{r_2^4} + \frac{16\xi(x_1 + \xi)^3}{r_2^6} - \frac{16\xi^2(x_1 + \xi)^2}{r_2^6} \right] \\
G_2^{11}(x; \xi, \chi) &= -\frac{x_1 - \xi}{r_1^2} + \frac{x_1 + \xi}{r_2^2} - \frac{2\xi}{r_2^2} + \frac{2(x_1 - \xi)^3}{r_1^4} - \frac{2(x_1 + \xi)^3}{r_2^4} \\
&\quad - \frac{8\xi(x_1 + \xi)^2}{r_2^4} + \frac{12\xi^2(x_1 + \xi)}{r_2^4} + \frac{16\xi(x_1 + \xi)^4}{r_2^6} - \frac{16\xi^2(x_1 + \xi)^3}{r_2^6} \\
G_1^{12}(x; \xi, \chi) &= -\frac{x_1 - \xi}{r_1^2} + \frac{x_1 + \xi}{r_2^2} - \frac{2\xi}{r_2^2} + \frac{2(x_1 - \xi)^3}{r_1^4} - \frac{2(x_1 + \xi)^3}{r_2^4} \\
&\quad + \frac{16\xi(x_1 + \xi)^2}{r_2^4} - \frac{12\xi^2(x_1 + \xi)}{r_2^4} - \frac{16\xi(x_1 + \xi)^4}{r_2^6} + \frac{16\xi^2(x_1 + \xi)^3}{r_2^6} \\
G_2^{12}(x; \xi, \chi) &= (x_2 - \chi) \left[-\frac{1}{r_1^2} + \frac{1}{r_2^2} + \frac{2(x_1 - \xi)^2}{r_1^4} - \frac{2(x_1 + \xi)^2}{r_2^4} \right. \\
&\quad \left. - \frac{4\xi(x_1 + \xi)}{r_2^4} + \frac{4\xi^2}{r_2^4} + \frac{16\xi(x_1 + \xi)^3}{r_2^6} - \frac{16\xi^2(x_1 + \xi)^2}{r_2^6} \right] \\
G_1^{22}(x; \xi, \chi) &= (x_2 - \chi) \left[-\frac{1}{r_1^2} + \frac{1}{r_2^2} + \frac{2(x_1 - \xi)^2}{r_1^4} - \frac{2(x_1 + \xi)^2}{r_2^4} \right. \\
&\quad \left. + \frac{12\xi(x_1 + \xi)}{r_2^4} - \frac{4\xi^2}{r_2^4} - \frac{16\xi(x_1 + \xi)^3}{r_2^6} + \frac{16\xi^2(x_1 + \xi)^2}{r_2^6} \right] \\
G_2^{22}(x; \xi, \chi) &= +\frac{3(x_1 - \xi)}{r_1^2} - \frac{3(x_1 + \xi)}{r_2^2} - \frac{2\xi}{r_2^2} - \frac{2(x_1 - \xi)^3}{r_1^4} + \frac{2(x_1 + \xi)^3}{r_2^4} \\
&\quad + \frac{16\xi(x_1 + \xi)^2}{r_2^4} - \frac{12\xi^2(x_1 + \xi)}{r_2^4} - \frac{16\xi(x_1 + \xi)^4}{r_2^6} + \frac{16\xi^2(x_1 + \xi)^3}{r_2^6}
\end{aligned} \tag{34}$$

where

$$\begin{aligned}
r_1 &= \sqrt{(x_1 - \xi)^2 + (x_2 - \chi)^2} \\
r_2 &= \sqrt{(x_1 + \xi)^2 + (x_2 - \chi)^2}.
\end{aligned} \tag{35}$$

Since we are only interested in the tractions appearing along Γ_c , we have that $0 \leq x_1 \leq a, x_2 = 0$. Since we only distribute dislocations along Γ_c , we also have that $0 \leq \xi \leq a, \chi = 0$. Thus, G_1^{11} , G_2^{12} and G_1^{22} vanish. Furthermore, G_2^{11} is not interesting in this case since it does not appear in (32). Hence we are left with the first and second components of the influence functions G^{12} and G^{22} respectively, which in this case turn out to be equal and can be written as

$$G_1^{12} = G_2^{22} = \frac{1}{x_1 - \xi} - \frac{1}{x_1 + \xi} - \frac{2\xi}{(x_1 + \xi)^2} + \frac{4\xi^2}{(x_1 + \xi)^3}. \quad (36)$$

In analogy with (33), the stress σ_{ij}^B that is induced at x by the distribution $B = (B_1, B_2)^T$ of infinitesimal dislocations along the crack, can be obtained as Cauchy's principal value of the integral of the scalar product of B with G^{ij} along Γ_c :

$$\sigma_{ij}^B(x) = \frac{C^{-1}}{\pi} \cdot (CPV) \int_{\Gamma_c} B(s) \cdot G^{ij}(x; s) d\Gamma_s, \quad i, j = 1, 2 \quad (37)$$

As can be seen from (34), all integrals of the above form are divergent, so in the following it is to be understood that the appearing integrals should be treated in the CPV-sense. With the crack contour parametrized in ξ , the equations (32) can be written as

$$\begin{aligned} \frac{1}{\pi} \int_0^a B(\xi, 0) \cdot G^{12}(x; \xi, 0) d\xi &= 0 \\ \frac{1}{\pi} \int_0^a B(\xi, 0) \cdot G^{22}(x; \xi, 0) d\xi &= -C\sigma^\infty(x), \quad x \in \Gamma_c \end{aligned} \quad (38)$$

and these are the equations we will try to solve for $B(\xi) := B(\xi, 0)$. We note first that since $G_2^{12} = G_1^{22} \equiv 0$ (as can also be seen from figures 5 and 2), the equations are uncoupled. Therefore it is easy to solve the first equation in (38), since this can be satisfied by setting $B_1 \equiv 0$. We are left with the equation

$$\frac{1}{\pi} \int_0^a B_2(\xi) \left(\frac{1}{x_1 - \xi} - \frac{1}{x_1 + \xi} - \frac{2\xi}{(x_1 + \xi)^2} + \frac{4\xi^2}{(x_1 + \xi)^3} \right) d\xi = -C\sigma^\infty(x_1, 0), \quad 0 < x_1 < a. \quad (39)$$

It is noted that the kernel of the left-hand side integral operator is generalized Cauchy. In order to formulate a BE-method for this equation, we must choose the appropriate shape functions. To do this we need to know the shape of B , or more specifically the shape of B near the crack tip. It has been mentioned that B is singular, and in chapter (3), the severity of this singularity will be discussed further. For this simple problem we content ourselves with a slightly restricted argument; It is well-known that the crack opening displacement varies with the distance r from the crack tip as the square root of r . Thus the identity (29) implies that

$$\frac{dCOD(x)}{dx} = -B_2(a - x), \quad (40)$$

and since $COD(r)$ varies as \sqrt{r} , this suggests why the same order of singularity as in σ^B (square root singular) appears also in the ansatz for B .

To support the choice of the different BE-formulations in this comparison of methods, we reason as follows; First we want to try out formulations using global shape functions, i.e. one single geometrical element. The well-known Gauss-Chebyshev method ([25]) is applicable, but since we are primarily interested in the value of B at the crack tip, we prefer a method that is based upon a closed or a semi-closed quadrature scheme. Thus we turn to the Bouzitat formulas for regular integrals, that can be found in [24]. Based upon these formulas, a complete closed-type method with affiliated collocation points for singular integral equations is developed in [28] and [29]. It is shown that this method, called the Lobatto-Jacobi method, is applicable to Cauchy principal value equations with generalized Cauchy kernels, such as the equation (39). Lobatto-Jacobi is attractive to us because of closed-typeness and the fact that it is based upon Jacobi polynomials, which allows us to control the behaviour of the unknown at the ends of the integration interval in a detailed manner. By looking ahead at section 3 we can tell that it would be pleasing to have this control. Unfortunately, altering the strength of the endpoint singularities in the ansatz for B alters the equations for the abscissae and collocation points, making it impossible to precalculate the values. Since we must solve an equation such as the one found in [28] and [29] every time we need new abscissae and collocation points (in the closely related Gauss-Jacobi method, these equations are somewhat simpler, see [26]), we would be grateful if we could find a method in which these points can be found with less effort. So, how about the Lobatto-Chebyshev method ([27])? Well, this is a special case of the Lobatto-Jacobi method, in which the singularities all are of the square root size. The weights, abscissae and collocation points are relatively easy to obtain. But how do we control the behaviour of the unknown when it is not square root singular? According to [32] and [31] there is a way to do this; By cheating.

In the many papers found in the references, a bit of a quarrel has been carried out concerning what abscissae, weights and collocation points are the best. On the other hand, in the excellent article [30], it is emphasized that you should not worry too much about what quadrature rule you use, because the results are not too different anyhow.

Secondly, we want to try a method that more resembles the classic BE-formulation, with many geometrical elements and local basis functions. Such formulations are common when considering three dimensional crack problems. Though, this will not be tried here due to lack of time. Instead, we refer to [9], for a comparison of these kinds of formulations when applied to

a three dimensional crack problem.

As has been mentioned, it is vital that the ansatz captures the correct shape of the unknown at the ends of the crack. This will be done by incorporating into this ansatz a (or several) shape function(s) that behaves as $r_l^\alpha r_r^\beta$, where r_l and r_r is the distance from the left and right endpoint respectively. Each method is applied to the normalized equation that is obtained by changing the variables of (39) into $s = 2\frac{\xi}{a} - 1$ and $t = 2\frac{x_1}{a} - 1$:

$$\frac{1}{\pi} \int_{-1}^1 B_2(s) \left(\frac{1}{t-s} - \frac{1}{t+s+2} - \frac{2(s+1)}{(t+s+2)^2} + \frac{4(s+1)^2}{(t+s+2)^3} \right) ds = -C\sigma^\infty\left(\frac{a}{2}(t+1), 0\right),$$

$$-1 < t < 1$$
(41)

Let us compare the following methods:

1. The Gauss-Jacobi method with $\alpha = 1/2$ and $\beta = -1/2$, as decribed in [26]. This method is relatively easy to apply, because the number of integration points and collocation points are the same, so no side condition is needed, and furthermore, these points, together with the associated weights, are tabulated in [9]. In this method there is only one single geometrical element $([-1, 1])$, and shape function number j is defined by

$$\phi_j(\cdot) = P_j^{(\alpha, \beta)}(\cdot)(1 + \cdot)^\alpha(1 - \cdot)^\beta, \quad (42)$$

where $P_j^{(\alpha, \beta)}$ is the j :th Jacobi polynomial. These shape functions obviously render the mentioned shape of B . Our ansatz \tilde{B} that approximates B is hence

$$\tilde{B} = \sum_{k=0}^{p(N)} \tilde{B}_k \phi_k, \quad (43)$$

where $p(N)$ is the polynomial degree of the Gauss-Jacobi method of order N for generalized Cauchy integrals with weight function $(1 + \cdot)^\alpha(1 - \cdot)^\beta$. In the system of linear equations that are produced by the Gauss-Jacobi method, the number p is not a parameter, but rather the number N of abscissae used, so we use N as the measure of precision of this BE-formulation.

A drawback of this method seems to be that due to the value of α , the density is actually forced to vanish at the crack mouth, but as we will see, we will still obtain accurate values of K_I .

From [9] we know that

$$\frac{dCOD(r)}{dr} = C \frac{K_I}{\sqrt{2\pi r}}, \quad (44)$$

where the distance r from the crack tip is small. According to equation (40) we must thus have that

$$K_I = \lim_{r \rightarrow 0} (\sqrt{2\pi} C^{-1} \sqrt{r} B(1 - 2r/a)), \quad (45)$$

To obtain our approximation of K_I , we use \tilde{B} instead of B in the above equation, and thus we get, with $t = 1 - 2r/a$, that

$$\begin{aligned} K_I &\approx \lim_{r \rightarrow 0} (\sqrt{2\pi} C^{-1} \sqrt{r} \sum_{k=0}^p \tilde{B}_k \phi_k(t)) \\ &= \lim_{r \rightarrow 0} (\sqrt{2\pi} C^{-1} \sqrt{r} \sum_{k=0}^p \tilde{B}_k P_j^{(\frac{-1}{2}, \frac{1}{2})}(1 - 2r/a) \sqrt{\frac{a-r}{r}}) \\ &= \sqrt{2\pi} C^{-1} \lim_{r \rightarrow 0} (\sqrt{a-r} \sum_{k=0}^p \tilde{B}_k P_j^{(\frac{-1}{2}, \frac{1}{2})}(1 - 2r/a)) \\ &= \sqrt{2\pi a} C^{-1} \lim_{r \rightarrow 0} (\sum_{k=0}^p \tilde{B}_k P_j^{(\frac{-1}{2}, \frac{1}{2})}(1 - 2r/a)) \\ &= \sqrt{2\pi a} C^{-1} (\sum_{k=0}^p \tilde{B}_k P_j^{(\frac{-1}{2}, \frac{1}{2})}(1)) \end{aligned} \quad (46)$$

The Gauss-Jacobi method provides the values of the polynomial part $\sum_{k=0}^p \tilde{B}_k P_j^{(\alpha, \beta)}$ of \tilde{B} at the integration points. Unfortunately, this quadrature scheme is not closed, so we have to extrapolate these values to obtain $\sum_{k=0}^p \tilde{B}_k P_j^{(\alpha, \beta)}(1)$. Fortunately, there is a formula specially adopted for this task, and which can be found in [9].

2. The Lobatto-Chebyshev method with the kind of endpoint singularity correction that is described in [27] and [31]. The Lobatto quadrature is closed, so no extrapolation is needed to obtain approximations of the stress intensity. Hopefully, this advantage will compensate for the lower polynomial degree of the Lobatto scheme. Furthermore, in this method we wish to obtain a $\alpha = 0, \beta = \frac{-1}{2}$ shape by first solving with $\alpha = \beta = \frac{-1}{2}$, and then correct the left endpoint shape by dividing the obtained solution by $(1 + \cdot)^{\frac{1}{2}}$. This correction actually imposes the wrong shape of the unknown, so we expect

the approximation of the stress field to be somewhat misleading, but we still hope for good stress intensity approximations. When $\alpha = \beta = \frac{-1}{2}$, the Jacobi polynomials in (42) are equal to the Chebyshev polynomials (hence the name Lobatto-Chebyshev), and in this case the abscissae, weights and collocation points are tabulated in [9]! Though, the collocation points are one less than the integration points, so we need one more equation to render the resulting linear system determined. It is common to apply a condition saying that the integral of the density along the crack should equal a constant. It is also possible to require the crack faces at the mouth of the crack to be parallel by simply requiring the density to be zero at this point. We will try these different side conditions.

We do not have to derive an expression for the approximate stress intensity factor in this case, since this has already been done in [32]. The expression is:

$$K_I \approx \sqrt{\pi a/2} C^{-1} \left(\sum_{k=0}^p \tilde{B}_k P_j^{(\frac{-1}{2}, \frac{-1}{2})}(1) \right) \quad (47)$$

For each of the above methods, we now graph the errors in the computed values for K_I for different N . For $a = 1/\pi$, the correct value is 1.1215 ([33]), and this is also the parameter value that is used in the computations. Figure 7 shows a log-log plot of the errors obtained by the two methods versus the number N of unknowns in the resulting linear systems, as N ranges from 10 to 60. The slightly curved graph corresponds to the Gauss-Jacobi method. The other graph is actually composed of several coinciding graphs that has been obtained by using the different side conditions that are associated with the Lobatto-Chebyshev method. The graphs are indistinguishable even on a fine scale, which proves that the side condition has little effect on the computed stress intensity factor. Furthermore, the result of fitting a line to these graphs suggests that both methods converge quadratically.

Let us also note something about the conditioning of the system matrices for each of these methods. As is usual, we expect an increase in the condition numbers as the precision increases. The reason for this is that the distance between the collocation points near the ends of the interval decreases rapidly as N increases. This is where the Lobatto-Chebyshev method hints its superiority; As $N = 600$ the condition number in method 2 does not exceed 400,

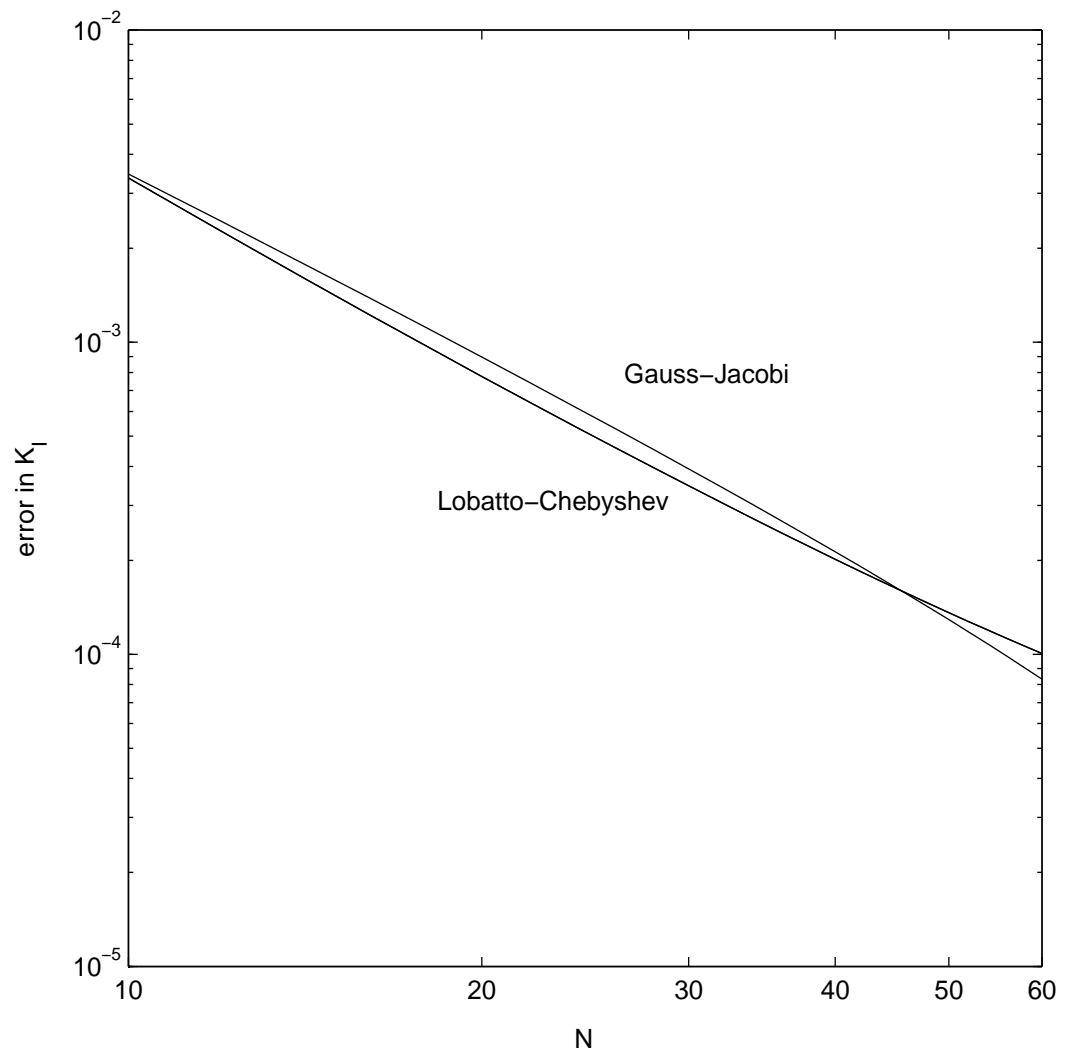


Figure 7: A comparison

while the condition number in method 1 is over 70000 as N is only 400. The conditioning of method 2 is though somewhat dependent on the side condition. The best results in this respect were obtained when a side condition requiring the crack faces at the crack mouth to be parallel was used.

1.4 Simplifications of the problem and assumptions on its data

In this section some simplifications of the formulated problem will be presented. The need for these simplifications can in some cases be explained by reference to the discussion in this introductory chapter, while some simplifications and assumptions are necessary to limit the extent of this Master project.

The analysis will be carried out in two dimensions, by imposing plane deformation conditions and letting the crack front be orthogonal to the plane under consideration. This implies that only mode I and II stress intensity factors will appear, and only straight edge dislocations will be treated (with the dislocation edges parallel with the crack front). As was mentioned in the problem formulation, only components made up from crystalline composites will be studied. Furthermore, the grain boundary is assumed to be the shape of a polygon.

Our current approach, modelling plasticity by dislocation emission and motion, is a method that in a detailed fashion treats the effects of the stress concentrations around the crack tip, as is appropriate for our small scale problem. Considering that the redistribution of stresses near the crack tip due to plastic work is achieved by a distribution of discrete dislocations, it is adequate to consider the material of our component to be perfectly elastic.

We aim at placing discrete dislocations at carefully selected points in Ω_g . Naturally, we must know how these dislocations influence the stress field in the grain. It should be clear from the discussion in (1.3.2) that we are forced to assume both elastic isotropy and constant material properties throughout Ω_h . An important expression is hence the expression (33) for the influence of a dislocation on the state of stress in a homogenous half plane. We will not derive this expression, but assume it. Note that we will consider anisotropy when calculating the motions of dislocations.

We assume that there is exactly one simply connected crack contour, and that this contour is piecewise linear and continuous.

The external load is assumed to consist of a time dependent tensile stress σ^∞ that is applied symmetrically to the remote northern and southern boundaries. σ^∞ is characterized by its minimum and maximum value during a cycle. Experience has shown that it is reasonable to take no notice of its variation between these extreme values. Furthermore, we assume that the frequency of the loading is small enough for it to be reasonable to dismiss any influence the acceleration of mass in the body might have on the solution procedure. Also, we let σ^∞ be such that the crack opening displacement along the entire length of the crack and during the whole loading sequence, is greater than the cohesive range of the particles in the lattice. This relieves us from the need of considering friction and contact forces, and it also prevents crack re-welding. As we will see in chapter (3), it is not enough to assume that σ^∞ is strictly tensile, since plasticity induced crack closure might occur even though σ^∞ is positive.

2 A dislocation based model of the fatigue growth of initiated microcracks

In this chapter a mathematical model for the simulation of the fatigue growth of initiated microcracks is proposed. As was specified in the problem formulation, the crystalline state will be considered, and dislocations will frequently be used for modelling different aspects of the fatigue growth. The simplifications in section 1.4 will help to limit the vastness of the general case model. In Chapter 3, we attempt to translate this model into a mathematical technique that will also be implemented to perform the simulation.

The chapter begins with a few sections each devoted to one of the following major modelling issues: Load stepping, the modelling of the grain boundaries, glide planes and crack, the definition of the boundary value problem for the stress field and how to obtain its data, the modelling of the plasticity, the dislocation emission and annihilation model and the crack growth model. In figure 9 at the end of the chapter, a flow scheme for the simulation model is depicted.

2.1 Load stepping

During the fatigue, the external load is assumed to vary periodically. Since the cycle is determined by the pair $(\sigma_{min}^\infty, \sigma_{max}^\infty)$, we must decide the behaviour of the loading when it is between these two values. It is not necessary to consider all values of the load during a cycle and thus having to model a continuous change in the load by means of some subtle analysis, but instead we choose a finite sequence $\{\sigma_i^\infty\}_i$ of load values that increase from σ_{min}^∞ to σ_{max}^∞ and then decrease from σ_{max}^∞ back to σ_{min}^∞ simply by picking a suitable size of the load step that will be used throughout the whole cycle.

2.2 The modelling of the grain boundaries, glide planes and crack

The modelling of the grain boundaries is perhaps the most central issue in this study. We have assumed that the grain boundary Γ_g is a polygon. As before, we denote by Ω_g the plane set bounded by this polygon. There are at least two possible ways to model the grain boundaries; One way is to define them by a local increase in τ_{crit} (see section 1.3.1) which surely will make Γ_g

act as barrier for dislocation glide. Another way is to distribute dislocations along Γ_g . The latter approach is actually the more realistic one, since grain boundaries in a wider sense are nothing but distributions of dislocations. More specifically, a grain boundary is a displacement, and hence it is close at hand to model the grain boundaries by a set of dislocation dipoles, which is what we do here. In a way we have already encountered an application of this technique as we discussed the modelling of finite bodies that is performed in [17], where traction free grain boundaries are achieved by introducing an extra set of equations for the grain boundary dipole strengths in Ω_g , expressing the condition that the stress on the grain boundaries induced by the external load must be matched by the traction stresses induced by the boundaries themselves and other internal sources of stress in Ω_g . This would probably make Γ_g act as barrier for both dislocation glide and crack advance, but this technique is a little too advanced for our purposes. In this model, we employ the simpler strategy of merely placing finite length dipoles in a suitable way along Γ_g to mimic the grain boundaries. Since the grain boundaries are defined by some displacements, it can be understood why we choose to distribute dipoles and not single dislocations. Thus, Γ_g is a finite set of finite length dislocation dipoles, i.e. their strengths, lengths and orientations.

To simulate the crack growth, we also have to specify the glide planes of the grain. Since this is a two dimensional simulation, all glide planes that we consider must be parallel to the crack front, so that they can be represented by lines. This is of course not the case for all glide planes in every crystal, so the actual number of glide planes must perhaps be reduced and the model of the crystal must perhaps be simplified before the simulation is applied.

We also need to represent the crack line Γ_i at load step i . Since it is assumed that there is exactly one simply connected piecewise linear crack contour, we can represent Γ_i by the coordinates of a finite set of ordered and distinct kinks. Thus we write Γ_i^k for the coordinates of kink number k at load step i . It follows that $\Gamma_i^1 \in \Gamma_h$, and every time the crack increments all we need to do is add an element to $\{\Gamma_i^k\}_{k=1}$. We also write $C^i + 1$ for the number of elements in $\{\Gamma_i^k\}_{k=1}$. By a slight abuse of notation, we will in the following write Γ_i for the crack locus, and $\{\Gamma_i^k\}_{k=1}$ for the kinks. This will probably not cause any confusion.

The actual modelling of the crack is brought about by a distribution of dislocations along Γ_i . We now suggest how to find this distribution.

2.3 The governing boundary value problem and how to obtain its data

During the simulation, we will need to compute the stresses at different points in Ω_g . The state of stress in a static body is governed by the equations of elasticity. There is no need to incorporate into these equations a term involving the derivatives of the displacements with respect to time, in order to model the possible acceleration of various points in the body. This is because the body will reach equilibrium very quickly. It is thus clear from the discussion in chapter (1), that the governing boundary value problem can be expressed as the problem of finding the distribution of dislocations along the crack line that leaves the crack free of any traction stress. In this way the boundary value problem at load step i is reduced to the following:

Given $\hat{\sigma}_i^A$, $\sum_{d \in P_i} \hat{\sigma}_i^d$ and $\hat{\sigma}_i^G$, find $B_i : \Gamma_i \rightarrow \mathfrak{R}^2$ such that

$$\hat{\sigma}_i^B = -\hat{\sigma}_i^A - \sum_{d \in P_i} \hat{\sigma}_i^d - \hat{\sigma}_i^G \quad \text{on } \Gamma_i, \quad (48)$$

where $\hat{\sigma}_i^A, \hat{\sigma}_i^d, \hat{\sigma}_i^G, \hat{\sigma}_i^B : \Gamma_i \rightarrow \mathfrak{R}^2$ are the direct and shear traction stresses normal to the crack line induced by σ_i^∞ , the dislocation d , Γ_g and B_i respectively, and P_i is a set of free dislocations in Ω_g (see section 2.4).

Once we have solved (48), we can obtain the overall stress field σ_i at load step i , adding together the stress fields σ_i^A , $\sum_{d \in P_i} \sigma_i^d$, σ_i^G and σ_i^B induced in Ω_g by σ_i^∞ , the dislocations d in the set P_i (see section 2.4), the grain boundaries Γ_g , and the dislocation density B_i respectively. This operation must of course be preceded by the calculation of these terms; σ_i^g and σ_i^d are easily computed by using (33). Furthermore, we obviously have that

$$\sigma_i^A = \begin{bmatrix} 0 & 0 \\ 0 & \sigma_i^\infty \end{bmatrix}. \quad (49)$$

Also, σ_i^B can be obtained from (37).

We need no condition on the stress saying that Γ_h is traction free, or a condition saying that $\sigma_i^A(x) + \sigma_i^B(x) + \sum_{d \in P_i} \sigma_i^d(x) + \sigma_i^g(x)$ should tend to the far field loading as $\|x\|$ tends to infinity, since these conditions are automatically satisfied by the nature of the expressions (see (34)) for the stress fields around a dislocation.

Obtaining the correct data for (48) is a separate, but not overwhelming, task. Knowing σ_i^A , σ_i^d and σ_i^G we can easily compute $\hat{\sigma}_i^A$, $\hat{\sigma}_i^d$ and $\hat{\sigma}_i^G$ by performing a transformation of the form

$$\begin{aligned}
\hat{\sigma}_{i_1}^x &= \frac{1}{2}(\sigma_{i_{11}}^x + \sigma_{i_{22}}^x) - \frac{1}{2}(\sigma_{i_{11}}^x - \sigma_{i_{22}}^x) \cos 2\theta - \sigma_{i_{12}}^x \sin 2\theta \\
\hat{\sigma}_{i_2}^x &= -\frac{1}{2}(\sigma_{i_{11}}^x - \sigma_{i_{22}}^x) \sin 2\theta + \sigma_{i_{12}}^x \cos 2\theta
\end{aligned} \tag{50}$$

$x = A, d, G,$

where θ is the counter clockwise angle that the crack line makes with the global x-axis.

We now understand that the crack is nothing but a vector valued function B_i ! The crack locus Γ_i is built into this definition of the crack, since Γ_i is the domain B_i , which is a vital part of the function. Hence, B_i is a complete description of the crack, since we can extract both the crack locus and the crack opening displacement from its definition.

2.4 Modelling plasticity

In a solid that is not perfectly elastic, a plastic zone will inevitably appear around the crack tip, even when the applied loads are small. Dislocation based models accurately describe this zone at load step i , by a set P_i of free dislocations placed at carefully selected points in Ω_g . A dislocation d in P_i might relocate if the stress situation at the location d_l of d fulfils some criterion. This criterion is detailed below.

2.4.1 Dislocation glide and climb

In reality, dislocation glide is initiated only if the shear stress τ acting along the glide plane of the dislocation at the location of the dislocation exceeds the critical value τ_{crit} (see section 1.3.1). τ_{crit} is assumed to be a material property, and can be thought of as a friction coefficient. For our purposes, it is more convenient to let the glide be determined by the relative discrepancy between τ and τ_{crit} , and so we instead choose to initiate glide as $\frac{|\tau| - \tau_{crit}}{\tau_{crit}} < tol$, where tol is a specified tolerance. One might argue that the condition for the glide of the dislocation d should be dependent on the burgers vector d_b of d , which is why one might employ instead an alternative glide condition used in [15]; One computes the size of the Peach-Koehler slip force F_d acting on d (which requires only the knowledge of the stress intensities and the locations and burgers vectors of the dislocations, see [19] and [20]), and then compare it to the material's extrinsic resistance to dislocation motion (see [10]). This approach is in some cases superior since it takes into account the size of the

dislocation and requires no knowledge of the external tensile loading and crack opening, but is tedious when there are several glide planes and the crack is allowed to kink. In our case we will also see in section 2.5 that the mobile dislocations all have the same length of their burgers vectors, so the slip force approach is superfluous.

As can be understood by examining the formerly mentioned Andrades model, the dislocation glides so to speak 'opposite' to the applied shear stress. What 'opposite' means is of course a question of the orientation of the burgers vector. Let us decide that the orientation of d_b is such that d glides in the positive burgers vector direction, as a big enough *positive* shear stress is applied.

In this study, dislocation climb is not considered.

Due to the presence of the free boundary, a dislocation d in a half plane exerts an image force on itself. This force is relatively small, and will be ignored when computing the stress induced at d_l by the free dislocations (the image forces of all dislocations other than d are considered though). Still, this image force plays a role as a load on the crack, and thus influences the state of stress at d_l .

2.4.2 The Equilibrium Arrangement of Dislocations and the EAD-iteration

As the simulation moves from load step σ_i^∞ to load step σ_{i+1}^∞ , all discrete dislocations in P_i are at rest. As the load is incremented, the state of stress in Ω_g will change; Specifically the stress acting at the locations of every mobile dislocation d in P_i will change. To obtain information about this state, we solve (48). Once this is done, we can calculate the specific values of the global stress components at d_l , and then calculate the shear along d_b at d_l by a Mohr's transformation. This is valuable information since this value will govern whether the dislocation d will move or not. Let us imagine that some dislocations actually move every time the load is incremented. The dislocations all relocates to positions where the stress is such that the glide criterion is no longer fulfilled, i.e. an Equilibrium Arrangement of Dislocations (EAD) has been reached. It is of course necessary for the further simulation to find these positions. This model approximates the EAD-positions of the dislocations by what we call an EAD-iteration. The first step of the EAD-iteration consists of calculating the shear stress τ along d_b at d_l for every $d \in P_i$. As we have seen in (2.3), this comprises the calculation of the stress induced

by the far field loading, the grain boundaries, the free dislocations and the crack. In the second step the glide condition is checked for every $d \in P_i$, and if fulfilled, d_l is set to $d_l + c d_b \text{sign}(\tau) \frac{|\tau| - \tau_{crit}}{\tau_{crit}}$, where c is a constant that must be chosen. It can be seen that this glide model takes into account the actual discrepancy between the shear stress and the critical shear stress, while many other dislocation based models (such as [15] and [11]) move a dislocation a fixed distance such as 5 or 10 burgers vectors every time this glide condition is fulfilled. Together with the check for dislocation annihilation (explained below), the two steps described above makes up the only three steps that are performed in every iteration in the EAD-iteration. The stop criterion for the EAD-iteration is simply that no dislocation in P_i relocates during an iteration.

2.4.3 Dislocation annihilation

During every iteration of the EAD-iteration, we check if a discrete dislocation is within distance of ba burgers vectors from the crack tip, where ba is a parameter that is chosen. Those that are, are annihilated, that is, they are simply removed from P_i .

The procedure of approximating the EAD-configuration is schematically described in figure 8.

2.5 Dislocation emission and crack tip shielding

Once the overall stress field σ_i is obtained, the stress intensity factors can be calculated. The stress intensity factors obtained from the solution of (48) are sometimes referred to as the 'local' stress intensity factors because they consider the local conditions around the crack tip, i.e. the dislocation loads in (48). The size of these factors will influence whether discrete dislocations will be emitted during load step number i . Dislocation generation is restricted to the crack tip. Since the stress intensity factors are relatively small (HCF-condition), other dislocation sources are not likely to appear. Actually, we let the dislocations be 'born' at a distance of be burgers vectors ahead of the crack tip, where be is a parameter that is chosen. This is common practice in dislocation modelling, and helps to simplify the problem since the dislocation mechanics *at* the crack tip is more complicated than elsewhere in the body. Furthermore, since dislocation climb is not allowed in this model, all emitted dislocations belong to a specific glide plane. Our aim is thus to define a

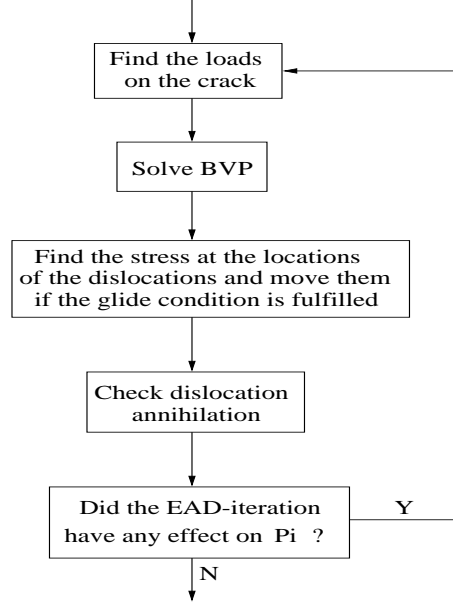


Figure 8: The EAD-iteration

condition for dislocation emission along the glide plane R_ρ , in terms of the stress intensity factors K_I and K_{II} , and the angle ρ that the glide plane makes with the crack tip line ($\Gamma_i^{C^{i+1}} - \Gamma_i^{C^i}$). To define such a condition we weigh together the values of K_I and K_{II} using ρ -dependent weights, and check if the absolute value of this linear combination K_ρ exceeds a critical value. If so, a dislocation d that glides along R_ρ is emitted, that is, created at the distance be burgers vectors along the plane R_ρ in front of the crack tip. The linear combination K_ρ that also determines the direction of d_b , is defined by

$$K_\rho = \sin(\rho) \cos(\rho) K_I + \cos(2\rho) K_{II}. \quad (51)$$

To simplify the simulation, we decide that all emitted dislocations are of the same size. We know a priori that the stress intensity can be strictly negative even though we have assumed tensile (not compressive) loading (see [14]), and thus can K_ρ also be negative. Hence, even though all the burgers vectors of the dislocations emitted on a plane are of the same size, they may differ in direction. We must therefore be careful to emit dislocations with properly oriented burgers vectors; If K_ρ is positive, the burgers vector points

away from the crack tip, and vice versa.

It remains to define the critical value K_e for dislocation emission, that is, the value that K_ρ is compared to when determining emission. At this stage it should be noted that the stress intensity factors that we have computed describe the exact conditions around the crack tip, including the local effects of the dislocations in P_i . This means that we do not have to alter the values K_I and K_{II} (as is done in for example [20] and [16]) to take into account the effects of the emitted dislocations. This effect that a dislocation $d \in P_i$ has on the crack tip stress intensities is often referred to as the shielding effect of d . (Actually, the reason why we introduced P_i in the first place was for its shielding effect.) This shielding effect could be either positive or negative (anti-shielding) depending on the orientation and location of d . That our model automatically treats the discussed shielding effect without altering K_I and K_{II} is confirmed in section 4.3 and especially by figure 15. Hence, we consider K_e to be a material property.

2.6 Crack growth

The crack increments as discrete dislocations are emitted. The crack always increments along one of the specified glide planes. It remains to determine the angle that this glide plane makes with the crack tip line. If the cracked material were to be considered isotropic, we could use the maximum normal stress criterion given in [31] to find the fracture angle θ ;

$$K_I \sin \theta + K_{II}(3 \cos \theta - 1) = 0 \quad (52)$$

Our material is not considered isotropic, which is why the above equation cannot be used for finding θ . This is because there is not necessarily a glide plane that makes the angle θ with the crack tip line. Though, we could employ a slightly altered approach. We let the fracture angle θ be defined by the equation

$$\theta = \operatorname{argmin}_{\theta' \in R} (K_I \sin \theta' + K_{II}(3 \cos \theta' - 1)), \quad (53)$$

where R is the set of angles that the glide planes make with the crack tip line. This way, R_θ is always a glide plane.

The length of the crack increment depends on the angles between the burgers vectors of the emitted dislocations and the glide plane along which

the crack grows. The length of the increment is simply taken as the sum of the projections of the burgers vectors on this glide plane ([18]).

2.7 A flow scheme for the simulation

The flow scheme for the simulation is depicted in figure 9.

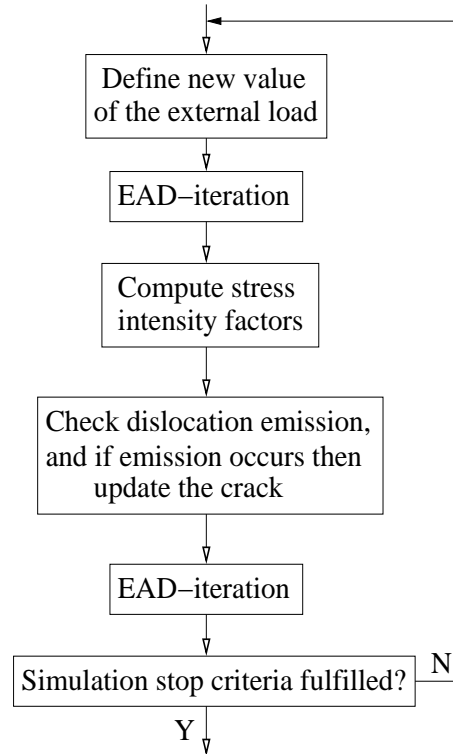


Figure 9: Flow scheme for simulation

3 A technique for simulating the fatigue growth of initiated microcracks based upon the model

In this section we develop a complete mathematical technique for the simulation of fatigue crack growth. This we do by detailing each of the actions that are described in figure 9.

3.1 The boundary equation formulation of the governing boundary value problem

At each load step, it is convenient to express (48) as a coupled system of C^i pairs of equations. We consider equation *pairs* since in the entire system, exactly two equations have the same domain; One saying that the direct stress normal to crack segment number k must be zero, and one saying that the shear stress normal to crack segment number k must be zero. The unknowns will for later convenience be expressed in coordinate systems local to the crack segments; This will not complicate anything since the density behaves as a vector and one can easily transform it to another coordinate system by premultiplying it by a rotation matrix. The parametrization γ_k in s of segment k is defined from

$$\gamma_k(s) = \Gamma_i^k + \frac{1+s}{2}(\Gamma_i^{k+1} - \Gamma_i^k), \quad -1 \leq s \leq 1. \quad (54)$$

According to (37), we have that

$$C\sigma_{i_{mn}}^B(\gamma_k(t)) = \sum_{j=1}^{C^i} \frac{1}{\pi} \int_{\gamma_j} B_i \cdot G^{mn}(\gamma_k(t); \cdot) d\gamma_j, \quad (55)$$

Using the parametrization γ_j in the above integral gives

$$C\sigma_{i_{mn}}^B(\gamma_k(t)) = \sum_{j=1}^{C^i} \frac{1}{\pi} \int_{-1}^1 B_i(\gamma_j(s)) \cdot G^{mn}(\gamma_k(t); \gamma_j(s)) |\gamma_j'(s)| ds \quad (56)$$

Along segment number j we wish to describe B_i with respect to a coordinate system which first axis is parallel with the crack segment γ_j and origin at the segment midpoint. Thus we write $\hat{B}_i^j(s)$ for the local density at $\gamma_j(s)$, and apply a rotation to $\hat{B}_i^j(s)$ to transform back into the global system. If we treat $\hat{B}_i^j(s)$ and G^{mn} as column vectors, and let a_j denote the (global) half length of segment j , we can write

$$C\sigma_{i_{mn}}^{\hat{B}}(\gamma_k(t)) = \sum_{j=1}^{C^i} \frac{1}{\pi} \int_{-1}^1 \hat{B}_i^j(s)^T \begin{bmatrix} \cos \theta^j & -\sin \theta^j \\ \sin \theta^j & \cos \theta^j \end{bmatrix}^T a_j G^{mn}(\gamma_k(t); \gamma_j(s)) ds, \quad (57)$$

where θ^j is the angle that γ_j makes with the global horizontal axis. Writing R^j for the inverse of the rotation matrix, we get

$$C\sigma_{i_{mn}}^{\hat{B}}(\gamma_k(t)) = \sum_{j=1}^{C^i} \frac{1}{\pi} \int_{-1}^1 \hat{B}_i^j(s)^T a_j R^j G^{mn}(\gamma_k(t); \gamma_j(s)) ds. \quad (58)$$

Since we, according to the formulation (48) of the boundary value problem, aim at annulling the 12- and 22-stresses *normal* to the crack line, we must also transform the above expression for the stress into the we local coordinate system of the segment γ_k . The Mohr transformation (50) that performs this task can be represented by a matrix. Hence,

$$\hat{\sigma}_i^{\hat{B}}(\gamma_k(t)) = M^k \begin{bmatrix} \sigma_{i_{11}}^{\hat{B}}(\gamma_k(t)) \\ \sigma_{i_{22}}^{\hat{B}}(\gamma_k(t)) \\ \sigma_{i_{12}}^{\hat{B}}(\gamma_k(t)) \end{bmatrix}, \quad (59)$$

where

$$M^k = \begin{bmatrix} \sin^2 \theta^k & \cos^2 \theta^k & -\sin 2\theta^k \\ -\sin \theta^k \cos \theta^k & \sin \theta^k \cos \theta^k & \cos 2\theta^k \end{bmatrix} \quad (60)$$

Inserting (58) into (59) we see that the matrix premultiplication by M^k can be turned into a Kronecker tensor product with R^j , and the equation pair number k can be written as a single vector equation, provided that we introduce some new notation:

$$C\hat{\sigma}_i^{\hat{B}}(\gamma_k(t)) = \sum_{j=1}^{C^i} \frac{1}{\pi} \int_{-1}^1 \begin{bmatrix} \hat{B}_i^j(s)^T & 0 & 0 \\ 0 & 0 & \hat{B}_i^j(s)^T \end{bmatrix} a_j (M^k \otimes R^j) G(\gamma_k(t); \gamma_j(s)) ds, \quad (61)$$

where

$$G = \begin{bmatrix} G_1^{11} \\ G_2^{11} \\ G_1^{22} \\ G_2^{22} \\ G_1^{12} \\ G_2^{12} \end{bmatrix}. \quad (62)$$

Using the above expression for the stress induced by the dislocation density along the crack, we find that (48) is equivalent to the equations

$$\begin{aligned} \sum_{j=1}^{C^i} \frac{1}{\pi} \int_{-1}^1 \begin{bmatrix} \hat{B}_i^j(s)^T & 0 & 0 \\ 0 & 0 & \hat{B}_i^j(s)^T \end{bmatrix} a_j(M^k \otimes R^j) G(\gamma_k(t); \gamma_j(s)) ds = \\ -C \hat{\sigma}_i^A(\gamma_k(t)) - C \sum_{d \in P_i} \hat{\sigma}_i^d(\gamma_k(t)) - C \hat{\sigma}_i^g(\gamma_k(t)), \quad k = 1, \dots, C^i, -1 \leq t \leq 1. \end{aligned} \quad (63)$$

The term $\hat{\sigma}_i^A(\gamma_k(t))$ is constant in t since the remotely induced traction stress does not change along a segment, and the term $\hat{\sigma}_i^g(\gamma_k(t))$ is constant in i because the grain boundaries do not change in time; Let us denote them by the column vectors RIS_i^k and $GIS^k(t)$ respectively. Summing up, we have arrived at a nice boundary equation formulation of our crack problem:

$$\begin{aligned} \sum_{j=1}^{C^i} \frac{1}{\pi} \int_{-1}^1 K_{kj}(t; s) \hat{B}_i^j(s) ds = & -C(RIS_i^k + GIS^k(t) + \sum_{d \in P_i} \hat{\sigma}_i^d(\gamma_k(t))) \\ & k = 1, \dots, C^i, -1 \leq t \leq 1, \end{aligned} \quad (64)$$

where¹

$$vec(K_{kj}(t; s)^T) = a_j(M^k \otimes R^j) G(\gamma_k(t); \gamma_j(s)). \quad (65)$$

It is the problem (64) that we now proceed to solve.

3.2 Discretizing the equations

3.2.1 The ansatz

To make the adequate ansatz we must know the strengths of the endpoint singularities of the unknown density along each crack segment, i.e. we must

¹if A is a matrix, then $vec(A)$ is the vector made from putting the columns of A on top of each other.

know the parameters α and β . By carefully studying [26] we conclude that the singularities in the densities should be of the same order as the singularity in the 'near kink' stress field. Since we have assumed that the crack is open along its entire length during the whole simulation, we can consider the magnification of each kink as the apex of two notched components with traction free notch-faces, and subjected to some form of external loading, as in figure 10.

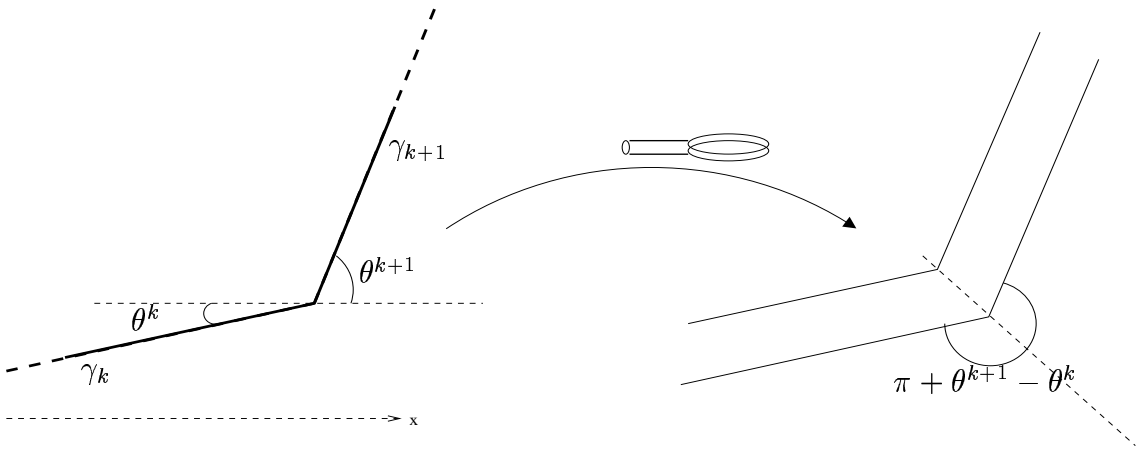


Figure 10: Magnification of a kink

We can now rely on Williams classic analysis (see eg [5],[8],[9]) to tell us the singularity of the stress around the notch, and hence also the parameters α and β in our ansatz. We will not detail this procedure here, since it turns out that our numerical method disregards the actual values of α and β and treats all near kink stress fields as square root singular. Anyhow, for theoretical reasons, we may observe that the ideal ansatz $\hat{B}_i^k : \mathfrak{R} \rightarrow \mathfrak{R}^2$ along segment k should be expressed in local coordinates as

$$\hat{B}_i^k(\cdot) = (\phi_1^k(\cdot)(1 + \cdot)^{\alpha_k}(1 - \cdot)^{\beta_k}, \phi_2^k(\cdot)(1 + \cdot)^{\alpha_k}(1 - \cdot)^{\beta_k})^T, \quad (66)$$

where ϕ_1^k and ϕ_2^k are polynomials of degree J , J is determined by the precision of the method that will be used, and α_k and β_k are the endpoint singularities of the segment which have been found by the technique explained above.

3.2.2 The Gauss-Jacobi method, the Lobatto-Chebyshev method and crack kink singularity correction

Our integral equations now have the form

$$\begin{aligned} & \sum_{j=1}^{C^i} \frac{1}{\pi} \int_{-1}^1 K_{kj}(t; s) \begin{bmatrix} \phi_1^j(s) \\ \phi_2^j(s) \end{bmatrix} (1+s)^{\alpha_k} (1-s)^{\beta_k} ds \\ &= -C(RIS_i^k + GIS^k(t) + \sum_{d \in P_i} \hat{\sigma}_i^d(\gamma_k(t))) \\ & k = 1, \dots, C^i, -1 \leq t \leq 1. \end{aligned} \quad (67)$$

Ideally, a quadrature scheme based on the Jacobi polynomials should be employed in a situation like this. But, as mentioned already, these are cumbersome to employ, so we seek alternative methods. We thus follow [31] and [32] in rewriting the above equations as

$$\begin{aligned} & \sum_{j=1}^{C^i} \frac{1}{\pi} \int_{-1}^1 K_{kj}(t; s) \begin{bmatrix} \phi_1^j(s)(1+s)^{\alpha_k+1/2}(1-s)^{\beta_k+1/2} \\ \phi_2^j(s)(1+s)^{\alpha_k+1/2}(1-s)^{\beta_k+1/2} \end{bmatrix} (1+s)^{-1/2}(1-s)^{-1/2} ds \\ &= -C(RIS_i^k + GIS^k(t) + \sum_{d \in P_i} \hat{\sigma}_i^d(\gamma_k(t))) \\ & k = 1, \dots, C^i, -1 \leq t \leq 1. \end{aligned} \quad (68)$$

If we make the substitution

$$(\Phi_1^j(s), \Phi_2^j(s)) = (\phi_1^j(s), \phi_2^j(s))(1+s)^{\alpha_k+1/2}(1-s)^{\beta_k+1/2}, \quad (69)$$

we are left with equations in (Φ_1^j, Φ_2^j) all of which have the $(1+s)^{-1/2}(1-s)^{-1/2}$ factor instead of the $(1+s)^{\alpha_k}(1-s)^{\beta_k}$ factor:

$$\begin{aligned} & \sum_{j=1}^{C^i} \frac{1}{\pi} \int_{-1}^1 K_{kj}(t; s) \begin{bmatrix} \Phi_1^j(s) \\ \Phi_2^j(s) \end{bmatrix} (1+s)^{-1/2}(1-s)^{-1/2} ds \\ &= -C(RIS_i^k + GIS^k(t) + \sum_{d \in P_i} \hat{\sigma}_i^d(\gamma_k(t))) \\ & k = 1, \dots, C^i, -1 \leq t \leq 1. \end{aligned} \quad (70)$$

One can now solve these equations using the Lobatto-Chebyshev method, and then multiply the obtained answer by $(1+s)^{-\alpha_k-1/2}(1-s)^{-\beta_k-1/2}$ to obtain the values of ϕ_1^j and ϕ_2^j . It turns out though, that we will never need the actual values of ϕ_1^j and ϕ_2^j , we will only need the integral of these functions, and when we integrate we use the same quadrature that was used when the equations were solved, which involves changing ϕ_1^j and ϕ_2^j back into Φ_1^j and Φ_2^j .

Thus it is not relevant to find ϕ_1^j and ϕ_2^j , but we rather treat Φ_1^j and Φ_2^j as our unknowns. This is of course cheating, since what we have done is that we have assumed that all singularities are of square root size. There is though one endpoint that we can treat appropriately. This is the left endpoint of the surface-breaking segment. We know that there should be no singularity there at all. By performing the above singularity correction at the right endpoint, we can thus assume that the unknown along the first segment is of the form $(\Phi_1^1(\cdot), \Phi_2^1(\cdot))(1 - \cdot)^{-1/2}(1 + \cdot)^{1/2}$. This ansatz produces equations that are best solved by the Gauss-Jacobi method. In the introductory section we also solved this equation using the Lobatto-Chebyshev method after having corrected the left endpoint singularity. This produced fine stress intensity approximations, but the wrong shape at the crack mouth produces an erroneous stress field. We thus discretize the first segment by the Gauss-Jacobi method and the others by the Lobatto-Chebyshev method.

It should be mentioned that of all the integrals in (64), only the ones whos domains are supersets of the collocation points are singular. Thus only a part of the integrals in the whole system of equations are singular integrals. Fortunately, the methods we intend to use works also for regular integral equations, so we can discretize all integrals using only these methods.

Let us denote by N the number of abscissae used on each segment. The integration points $\{s_{GJ}(n)\}_{n=1}^N$, collocation points $\{t_{GJ}(m)\}_{m=1}^N$ and weights $\{W_{GJ}(n)\}_{n=1}^N$ in the Gauss-Jacobi method are defined by

$$\begin{aligned} s_{GJ}(n) &= \cos\left(\pi \frac{2(N-n)+1}{2N+1}\right), n = 1, \dots, N \\ t_{GJ}(m) &= \cos\left(\pi \frac{2(N-m)+1}{2N+1}\right), m = 1, \dots, N \\ W_{GJ}(n) &= \frac{2(1+s(n))}{2N+1}, n = 1, \dots, N, \end{aligned} \quad (71)$$

and the corresponding numbers in the Lobatto-Jacobi method are defined by

$$\begin{aligned} s_{LC}(1) &= -1 \\ s_{LC}(n) &= \cos\left(\pi \frac{N-n}{N-1}\right), n = 2, \dots, N-1 \\ s_{LC}(N) &= 1 \\ t_{LC}(m) &= \cos\left(\pi \frac{2(N-m)-1}{2N-2}\right), m = 1, \dots, N-1 \\ W_{LC}(1) &= \frac{1}{2N-2} \\ W_{LC}(n) &= \frac{1}{N-1}, n = 2, \dots, N-1 \\ W_{LC}(N) &= \frac{1}{2N-2}. \end{aligned} \quad (72)$$

We now apply the Gauss-Jacobi method to approximate the first integral in (70) by a discrete sum, and the Lobatto-Chebyshev method will be used

to discretize the other equations. These sums are linear in the values of the integrands at the integration points, so for every collocation point we have one linear equation in $(\Phi_1^1(s(n)), \Phi_2^1(s(n)))$, $n = 1, \dots, N$. If we were free to collocate anywhere, we could easily produce a determined system, but the approximations of the integrals are valid only at the collocation points. If there is only one segment, we have as many collocation points as integration points, and so we can solve for the unknowns $(\Phi_1^1(s_{GJ}(n)), \Phi_2^1(s_{GJ}(n)))$, $n = 1, \dots, N$. If there are two or more segments, we must supply two side conditions since the Lobatto-Chebyshev supplies one collocation point less than the number of integration points. Such conditions can be derived by requiring single valuedness of the dislocation density at the kinks. The density behaves as a vector, so we can simply rotate both local densities into the same coordinate system and set them equal at the point where the segments meet;

$$\hat{B}_i^{j-1}(1) = \begin{bmatrix} \cos(\theta^j - \theta^{j-1}) & -\sin(\theta^j - \theta^{j-1}) \\ \sin(\theta^j - \theta^{j-1}) & \cos(\theta^j - \theta^{j-1}) \end{bmatrix} \hat{B}_i^j(-1), j = 2, \dots, C^i \quad (73)$$

Since the densities are singular at the kinks, this condition cannot be applied in the above form. Instead we write the condition as

$$\lim_{r \rightarrow 0} \left[\hat{B}_i^{j-1}(1-r) - \begin{bmatrix} \cos(\theta^j - \theta^{j-1}) & -\sin(\theta^j - \theta^{j-1}) \\ \sin(\theta^j - \theta^{j-1}) & \cos(\theta^j - \theta^{j-1}) \end{bmatrix} \hat{B}_i^j(-1+r) \right]_{j=2, \dots, C^i} = 0, \quad (74)$$

If we write $\Phi^j = [\Phi_1^j, \Phi_2^j]^T$ and insert our ansatz

$$\begin{aligned} \hat{B}_i^1(\cdot) &= \Phi^1(\cdot)(1+\cdot)^{1/2}(1-\cdot)^{-1/2} \\ \hat{B}_i^j(\cdot) &= \Phi^j(\cdot)(1+\cdot)^{-1/2}(1-\cdot)^{-1/2}, j = 2, \dots, C^i \end{aligned} \quad (75)$$

we get

$$\begin{aligned} \lim_{r \rightarrow 0} \left[\frac{1}{r^{1/2}} (\Phi^1(1-r) \cdot (2-r)^{1/2} - R^1(R^2)^T \Phi^2(-1+r) \cdot (2-r)^{-1/2}) \right] &= 0 \\ \lim_{r \rightarrow 0} \left[\frac{1}{r^{1/2}} (\Phi^j(1-r) \cdot (2-r)^{-1/2} - R^{j-1}(R^j)^T \Phi^j(-1+r) \cdot (2-r)^{-1/2}) \right] &= 0, \\ & j = 3, \dots, C^i \end{aligned} \quad (76)$$

and consequently

$$\begin{aligned} \lim_{r \rightarrow 0} \left[\Phi^1(1-r) \cdot (2-r)^{1/2} - R^1(R^2)^T \Phi^2(-1+r) \cdot (2-r)^{-1/2} \right] &= 0 \\ \lim_{r \rightarrow 0} \left[\Phi^{j-1}(1-r) \cdot (2-r)^{-1/2} - R^{j-1}(R^j)^T \Phi^j(-1+r) \cdot (2-r)^{-1/2} \right] &= 0, \\ & j = 3, \dots, C^i \end{aligned} \quad (77)$$

which is the same thing as

$$\begin{aligned} \Phi^1(1)2^{1/2} - R^1(R^2)^T \Phi^2(-1)2^{-1/2} &= 0 \\ \Phi^{j-1}(1)2^{-1/2} - R^{j-1}(R^j)^T \Phi^j(-1)2^{-1/2} &= 0, \\ & j = 3, \dots, C^i \end{aligned} \quad (78)$$

The side conditions are thus expressed by the equations

$$\begin{aligned} 2\Phi^1(1) - R^1(R^2)^T \Phi^2(-1) &= 0 \\ \Phi^{j-1}(1) - R^{j-1}(R^j)^T \Phi^j(-1) &= 0, j = 3, \dots, C^i. \end{aligned} \quad (79)$$

To apply the first one of these conditions, we have to extrapolate the known values of Φ^1 on the first segment, just as we did in section 1.3.3.

An alternative way of defining the side conditions is by noting that (69) forces the unknowns to vanish at the endpoints. (This is dependent on the fact that $\alpha_k + 1/2$ and $\beta_k + 1/2$ are always greater than zero, which follows from William's analysis.) As we evaluate the code in section 4.1, one observation is that the choice of side condition has a minor effect on the computed stress intensities, but our approach is slightly better in most cases.

Applying the Gauss-Jacobi method and Lobatto-Chebyshev method and collocating gives

$$\begin{aligned} & \sum_{n=1}^N W_{GJ}(n) K_{k1}(t; s_{GJ}(n)) \Phi^j(s_{GJ}(n)) \\ & + \sum_{j=2}^{C^i} \sum_{n=1}^N W_{LC}(n) K_{kj}(t; s_{LC}(n)) \Phi^j(s_{LC}(n)) \\ & = -C(RIS_i^k + GIS^k(t) + \sum_{d \in P_i} \hat{\sigma}_i^d(\gamma_k(t))), \\ & k = 1, \dots, C^i, \end{aligned} \quad (80)$$

where $t \in \{t_{GJ}\}$ for $k = 1$ and $t \in \{t_{LC}\}$ for $k = 2, \dots, C^i$. By introducing the vector

$$\Phi = \begin{bmatrix} \Phi^1(s_{GJ}(1)) \\ \Phi^1(s_{GJ}(2)) \\ \vdots \\ \Phi^1(s_{GJ}(N-1)) \\ \Phi^1(s_{GJ}(N)) \\ \Phi^2(s_{LC}(1)) \\ \vdots \\ \Phi^2(s_{LC}(N)) \\ \vdots \\ \Phi^{C^i}(s_{LC}(N-1)) \\ \Phi^{C^i}(s_{LC}(N)) \end{bmatrix} \quad (81)$$

and incorporating the side conditions into the system of linear equations, we can write it as a $2NC^i \times 2NC^i$ matrix equation

$$A\Phi = -Cf, \quad (82)$$

where f is a vector containing the values of the load stresses at the collocation points together with the righthand sides of (79). We may now let a computer assemble the system (82) by using the formulas (80) and (79).

3.3 Solving the resulting linear system

Solving the linear system (82) is not a major issue. As we will see in chapter (4), the systems that are considered are rarely larger than say 500×500 , so solving by LU-factorization is sufficient. It should be noted that the system (82) is full, which further emphasizes that there is not much computational time to save by implementing an iterative solver. Furthermore, time efficiency of the code is not central in this kind of simulation.

3.4 The problem of plasticity induced crack closure

In chapter (2) we simply built our model upon the assumption that the crack is open along its entire length during the whole load cycle. It is not easy to know a priori what kind of loading and geometries that implies the validity of this assumption. Indeed, even a pure mode I crack subjected to a tensile load may close due to the influence of the dislocations that are left

behind in a 'wake' as the crack grows. This phenomenon is termed *plasticity induced crack closure* (see [12] for a discussion of this concept), and if it occurs, the simulation is no longer valid. To check that closure does not occur, one computes the crack opening displacement along the crack every time one calculates B^i , and make sure that it is strictly positive at a set of selected points on the crack. As we have seen, this amounts to checking that the integral of the dislocation density from the crack tip is strictly positive. Formally, we should require that

$$COD^j(r) = COD^j(1) + \int_0^r \hat{B}_i^j(1-s)ds > 0, \quad j = 1, \dots, C^i, 0 < r < 2, \quad (83)$$

where $COD^j(1)$ is the crack opening displacement at $\gamma_j(1)$ given rise to by segment number $j+1$. It will be noticed in chapter (5) that the requirement that the crack is open is not always satisfied, for in some cases negative stress intensities appear. In this cases one should be aware of the fact that the simulation is only approximate.

3.5 Computing stress intensity factors

The same formulas for the approximate stress intensity factors as those used in section 1.3.3 holds, i.e. the formulas (46) and (47), but now the crack length a should be replaced by the length of the last crack segment. Note also that the polynomial part of the density B_i should be evaluated *in local coordinates* at the crack tip. Since our solution vector is already expressed in local coordinates, we do not have to transform it. We must also take care to apply formula (46) only when there is only one crack segment, and use formula (47) otherwise. As before, the application of (46) must be preceded by an extrapolation.

4 An implementation of the technique

Based upon the technique described in the previous chapter, we have written a computer code that performs the simulation of the fatigue growth of a microcrack. The code consists of a few routines that assembles the system matrix and load vector, an object oriented part for the treatment of the free dislocations, and a simple visualization. The code was written in MATLAB except for a part of the computational kernel that was implemented in C.

In this chapter we evaluate our model and the associated technique by applying them to crack problems which previously have been successfully analyzed by other investigators.

The investigations carried out in this chapter (except for section 4.1) are meant to display how the code behaves qualitatively, so in many cases we mention nothing about the units or values of the parameters.

4.1 Evaluating the code by comparing stress intensity approximations with handbook tables

In this section, stress intensity approximations computed by our code is compared to the values tabulated in [33].

The stress intensity factors for single segment crack configurations converge well, with somewhat lesser accuracy when the angle with the boundary is small. This lack of precision for very slant cracks seems to be due to an inherent weakness of the solution technique. Even so, for cracks that make an angle of 40 degrees or more with the boundary we achieve a relative error below one percent using only $N \leq 10$. This strongly contrasts with the crack that makes the angle 10 degrees with the boundary, and for which we have to set $N = 140$ to achieve a relative error below 10 percent.

We also try some crack configurations where the crack has a kink, i.e. two inclined segments. The code efficiently computes accurate values of the stress intensities. In most cases we only need $N = 10$ to achieve a one percent relative error. In figure 11 we display the convergence for a crack that has initiated in shear at an angle of 45 degrees with the boundary, whereupon it turns orthogonal to it, and thus is a pure mode I crack. The lengths of the crack segments are $0.25\sqrt{2}$ and 0.75 respectively. In this case we have $K_{II} = 0$ and $K_I = 1.121\sigma_\infty\sqrt{\pi}$.

By studying the convergence of these testproblems we have learned that very little accuracy is gained from increasing N when N is greater than 30,

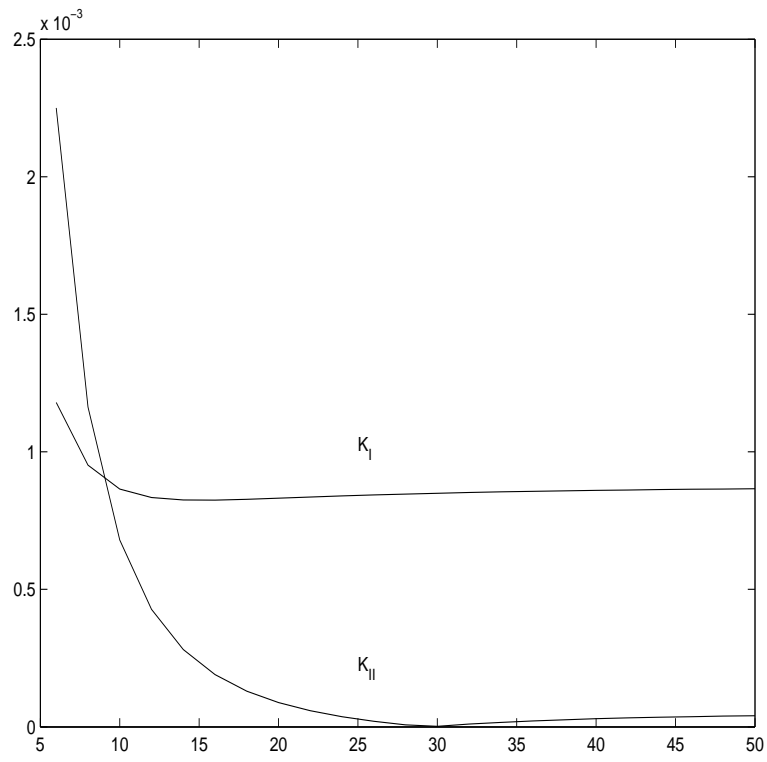


Figure 11: The error in K_I and K_{II} for a crack with a kink versus the number of abscissae used on each segment.

which is verified by figure 11. Thus there is no use in considering system matrices A that are of very great dimensions.

4.2 Evaluating the code by examining stress field approximations

To convince ourselves that the stress fields are also well approximated, we plot in figure 12 and 13 the shear stress field along the global horizontal axis around a kinked crack. The collocation points at the crack line can actually be distinguished, so we guess that a greater value of N is needed to obtain a good approximation of the stress field than is needed to obtain the stress intensities alone.

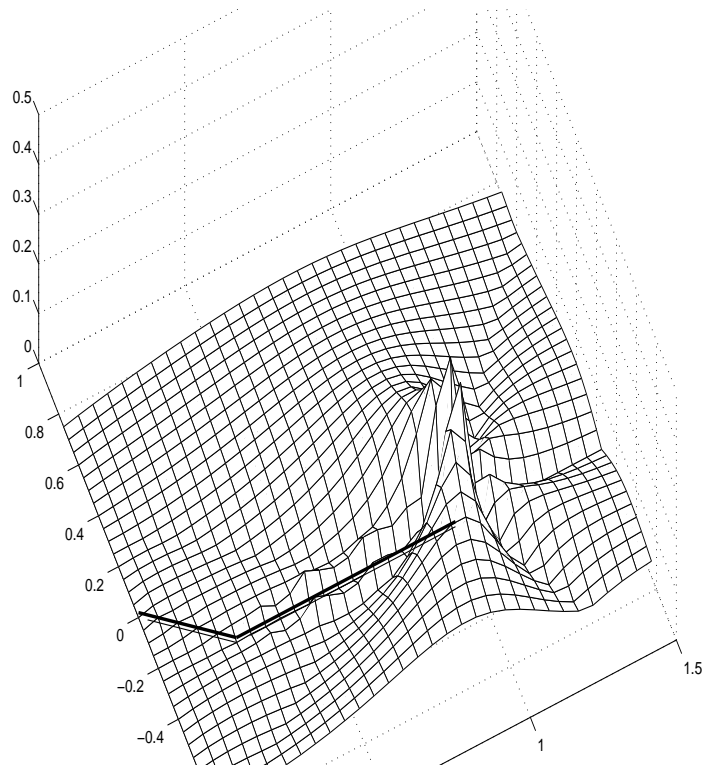


Figure 12: Using $N = 15$ and a course grid for plotting.

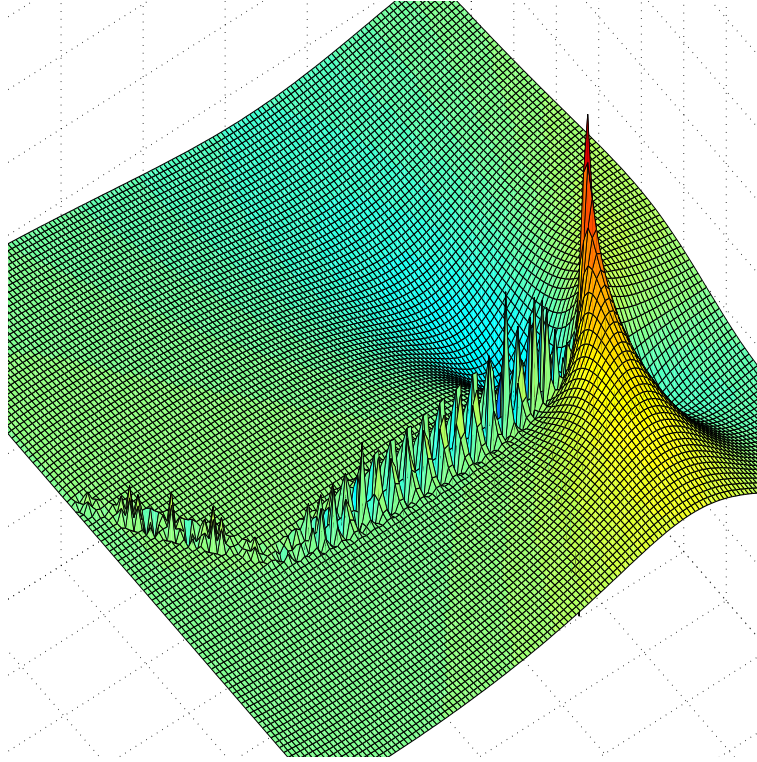


Figure 13: Using $N = 30$ and a fine grid for plotting. The upwards and downwards spikes at the crack tip verifies that the shear stress field has a singularity.

4.3 Examining the effects of dislocations on the stress intensity

We now investigate how a dislocation in front of the crack tip affects the stress intensity at the crack tip. More precisely, we examine straight edge cracks with dislocations with normalized burgers vectors parallel to the crack tip line and placed at different distances ahead of the crack tip. Our code shows the same qualitative results for all straight edge cracks, so let us concentrate on the edge crack that was also treated in section 1.3.3, but now let the crack be of length 10. As we have seen, the K_{II} -factor is zero if there are no dislocations present in the grain, and by looking at figure 14, we understand that we can expect the value of this factor to be decreased by a dislocation in front of the crack tip whose burgers vector points in the direction of the crack tip. This is in fact also the case, which can be seen from figure 15. If we let the burgers vector point in the opposite direction, the plot is reflected in the x-axis. Furthermore, the code shows (as we expect) that the K_I factor is unaffected by such a dislocation.

4.4 Evaluating the crack growth model

It is known that cracks tend to turn so that they grow in mode I, independently of how they are initiated. To verify this behaviour, we study the growth of a crack of length one that makes an angle of 45 degrees with the boundary. For now, we set $K_e = \infty$, so no dislocations will be emitted. Also we let all crack increments be of length one, and we define a large set of glide planes so that the transition into mode I growth is not instantaneous. Still, it can be seen from figure 16 that the crack has turned into a mode I crack after only 3 load steps.

Even in cases where the crack is assumed to have initiated in a more unrealistic way, as in figure 17, our crack growth model predicts that the crack will turn into mode I. Thus we are confident that our crack growth model is realistic.

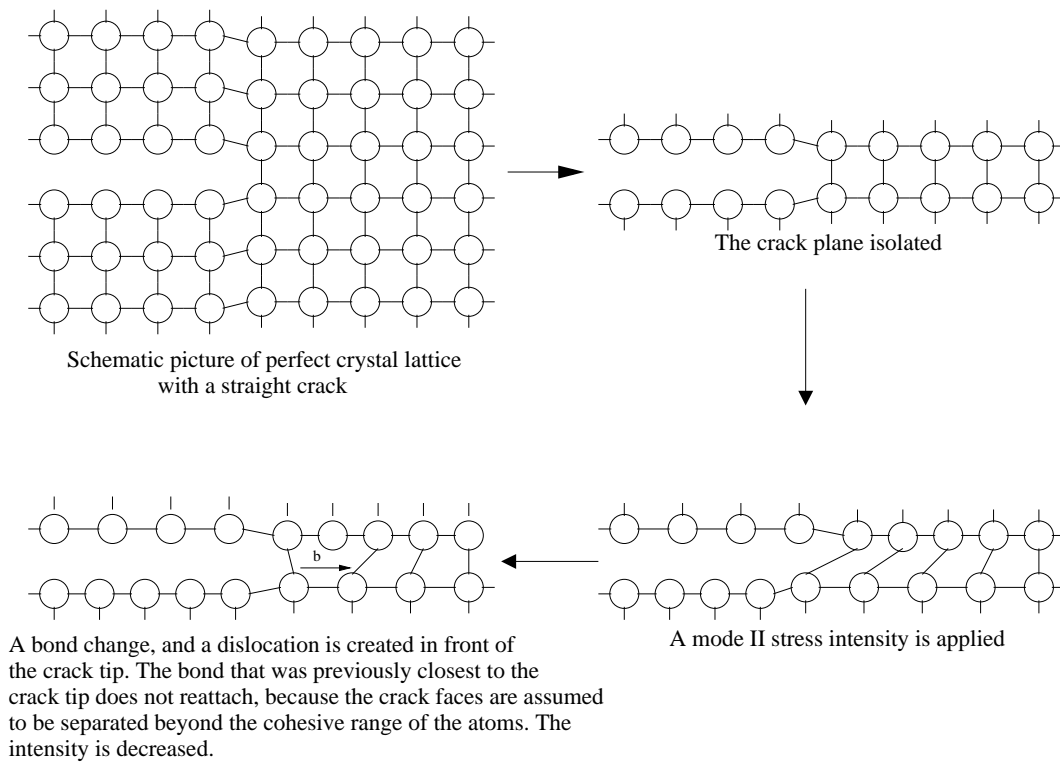


Figure 14: The emission of a glide dislocation onto the crack plane.

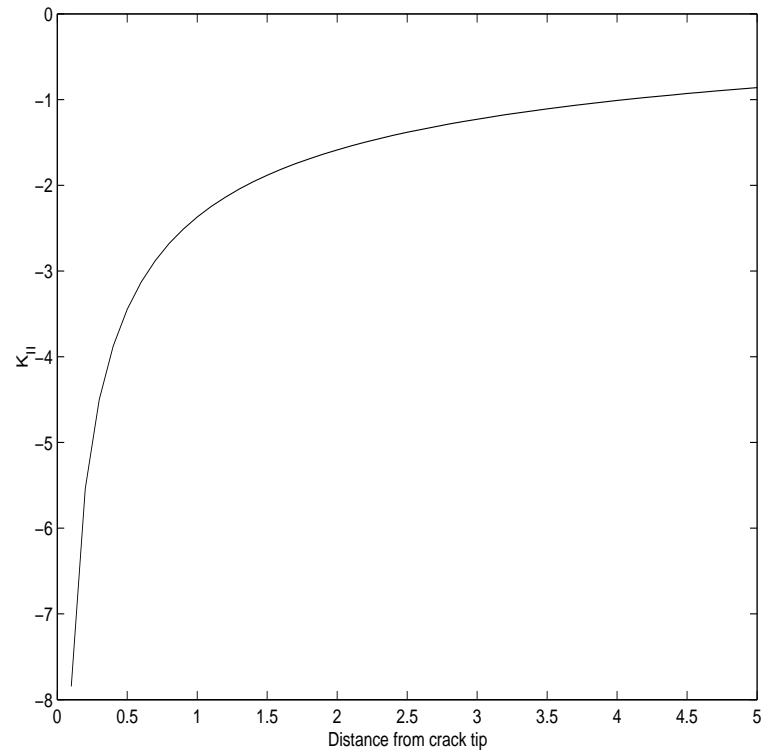


Figure 15: The effect of a dislocation in front of the crack tip.

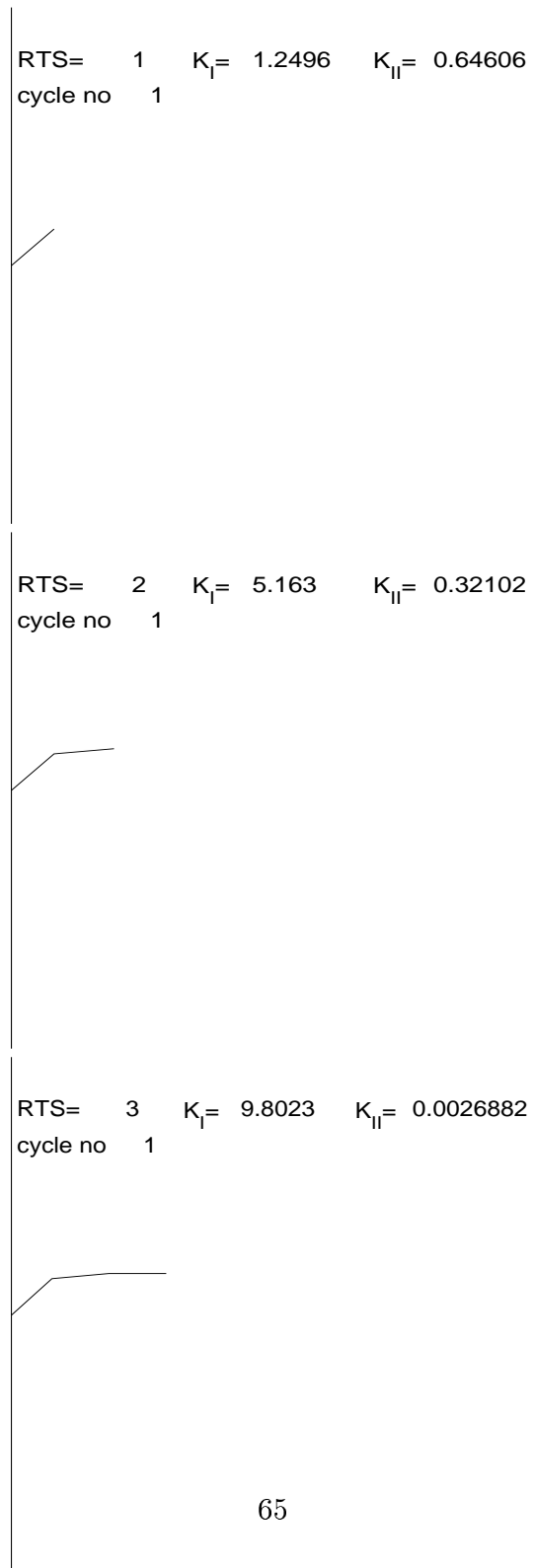


Figure 16: The growth of a slant crack. RTS stands for Remotely induced Tensile Stress.

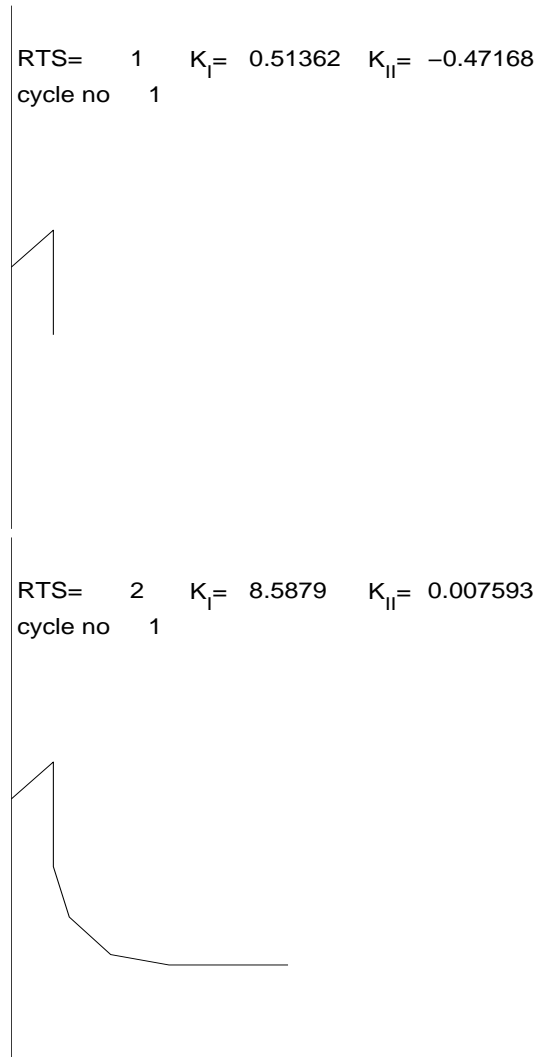


Figure 17: The growth of an oddly initiated crack. The load is increased from 1 to 4, then decreased to 2.

5 Applications of the implementation

Our experience from the previous chapter shows that many general conclusions can be obtained by studying pure mode I cracks, and so we do in the first two applications. In the third application below, we study a more general problem.

In all problem formulations below, we define one unit of length (L) such that $1L = 1\mu m$. The intrinsic burgers vector of the lattice is of order $1nm$, but its actual size will not matter, since we for computational reasons in many cases choose to emit 'superdislocations' with burgers vectors whose sizes are greater than the size of the intrinsic burgers vector. This we can do because the many smaller dislocations can be added together and treated as one dislocation with burgers vector equal to the sum of the many smaller burgers vectors, as explained in section 1.3.1.

5.1 A first application; No grain boundaries

In our first application, we study the behaviour of a microcrack in a material without a grain structure. We choose to emit dislocations with burgers vectors b such that $\|b\| = 0.1L = 10^{-7}m$. The values of the parameters are somewhat inspired by the choices made in [15]. Because of our different choice of $\|b\|$, we cannot practically use the parameter values used in [15] since the remote tensile loading required to induce the critical stress intensity for dislocation emission is so great that it alone induces a shear stress on the glide planes that is greater than the critical shear stress for dislocation glide. So, if we use the suggested parameter values and the amplitude of the loading is low, no emission will occur, and if the amplitude is not that low, the free dislocations will glide towards infinity. None of these situations are very interesting, so we avoid them both by using a higher material friction. The intrinsic burgers vector of the material is of order $0.001L$, so our superdislocations can be thought of as groups of approximately 100 elementary dislocations. Thus it seems reasonable to increase the critical resolved shear stress by a factor 100. There are many more parameter values that need to be chosen in order to run the simulation, and these are all listed below:

Material and load parameters

$$\begin{aligned}
C_0 &= 1 \\
\Gamma_0^1 &= (0, 0)L \\
\Gamma_0^2 &= (20, 0)L \\
R &= \{-70.5deg, 0deg, 70.5deg\} \\
\mu &= 80 \cdot 10^{-3} N/L^2 \\
\nu &= 0.3 \\
\tau_{crit} &= \frac{\mu}{20} N/L^2 \\
K_e &= \cos(70.5) \sin(70.5) \cdot 0.4 \cdot \mu \cdot \sqrt{\|b\|} \frac{N}{L\sqrt{L}} \\
\sigma_{min}^\infty &= 3 \cdot 10^{-3} N/L^2 \\
\sigma_{max}^\infty &= 4 \cdot 10^{-3} N/L^2
\end{aligned}$$

Technical parameters

$$\begin{aligned}
\text{loadstep} &\text{ is } \frac{\sigma_{max}^\infty - \sigma_{min}^\infty}{10} \\
N &= 30 \\
c &= 1 \\
tol &= 0.1 \\
ba &= 1 \\
be &= 1
\end{aligned}$$

In figures 18 through 24, we can follow the simulation of the crack growth. The behaviour we see is quite typical; The load is increased and dislocations are emitted, whereupon they glide away from the crack tip. The load is then further increased, and more dislocations are emitted. This continues until enough shielding of the crack tip has been achieved. No further crack growth occurs, since no more dislocations are emitted. Note that the crack would not have ceased to grow if we had not used a high material friction, since the dislocations then would have glided towards infinity and not produce any shielding effect.

By this application we have verified that a microcrack in a homogenous material with a relatively high material friction subjected to a load that induces a critical stress intensity, is predicted to stop growing. On the other hand, if the material friction is too low, the crack will continue to grow.

From this application we have also learned that the convergence in the EAD-iteration is slow, and that the EAD-positions are sensitive. It is for these reasons that we use the slightly altered glide condition and relatively high value of the parameter *tol*. Simulations have shown that a lower value

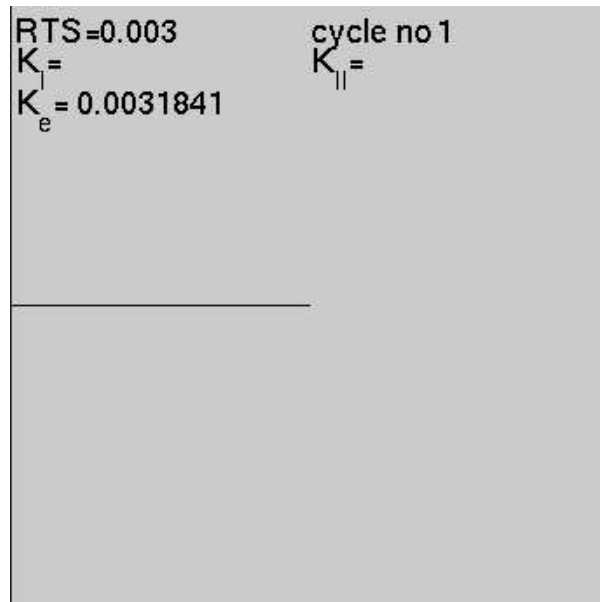


Figure 18: The initial crack

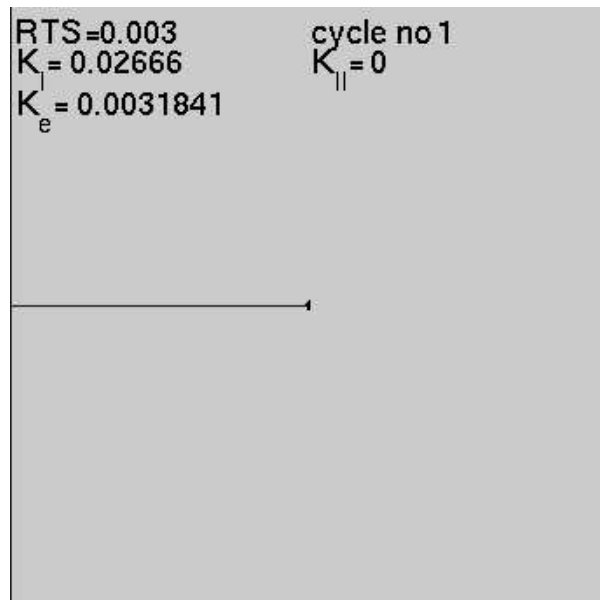


Figure 19: Due to the stress concentration around the crack tip, a pair of dislocations are emitted and the crack propagates.

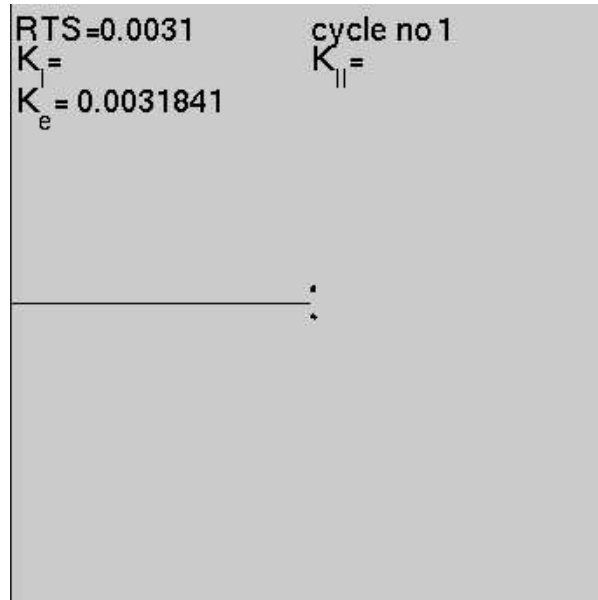


Figure 20: The dislocations glide to their EAD positions.

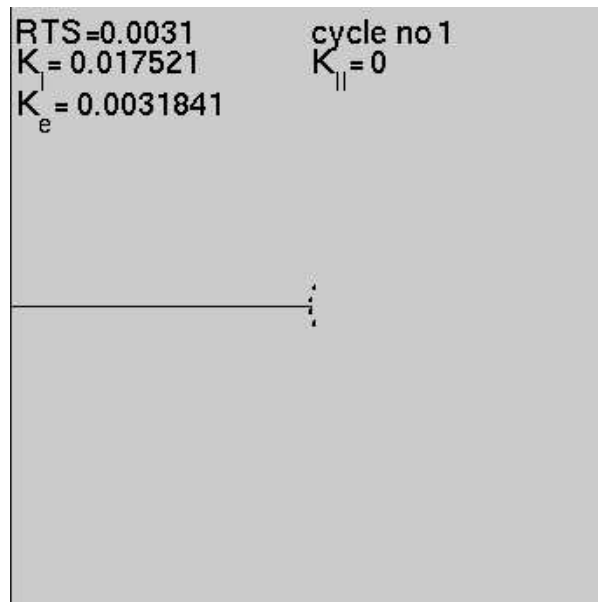


Figure 21: The load is increased and the dislocation cloud grows.

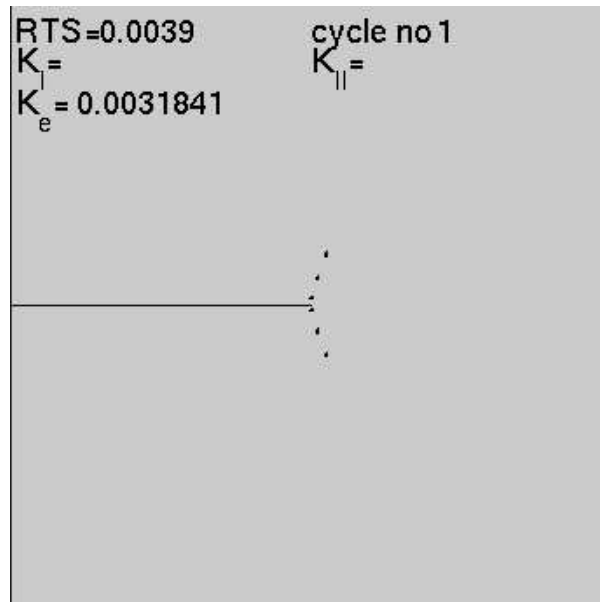


Figure 22: We can now distinguish the glide planes.

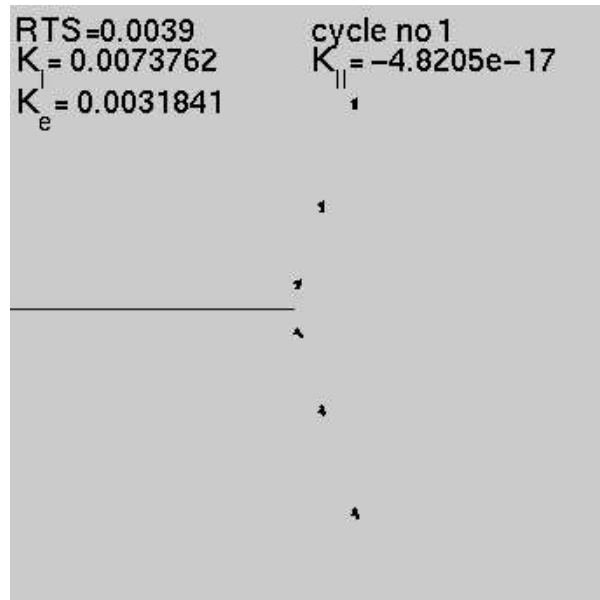


Figure 23: By zooming in on the crack tip, we clearly see the discrete nature of the plasticity.

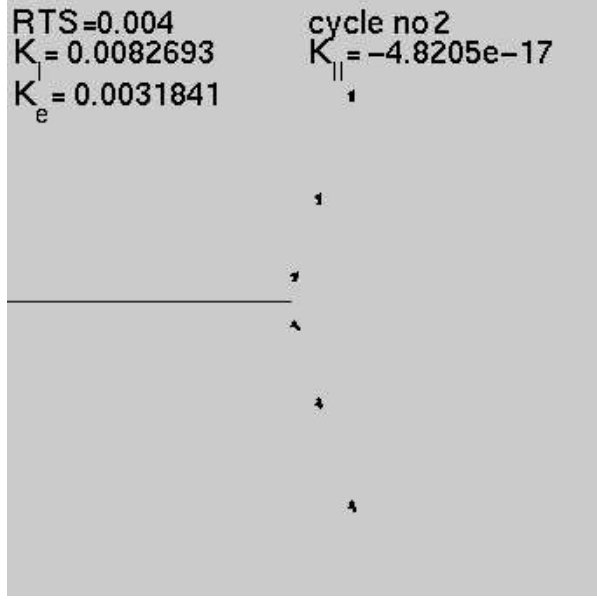


Figure 24: A further zoom. After one full load cycle enough shielding has been achieved to prevent crack growth during the following cycles.

of tol does not have any substantial influence on the EAD positions.

In this case, the crack growth stopped after only one load cycle. It might happen though that too much shielding is produced by the emitted dislocations, which makes the stress intensity become negative and dislocations with opposite direction burgers vectors are emitted. These raise the stress intensity and thus lower its magnitude. This situation has occurred in figure 25. One should keep in mind that in such cases the crack closure occurs along some parts of the crack, so the results are not reliable.

Let us also make a simulation in which we use $\|b\| = 0.25nm = 0.25mL$ and the exact parameter values given in [16], with the exceptions that the values of the remote loading is kept positive to prevent crack closure, and a factor $1/2$ is incorporated into the value for the critical stress intensity to accomodate to our alternative emission model. The values are chosen with the aim of simulating the crack growth in a base centered cubic crystal lattice. The changes in the parameter values are:

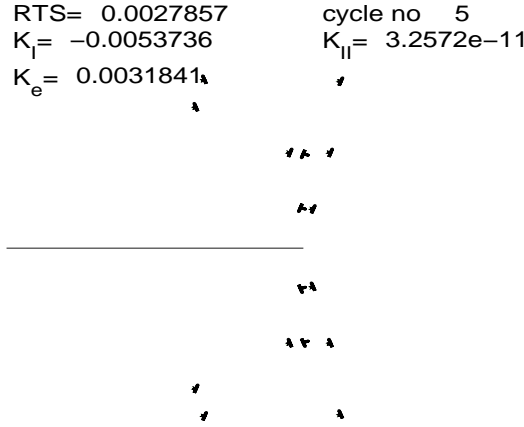


Figure 25: Due to the negative stress intensity, dislocations with burgers vectors pointing towards the crack tip have been emitted.

Material and load parameters

$$\begin{aligned}
 R &= \{-45deg, 0deg, 45deg\} \\
 \mu &= 80 \cdot 10^{-3} N/L^2 \\
 \nu &= 0.3 \\
 \tau_{crit} &= \frac{\mu}{2000} N/L^2 \\
 K_e &= (1/2) \cdot 0.4 \cdot \mu \cdot \sqrt{\|b\|} \frac{N}{L\sqrt{L}} \\
 \sigma_{min}^{\infty} &= 0 \\
 \sigma_{max}^{\infty} &= \frac{1.25 \cdot 2 \cdot K_e}{1.1215 \cdot \sqrt{\pi i * 20}}
 \end{aligned}$$

Technical parameters

$$\begin{aligned}
 \text{loadstep} &\text{ is } \frac{\sigma_{max}^{\infty} - \sigma_{min}^{\infty}}{10} \\
 N &= 50 \\
 c &= 2 \\
 tol &= 0.03 \\
 ba &= 10 \\
 be &= 10
 \end{aligned}$$

The results of this simulation can be seen in figures 26 through 33.
In [16], crack propagation is never prevented because dislocations are an-

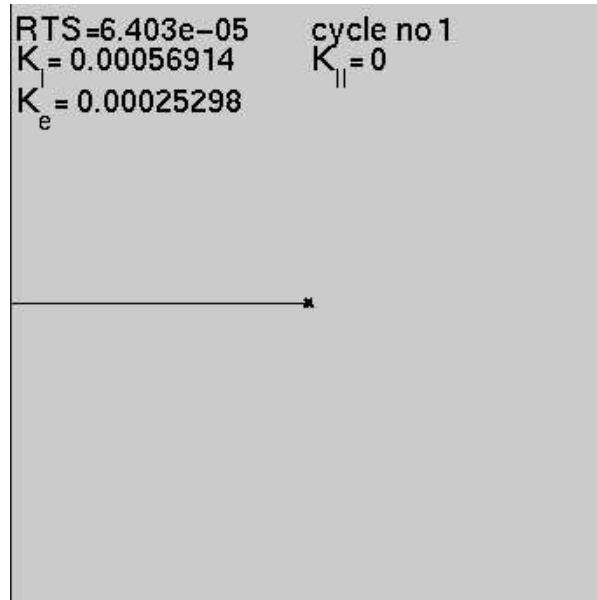


Figure 26: The first dislocation pair is emitted during load cycle number one.

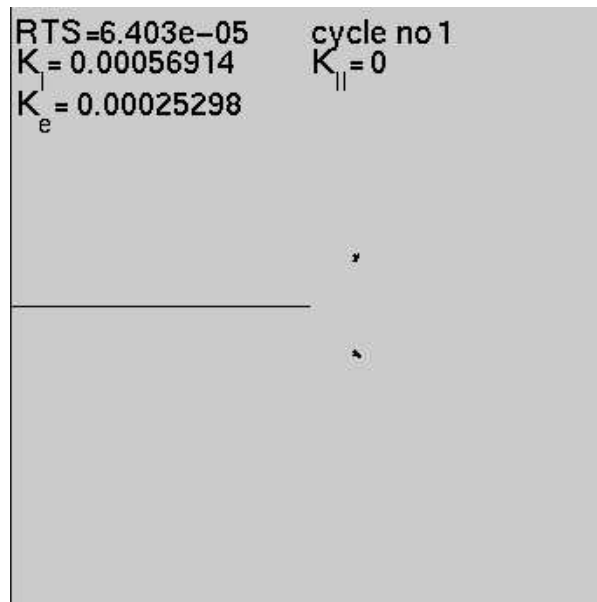


Figure 27: The EAD positions.

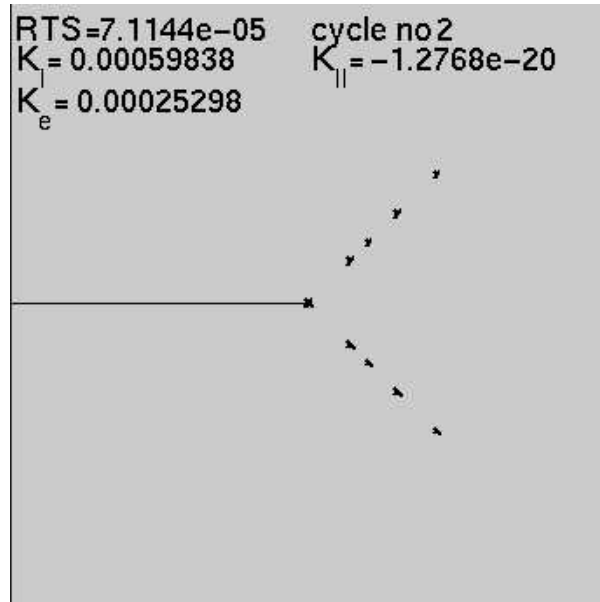


Figure 28: Emission at the peak of load cycle number two.

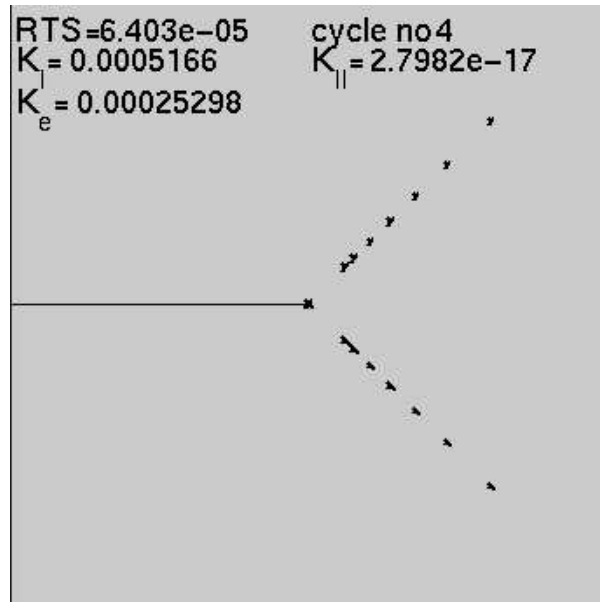


Figure 29: During load cycle number four, a pair of dislocations is emitted...

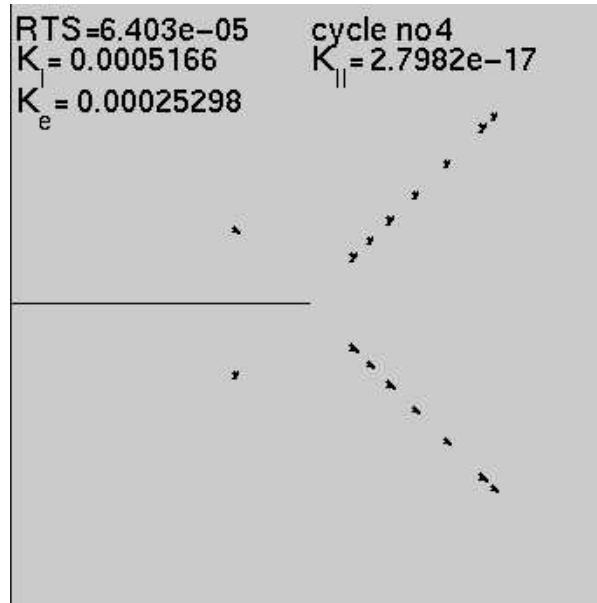


Figure 30: ...that glides in an unexpected direction. Even though the stress intensity at the crack tip is positive, the shear stress along the glide planes at ten burgers vectors in front of the crack tip has the opposite sign.

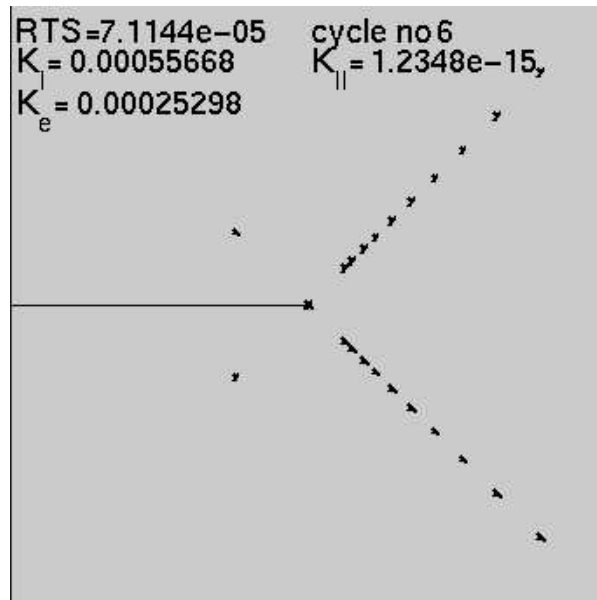


Figure 31: Dislocations are also emitted at the peak of load cycle number six.

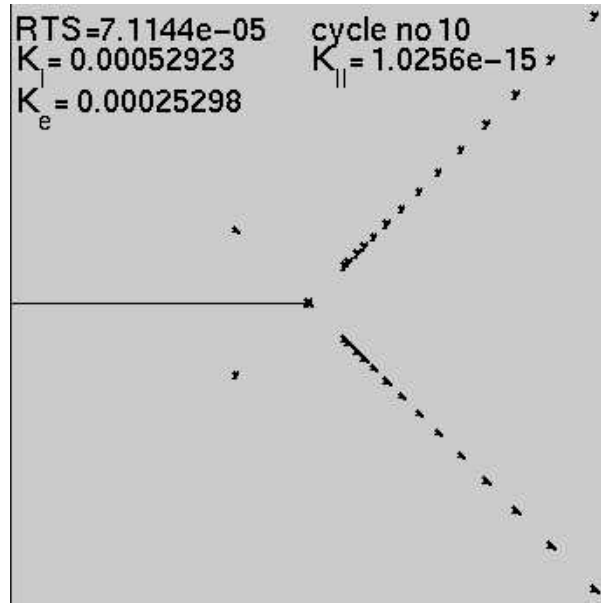


Figure 32: The last emission occurs at the peak of load cycle number ten. No more emission or glide occurs during the following load cycles.

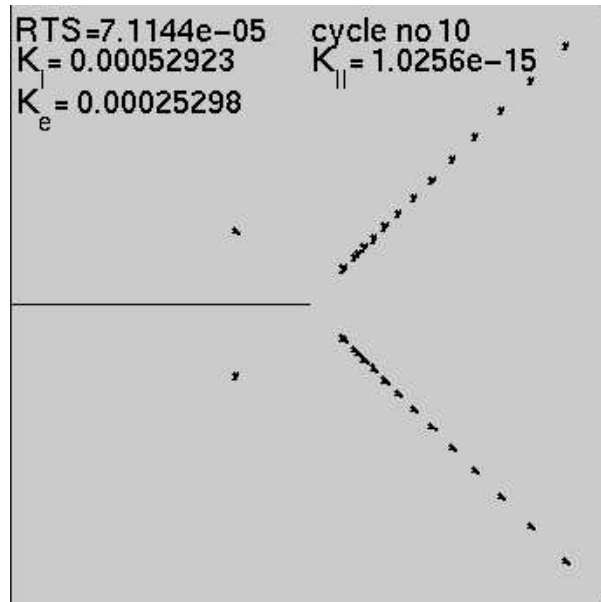


Figure 33: The final configuration. The total crack increment is approximately 40nm.

nihilated during the compressive loading sequence, thus lowering the shielding. In our case, the shielding increases until the crack is brought to a stop. So, It seems that the component's ability of resisting fatigue is better in the case when only a tensile load, and not a compressive load, is applied.

5.2 A second application; Simple grain boundaries

In the previous section we obtained results for cracks in a material without a grain structure. We now introduce grain boundaries with the intent of investigating how well these act as barriers for dislocation glide. If the dislocation does not glide too far, it most probably will shield the crack tip and prevent further crack growth, so the actual aim is to investigate how well the grain boundaries work as barriers for crack growth.

In this application we model the boundaries by a simple sequence of dislocation dipoles. A detail of the dipole constellation that models the grain boundaries is depicted in figure 34, and the whole grain with the initial crack can be seen in figure 35. The grain is not symmetric due to the non-symmetric boundaries. It can be seen that the dipoles are parallel to each other and of greatly varying strengths. Specifically, the lengths are approximately $0.2L$, and the strengths (lengths of burgers vectors) of the stronger dipoles are $3L$, and the strengths of the weaker dipoles are $0.001L$. The strengths of the stronger dipoles are unrealistically great, because the influence of any weaker dipoles is too low to have any considerable effect on the motions of the free super-dislocations. In the next section we will consider the motions of weaker dislocations (not superdislocations), and then the strenghts of the boundary dipoles will be more realistic, but for now well consider a scaled problem.

The grain is of size $20L$, so it is not appropriate to let the initial crack be of length $20L$ as in the previous section. Instead we let the crack be of length $(20/3)L$, and increase the load amplitude by a factor $\sqrt{3}$, so that we would have obtained the same stress intensities as before if there were no grain boundaries. In figures 36 through 47 we can follow the simulation of the fatigue process for the crack problem with the paramater set:

Material and load parameters

$$\begin{aligned}
C_0 &= 1 \\
\Gamma_0^1 &= (0, 0)L \\
\Gamma_0^2 &= (20/3, 0)L \\
R &= \{-70.5deg, 0deg, 70.5deg\} \\
\mu &= 80 \cdot 10^{-3} N/L^2 \\
\nu &= 0.3 \\
\tau_{crit} &= \frac{\mu}{2000} N/L^2 \\
K_e &= \cos(70.5deg) \sin(70.5deg) \cdot 0.4 \cdot \mu \cdot \sqrt{\|b\|} \frac{N}{L\sqrt{L}} \\
\sigma_{min}^\infty &= \sqrt{3} \cdot 3 \cdot 10^{-3} N/L^2 \\
\sigma_{max}^\infty &= \sqrt{3} \cdot 4 \cdot 10^{-3} N/L^2
\end{aligned}$$

Technical parameters

$$\begin{aligned}
\text{loadstep} &\text{ is } \frac{\sigma_{max}^\infty - \sigma_{min}^\infty}{5} \\
N &= 40 \\
c &= 10^{-2} \\
tol &= 0.1 \\
ba &= 2 \\
be &= 1
\end{aligned}$$

Using this parameter set without grain boundaries would make all emitted dislocations glide towards infinity and the crack would not cease to grow.

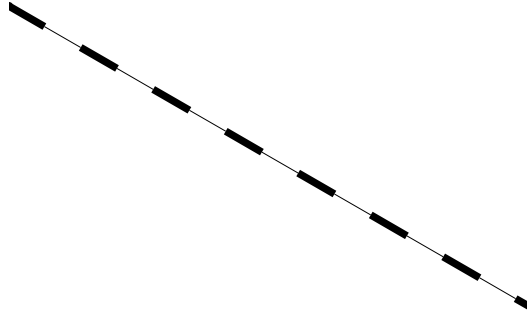


Figure 34: Detail of the grain boundary of the second application.

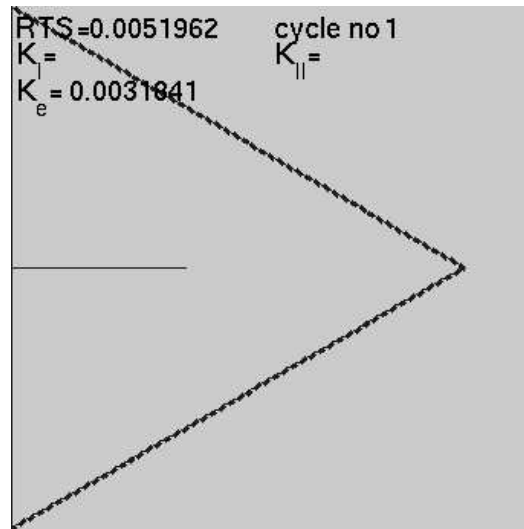


Figure 35: The grain and the initial crack in the second application.

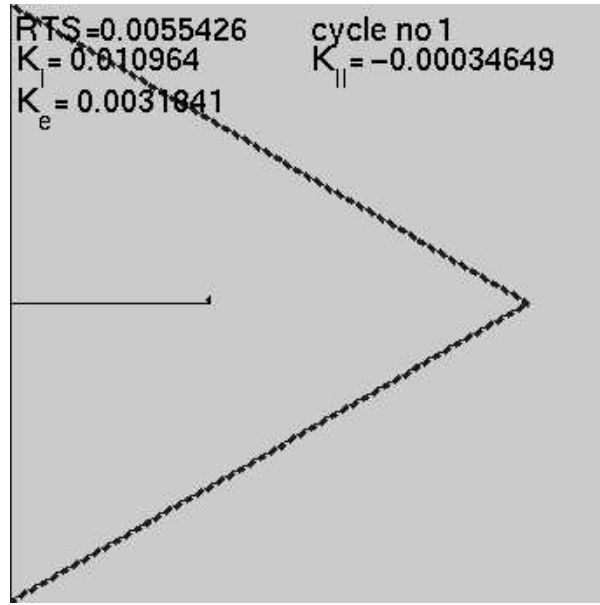


Figure 36: After a few loadsteps the stress intensity exceeds its critical value and a single dislocation is emitted. The crack increments.

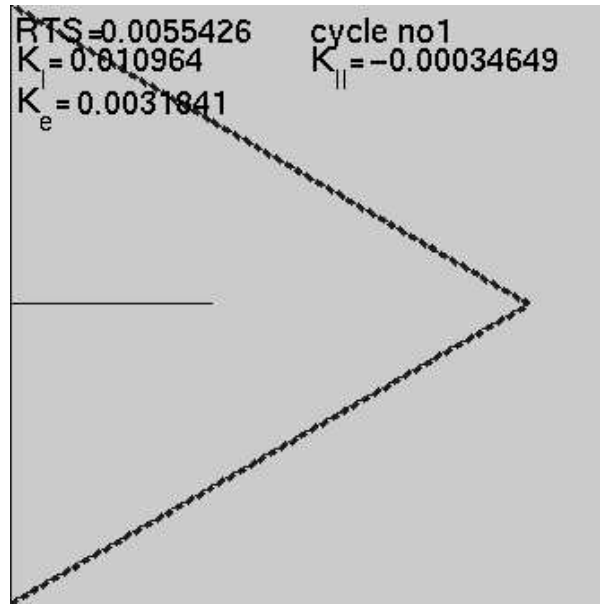


Figure 37: The stress along the glide plane is not high enough for the dislocation glide to be initiated, so the emitted dislocation is at once annihilated by the crack tip.

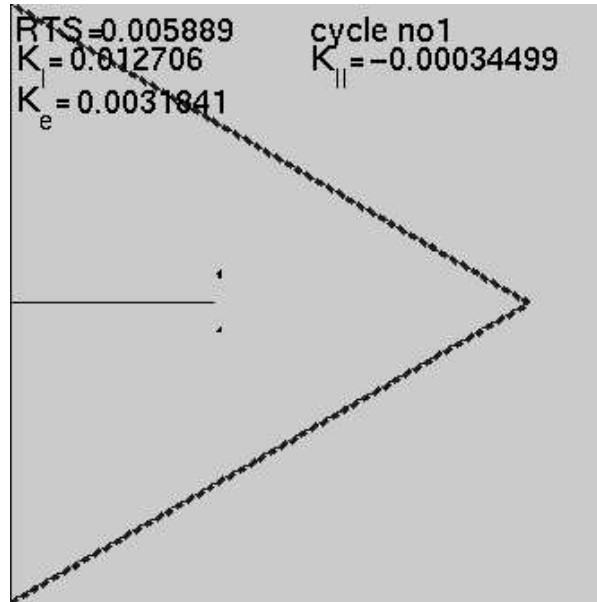


Figure 38: As the load is increased, a dislocation pair is emitted.

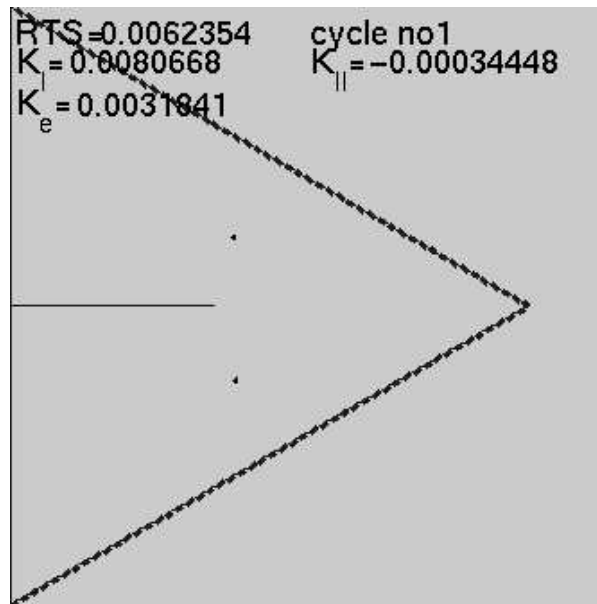


Figure 39: The dislocations have glided to their EAD positions.

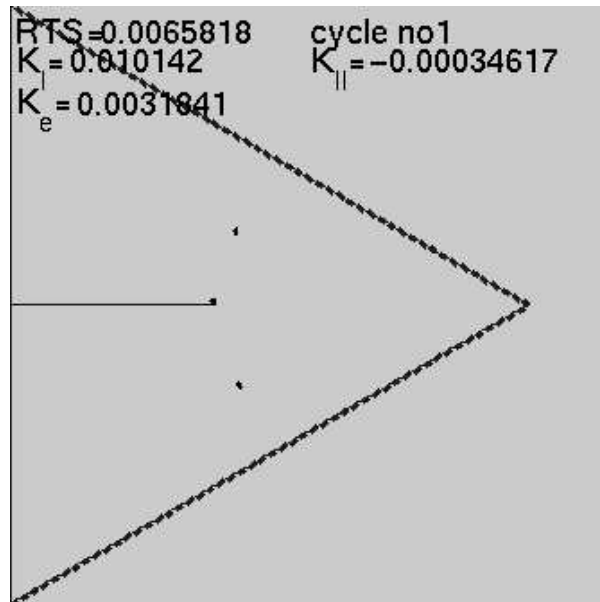


Figure 40: After a further increase in load, another dislocation is emitted...

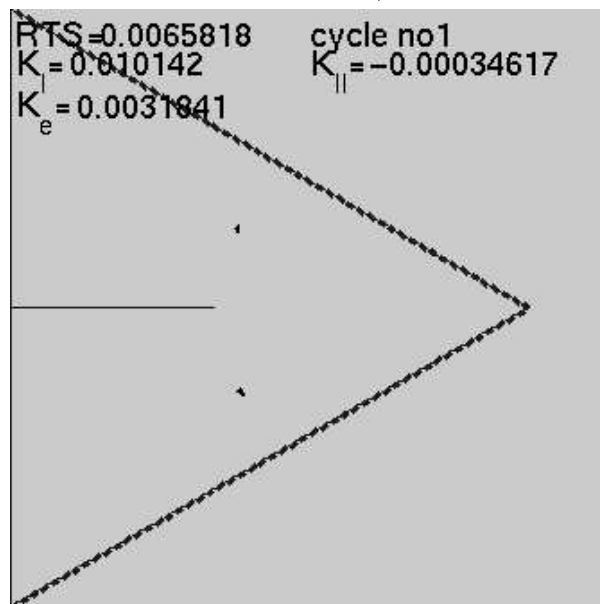


Figure 41: ...but is immediately annihilated.

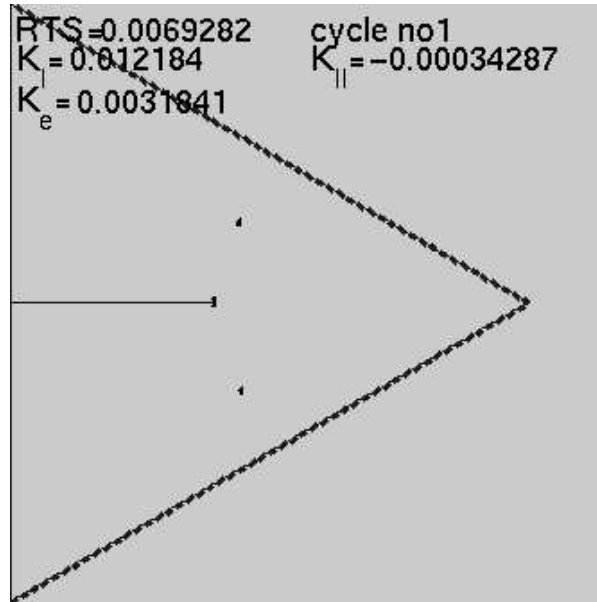


Figure 42: During the next load step another dislocation pair is emitted.

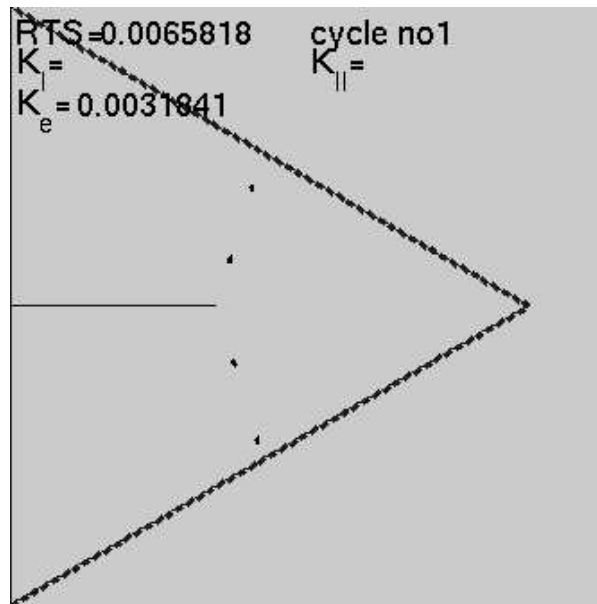


Figure 43: The dislocations glide away from the crack tip.

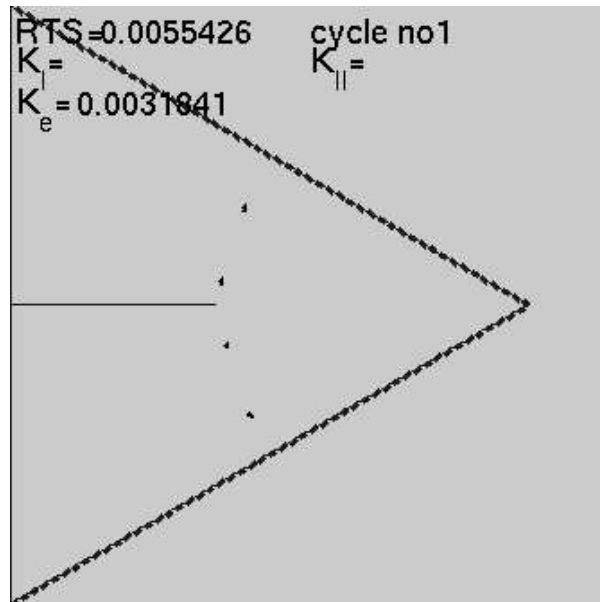


Figure 44: Due to the influence of the grain boundaries, the dislocations glide back towards the crack tip as the load is decreased!

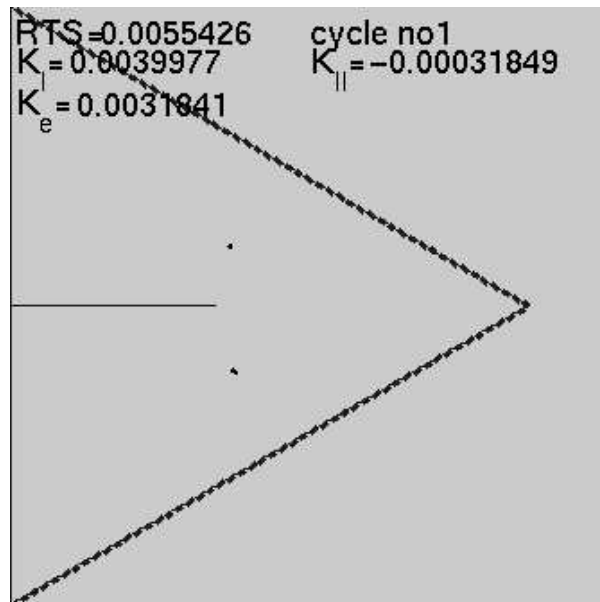


Figure 45: The innermost pair is annihilated!

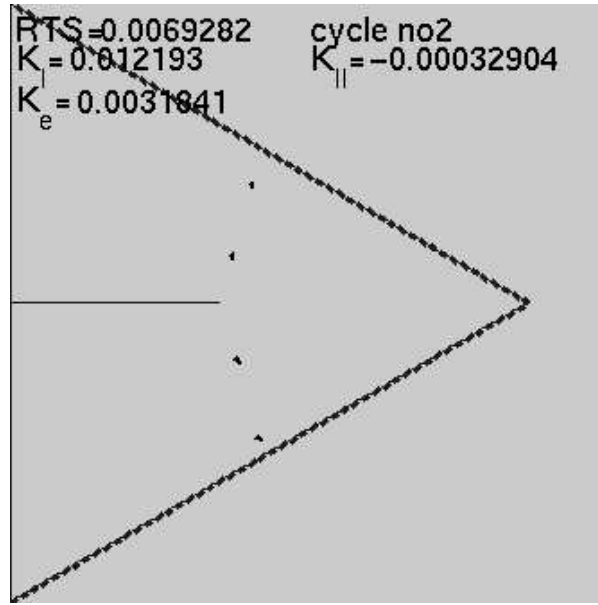


Figure 46: Approximately the same configuration is obtained at the peak of load cycle number two as at the peak of load cycle one. The slip bands of the parallel dislocations are now further apart, because the crack has grown during the loading sequence.

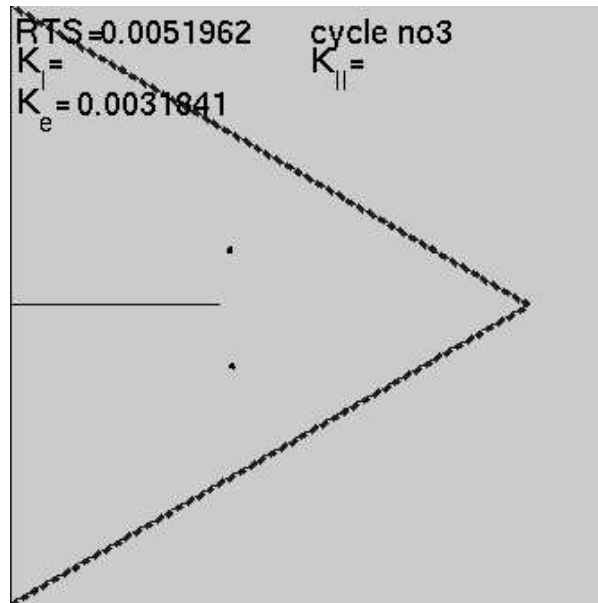


Figure 47: During the unloading sequence, the dislocations glide towards the crack, and a pair is annihilated.

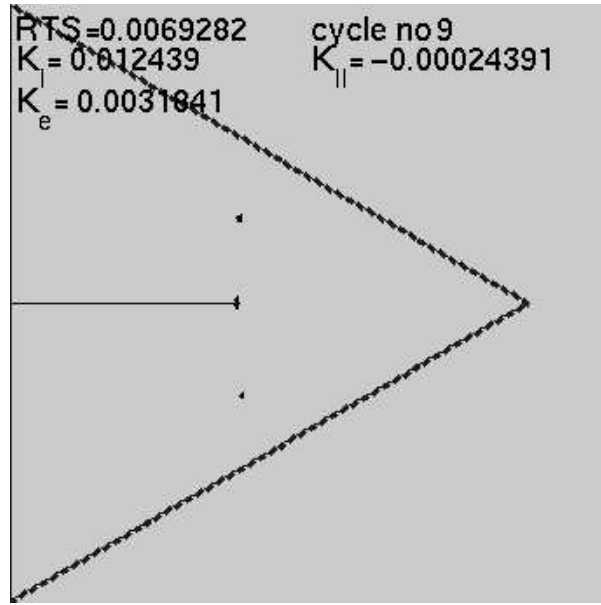


Figure 48: The same procedure as in load cycles number one and two is repeated during the following cycles; The first emitted pair of dislocations prevail, while others are emitted and annihilated. During this procedure the distance between the slip bands of the first emitted pair and the newly emitted pair grows. In load cycle number 9, the distance is so great that...

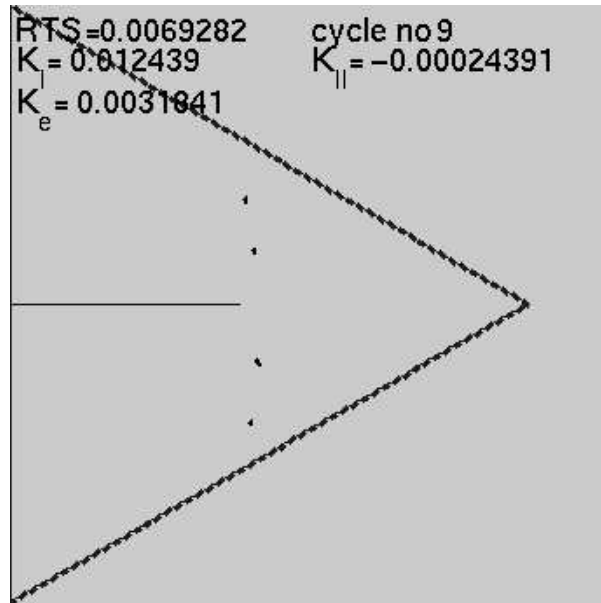


Figure 49: ...after the load peak has been reached...

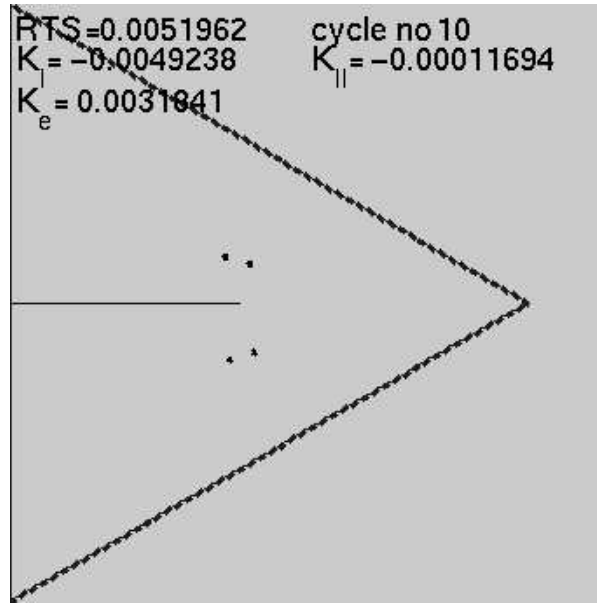


Figure 50: ...the dislocations are not pushed back enough towards the crack tip to be annihilated!

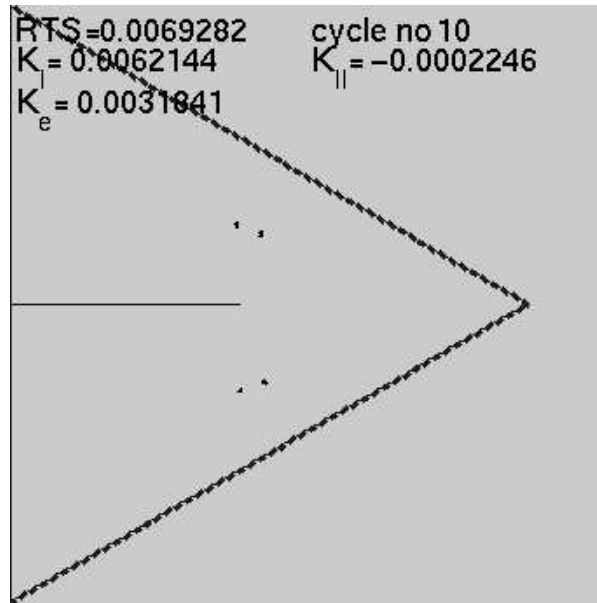


Figure 51: A configuration has been reached that prevents both emission and annihilation during the following cycles. The influence of the grain boundaries have brought the crack to a stop.

5.3 A third application; Sophisticated grain boundaries, a complicated geometry and several glide planes

We now investigate the behaviour of a kinked crack in a grain which boundaries are modelled by a sequence of inclined dipoles.

If we use $\|b\| = 0.25nm$ and allow the crack to kink, we encounter problems when solving the linear system. A new crack segment following a kink is approximately $1mL$, so the collocation points on the segment almost coincide. Thus the equations for the dislocation density arising from collocating on this segment are almost the same, which implies that the system matrix A is very ill-conditioned. Condition numbers in the order of 10^{20} appear. Though, the observations made in section 4.4 tells us that cracks tend to turn into mode I, so we might very well let the last segment of the initial crack be parallel to the x-axis. In this way the crack increments forward, and no short segments will appear.

We used values of tol between 0.1 and 1.5. When the value of tol is as high as 1.5, our glide model tells us that a dislocation will not move if $|\tau| < 1.5\tau_{crit}$ which contradicts the purpose of the material property τ_{crit} . Though, such high values of tol are only used in situations when problems with the convergence of the EAD-iteration appears, and these problems often concerns only few dislocations, whereas the for the other dislocations the more realistic criterion $|\tau| < \tau_{crit}$ is often fulfilled at the end of each EAD-iteration. Also, the dislocation speed c was set to 10^{-2} at the beginning of every EAD-iteration, whereupon it was lowered repeated times if convergence was not reached. Finally, we set $be = 200$ and ba between 300 and 500, because dislocations very close to the crack tip sometimes gives rise to somewhat chaotic behaviour (see further discussion below).

In figures 52 through 59 we can follow the simulation of the described crack problem. The parameter values we have not yet defined are:

Material and load parameters

$$\begin{aligned}
C_0 &= 4 \\
R &= \{-\pi/4, 0, \pi/4, \pi/2\} \\
\mu &= 80 \cdot 10^{-3} N/L^2 \\
\nu &= 0.3 \\
\tau_{crit} &= \frac{\mu}{2000} N/L^2 \\
K_e &= 0.4 \cdot \mu \cdot \sqrt{\|b\|} \frac{N}{L\sqrt{L}} \\
\sigma_{min}^\infty &= 0 N/L^2 \\
\sigma_{max}^\infty &= 3.5 \cdot 10^{-4} N/L^2
\end{aligned}$$

Technical parameters

$$\begin{aligned}
\text{loadstep} &\text{ is } \frac{\sigma_{max}^\infty - \sigma_{min}^\infty}{4} \\
N &= 20
\end{aligned}$$

We see dislocation pile-ups against the grain boundary. This behaviour is also observed in [12], even though the obstacles (such as a grain boundary) in [12] was modelled by a local increase in the material friction. During the simulation, dislocations do overcome the boundary due to the other dislocations in the pile-up that increase the force on the 'leading dislocation'. Furthermore, as dislocations are pushed back from the grain boundary, it happens that they actually glide pass the crack front without being annihilated. The technical parameters ba and c has a great influence on whether this happens or not, and this will be discussed in the final section.

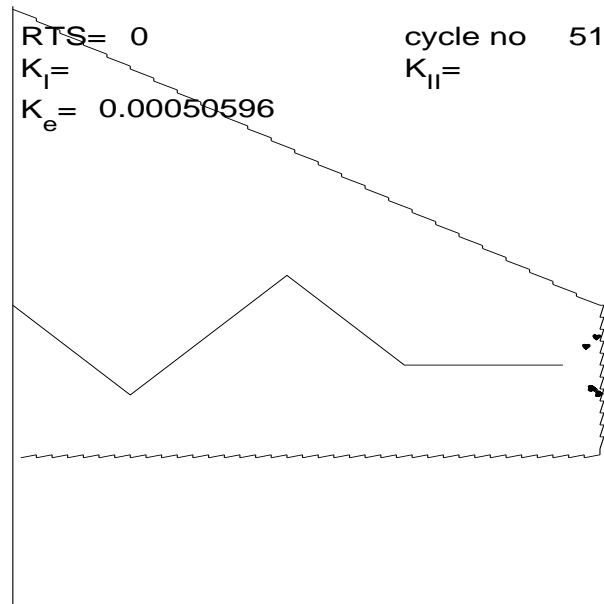


Figure 52: The configuration after 50 load cycles.

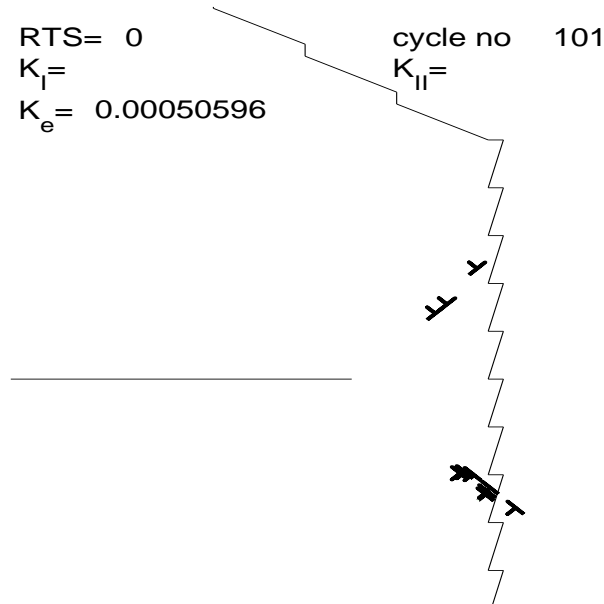


Figure 53: After 100 load cycles we clearly see dislocation pile-ups towards the grain boundary.

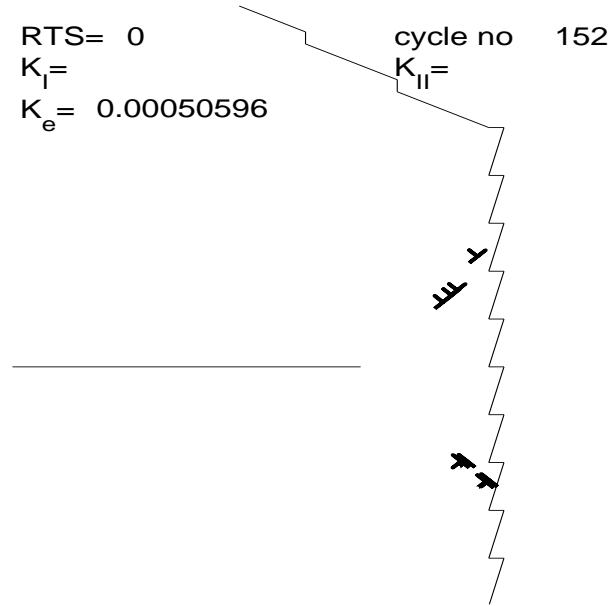


Figure 54: The barrier effects of the grain boundary depends on from which direction the dislocation approaches.

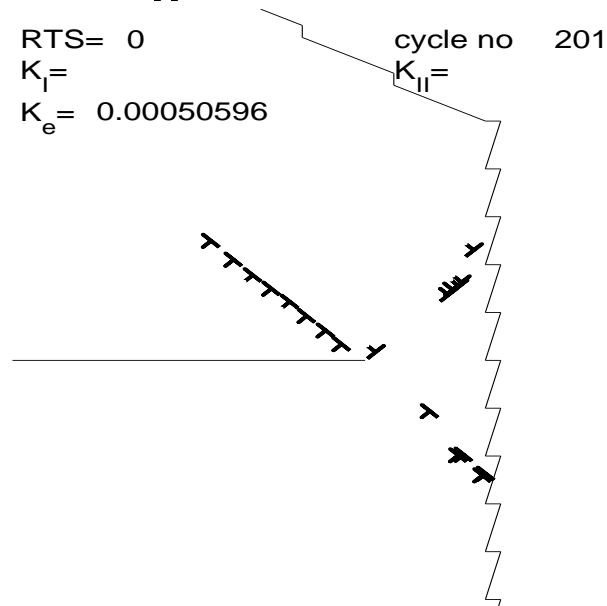


Figure 55: After 200 load cycles dislocations have been pushed back *beyond* the crack tip. The physical relevance of this is further discussed below.

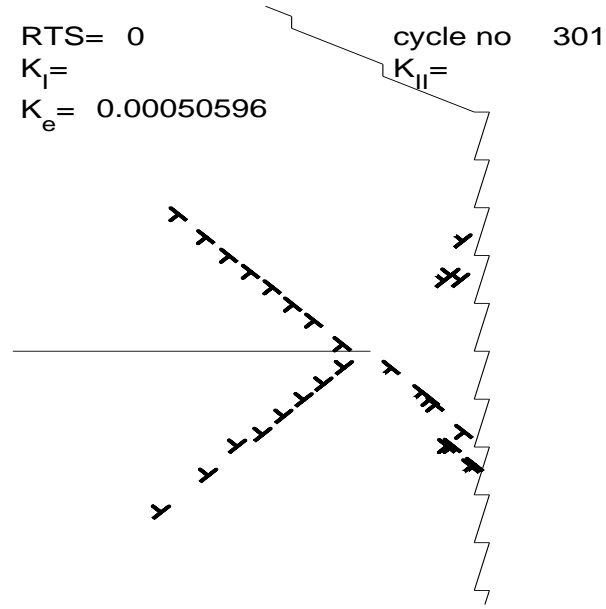


Figure 56: After 300 load cycles even more dislocations have been pushed back beyond the crack tip, and the size of the pile-ups against the grain boundary have increased.

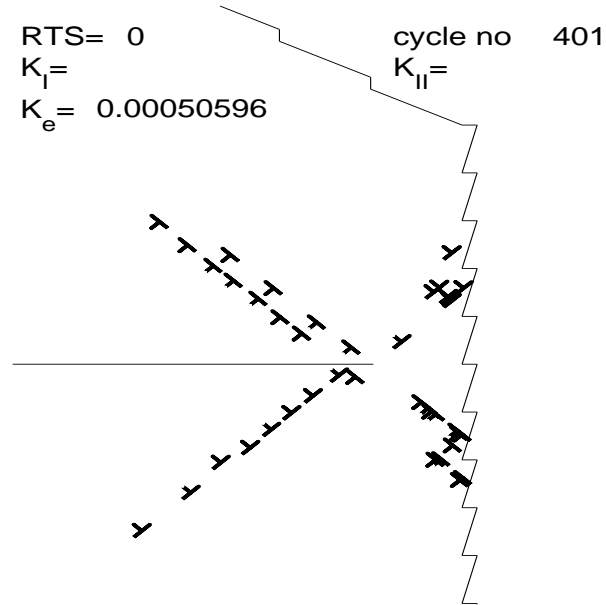


Figure 57: After 400 cycles the EAD-iterations are very slow because of the many free dislocations.

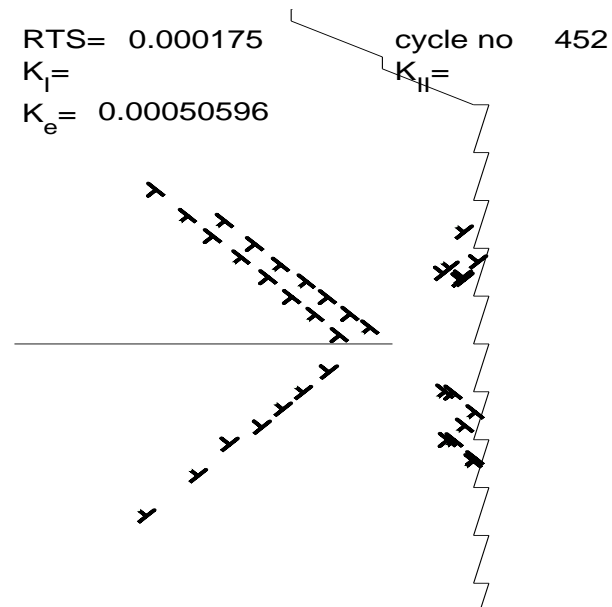


Figure 58: The dislocation configuration after 452 cycles.

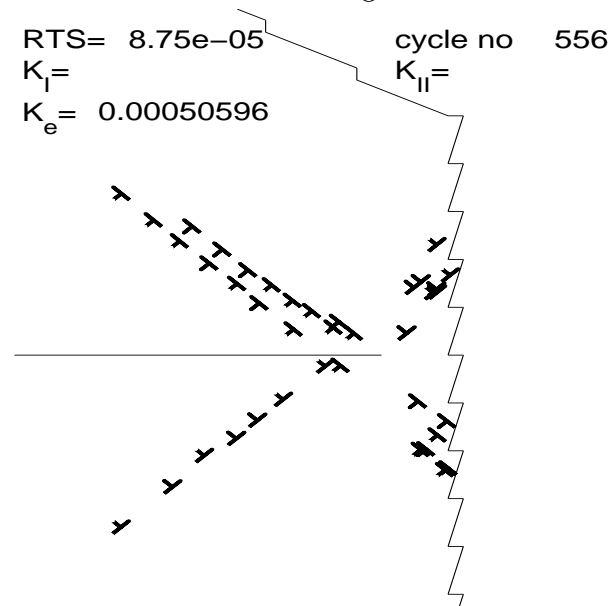


Figure 59: The dislocation configuration after 555 cycles.

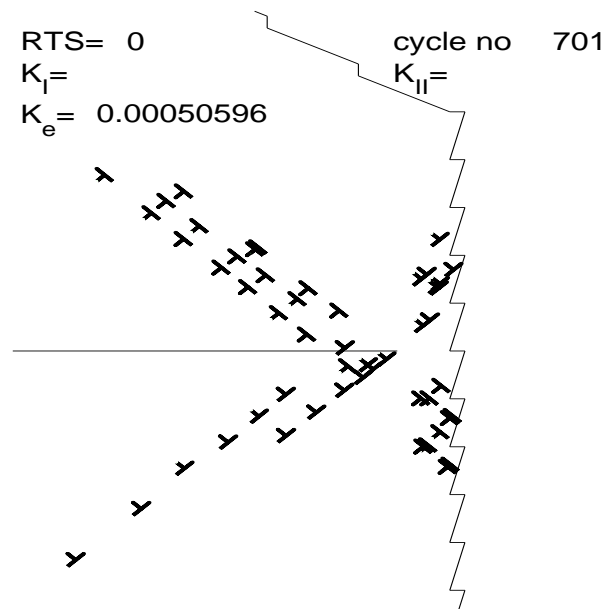


Figure 60: The dislocation configuration after 700 cycles. Several rays of dislocations are left behind in the plastic wake.

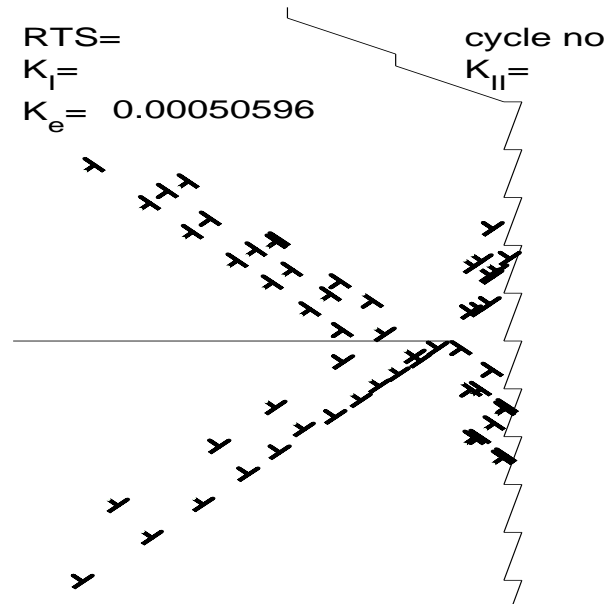


Figure 61: The dislocation configuration after 774 cycles.

5.4 Conclusions and future work

Some criticism of the very special emission and crack growth models that were used in this study is motivated. The formula that determines whether dislocations with specific burgers vectors should be emitted resembles a Mohr's transformation for computing the *shear* along inclined planes. Thus one can imagine that all dislocations are emitted due to shear, even if they are emitted along inclined glide planes. It might be worthwhile to try out a model that treats 'mode I emission' in more suitable way. The crack growth model works efficiently unless very short segments appear, as they do when one treats elementary dislocations (dislocations whos burgers vectors are the same size as the intrinsic burgers vector) and kinking is allowed. A remedy for this shortcoming could be to use a different number of collocation points on each segment. Though, if the segment is very short it would probably not fit more than a couple collocation points, so then the solution might very well be very inaccurate.

The values of the technical parameters have a great influence on the outcome. For example, one load step instead of ten during a load cycle will have the effect that one dislocation instead of ten dislocations are emitted during every load cycle. Since all dislocations are of equal strength, this difference has a significant impact on the crack. Such pitfalls could be avoided by treating free dislocations of different strengths, which requires a model for deciding these strenghts. Also the dislocation speed c has a great influence on the EAD-iteration. In the third application for example, as dislocations were pushed back from the grain boundary, the too high value of c made it possible for the dislocations to pass in front of the crack tip without being annihilated. A lower value of c would have slowed down the convergence of the iteration, so that the EAD might never have been reached. Also the value of the parameter ba could be increased to avoid this behaviour. On the other hand, it might be physically reasonable for this constellation to appear. The conclusion is that the technical parameters have a very great influence on the outcome of the simulation. Some more research concerning what paratemer values that are realistic is recomended.

The EAD-iteration is too slow. This problem could be solved by coding entirely in a compiling language, and treating superdislocations instead of many smaller dislocations.

Partially because we want to reduce the computational load in the EAD-iteration, we do not check whether mobile dislocations move across the crack

tip line far from the crack tip. The dislocations that make up the plastic wake in the third simulation move across a region close to the crack tip, and as mentioned, the reason why they are not annihilated can be derived from the values of c and ba .

To extend the code so that it can handle multiple and branched cracks is not difficult, it is just a matter of adding more equations and finding the correct conditions for the ends of the crack segments. Friction stresses due to crack face contact and the possible rewelding of the crack is not entirely trivial, see [11]. If one wishes to treat cracks of arbitrary shape, one can discretize the crack line into several linear segments. This way our code can handle also curved cracks.

It is simple to use this code for geometrical constellations other than the half plane, for example an infinite plane with a circular inclusion. The only condition on the geometry is that there must be available an expression for the influence of a dislocation. The crack must also initiate at a free surface, since this has a special influence on the BE-formulation of the equations. A crack that does not initiate at a free surface would actually require a *simplification* of the code!

An obvious generalization of the proposed model is that it should be applicable to cases in which you consider all three dimensions. This is not entirely trivial. The technique is the same, but all integrals will be two dimensional and 'even more' divergent than in the one dimensional case, and consequently they must be evaluated by special methods.

References

- [1] C. Giacomazzo, H.L Monaco, D. Viterbo, F. Scordari, G. Gilli, G. Zanotti, M. Catti, edited by C. Giacomazzo, (1992) *Fundamentals of Crystallography*, Oxford; Oxford University Press
- [2] I. Kovacs, L. Zsoldos (1973) *Dislocations and Plastic Deformation*, Oxford; Pergamon Press
- [3] J.P. Hirth, J. Lothe, (1968) *Theory of Dislocations*, New York; McGraw-Hill
- [4] T. Dahlberg, A. Ekberg, (2002) *Failure Fracture Fatigue*, Lund; Studentlitteratur
- [5] T.L. Anderson, (1995) *Fracture Mechanics; Fundamentals and Applications*, 2:nd ed., Boca Raton, Fla.; CRC, cop.
- [6] E.E. Gdoutos, (1990) *Fracture Mechanics; Criteria and Applications*, Dordrecht; Kluwer Academic Publishers
- [7] D.J. Cartwright, D.P. Rooke (1979) *Greens Functions in Fracture Mechanics* appearing in *Fracture Mechanics; Current Status, Future Prospects* edited by R.A. Smith, Conference Cambridge; Toronto cop.
- [8] M.H. Aliabadi, D.P. Rooke, (1991) *Numerical Fracture Mechanics*, Dordrecht; Kluwer Academic Publishers
- [9] D.A. Hills, P.A. Kelly, D.N. Dai, A.M. Korsunsky, (1996) *Solution of Crack Problems*, Dordrecht; Kluwer Academic Publishers
- [10] J. Weertman, (1996) *Dislocation Based Fracture Mechanics*, World Scientific
- [11] F.O. Riemelmoser, R. Pippan, O. Kolednik, (1997) *Cyclic crack growth in elastic plastic solids: a description in terms of dislocation theory*, Computational Mechanics, vol.20
- [12] F.O. Riemelmoser, P. Gumbsch, R. Pippan, (2001) *Dislocation Modelling of Fatigue Cracks; An Overview*, Materials Transactions, vol.42, no.1

- [13] F.O. Riemelmoser, P. Gumbsch, R. Pippan, (2000) *Plastic Deformation at Short Edge Cracks under Fatigue Loading*, Engineering Fracture Mechanics, vol.66
- [14] R. Pippan, F.O. Riemelmoser, (1995) *Dislocation Shielding of Fatigue Cracks*, Z. Metallkd., vol.86
- [15] F.O. Riemelmoser, P. Gumbsch, H.P. Stuwe, (1997) *A Comparison of a Discrete Dislocation Model and a Continouos Description of Cyclic Crack Tip Plasticity*, International Journal of Fracture, vol.85
- [16] C. Bjerken, S. Melin, (2002) *A tool to model short crack fatigue growth using a discrete dislocation formulation*, paper from Department of Mechanical Engineering, Lund University, Sweden
- [17] D.N Dai, (2002) *Modelling cracks in finite bodies by distributed dislocation dipoles*, International Journal of Fatigue and Fracture of Engineering Materials and Structures, vol. 25
- [18] F.O. Riemelmoser, P. Gumbsch, H.P. Stuwe, (1998) *An argument for a cycle-by-cycle propagation of fatigue cracks at small stress intensity ranges*, Acta Mater., vol 46
- [19] T. Zhu, W. Yang, T. Guo, (1996) *Quasi-cleavage processes driven by dislocation pileups*, Acta Mater., vol 44
- [20] I.-H. Lin, R. Thomson, (1986) *Cleavage, dislocation emission, and shielding for cracks under general loading*, Acta Metall., vol. 44, no.2
- [21] M.H. Aliabadi, (2002) *The Boundary Element Method, Volume 2*, Chichester; Wiley
- [22] M. Bonnet, (1995) *Boundary Integral Equations Methods for Solids and Fluids*, Chichester; Wiley
- [23] A. Andersson, (1996) *The Boundary element method in fracture mechanics*, Diploma report from Lund Institute of Technology, LUTFD2/(TFHF-5071)/1-65/1996
- [24] Z. Kopal, (1961) *Numerical Analysis*, London; Chapman and Hall

- [25] F. Erdogan, G.D. Gupta, (1972) *On the numerical solution of singular integral equations*, Quarterly of applied mathematics, vol.29
- [26] F. Erdogan, G.D. Gupta, T.S. Cook, (1973) *Numerical solution of singular integral equations*, appearing in *Methods of analysis and solutions of crack problems*, Leyden; Noordhoff international publishing
- [27] P.S. Theocaris, N.I. Ioakimidis, (1977) *Numerical integration methods for the solution of singular integral equations*, Quarterly of applied mathematics, vol.35
- [28] P.S. Theocaris, N.I. Ioakimidis, (1978) *Numerical solution of Cauchy type singular integral equations by use of the Lobatto-Jacobi numerical integration rule*, Aplikace Matematiky, vol. 23
- [29] P.S. Theocaris, N.I. Ioakimidis, (1979) *A Method of Numerical Solution of Cauchy-Type Singular Integral Equations with Generalized Kernels and Arbitrary Complex Singularities*, Journal of Computational Physics, vol. 30
- [30] A.V. Boiko, L.N. Karpenko, (1981) *On some numerical methods for the solution of the plane elasticity problem for bodies with cracks by means of singular integral equations*, International Journal of Fracture, vol. 17
- [31] C.-F. Sheng, L. Wheeler, (1981) *Crack Path Prediction for a Kinked Crack in the Neighborhood of a Circular Inclusion in an Infinite Medium*, Journal of Applied Mechanics, vol. 48
- [32] Y. Li, D.A. Hills, (1990) *Stress intensity factor solutions for kinked surface cracks*, Journal of Strain Analysis, vol. 25, no.1
- [33] Y. Murakami (editor-in-chief), (1987) *Stress intensity factors handbook*, vol.1, Oxford; Pergamon